**Investigating Electroweak Physics at the Large Hadron Collider**

A Dissertation presented

by

**Pin-Ju Tien**

to

The Graduate School

in Partial Fulfillment of the

Requirements

for the Degree of

**Doctor of Philosophy**

in

**Physics**

Stony Brook University

**May 2015**

**Stony Brook University**

The Graduate School

**Pin-Ju Tien**

We, the dissertation committee for the above candidate for the

Doctor of Philosophy degree, hereby recommend

acceptance of this dissertation

**Patrick Meade - Dissertation Advisor**

**Professor, C.N. Yang Institute for Theoretical Physics, Physics Department**

**George Sterman - Chairperson of Defense**

**Professor, C.N. Yang Institute for Theoretical Physics, Physics Department**

**Dmitri Tsybychev - Committee of Defense**

**Professor, Physics Department**

**Hooman Davoudiasl - Committee of Defense**

**Physicist, Brookhaven National Laboratory**

This dissertation is accepted by the Graduate School

Charles Taber

Dean of the Graduate School

Abstract of the Dissertation

**Investigating Electroweak Physics at the Large Hadron Collider**

by

**Pin-Ju Tien**

**Doctor of Philosophy**

in

**Physics**

Stony Brook University

**2015**

The basic principle of naturalness has driven the majority of the Large Hadron Collider (LHC) program, but so far all searches for new physics beyond the Standard Model (SM) have come up empty. On the other hand, a few existing measurements of SM processes contain interesting anomalies, for instance in the measurement of the WW cross section. The deviation of WW cross section was seen both at ATLAS and CMS and both at 7 and 8 TeV. The discrepancy also became larger at 8 TeV. Combined results with LHC 7 TeV and 8 TeV implies around a three sigma deviation from the SM NLO calculation. This allows for the possibility of new physics with mass scales very close to the Electroweak Scale. We show that the addition of physics beyond the SM at electroweak scale can improve the agreement with the data. In particular supersymmetric models involving charginos, stops and sleptons all provide better fits with the data. In the case of models of sleptons that agree better with the WW data, they can also explain dark matter and the (g-2) anomaly. Furthermore, we show that there are several different classes of stop driven scenarios that not only evade all direct searches, but improve the agreement with the data in the SM measurement of the WW cross section. We also demonstrate that even if these anomalies are not due to new physics, the WW channel can also be used to derive new exclusion limits which are more powerful than existing results using the same ATLAS and CMS datasets. By examining the differential WW cross section we show that the gap between LHC and LEP exclusions can be start to be closed. In particular, we lay out a program under which the difficult to search for regions of new physics models with large SM backgrounds can be investigated.

# Contents

## List of Figures

## List of Tables

## Publications

- David Curtin, Patrick Meade, Pin-Ju Tien, Natural SUSY in Plain Sight, Phys. Rev. D90 (2014) 115012
- David Curtin, Patrick Meade, Pin-Ju Tien, Casting Light on BSM Physics with SM Standard Candles, JHEP 1308 (2013) 068

# 1 Introduction

## 1.1 Why do we need new physics?

The Standard Model(SM) has been a successful theoretical model providing a remarkable description of nature. In particular, it explained the existence of lepton, quark, gauge bosons and the Higgs boson. Some of which of course were known before the SM and some were the predictions of the SM that have since been confirmed. It successfully explains eletromagnetic, weak and strong interaction. However, there are still some unsolved problems in nature which can not be explained by the SM. They are the hierarchy problem, dark matter, dark energy, baryon asymmetry, strong QCD phase, finite neutrino mass and the flavor structure. Although the discovery of Higgs boson in 2012 [14] makes the SM complete, the SM does not predict the Higgs mass. The Higgs Lagrangian of the SM is

$$\mathcal{L}_H = |D_\mu \phi|^2 + \mu^2 \phi^\dagger \phi - \lambda(\phi\phi^\dagger)^2. \tag{1.1}$$

where $\phi$ is a complex scalar field. When electroweak symmetry is broken and $\phi$ obtains a VEV, at tree level the Higgs mass $m_H = \sqrt{2}\mu$ and $v = \mu/\sqrt{\lambda}$. Before the discovery of the Higgs, $v$ was the only parameter which was known but $\mu$ and $\lambda$ were not determined completely.

At 1-loop, see Fig.1(a), there is a quadratic divergence to the Higgs mass when we integrate out loop momentum with cut-off $\Lambda$. Thus, $m_H^2 \sim (\mu^2 + \Lambda^2) \sim \Lambda^2$ assuming $\Lambda \gg \mu$. This implies that the cut-off scale $\Lambda$ should be around the TeV scale or else $m_H, v \sim \Lambda$ must

be larger than $v$ which would be a contradiction. The hierarchy problem is about how to tune $m_H^2 \sim \Lambda_{Planck}^2$ to $m_H^2 \sim v^2$. More explicitly, the main point is how to cancel this quadratic divergence "naturally" since the discovery of the Higgs boson. If new physics exists at the TeV scale, the Higgs mass can be potentially explained. However, ATLAS and CMS have not discovered any new physics with mass less than around $\mathcal{O}(\,\text{TeV})$ yet. Even if the new physics is found, we still need a mechanism to explain the relation between the Planck scale and the new physics scale.

Currently, there are two general sets of ideas for solutions to the hierarchy problem. One is supersymmetry, which we will primarily focus on. The other is the shift symmetry associated with the sigma model. The shift symmetry idea started from the papers of Georgi et al. [21] trying to realize the Higgs boson as a pseudo Nambu-Goldstone boson(pNGB). For example, in a composite Higgs model, the Higgs boson might be a bound state of a strongly-interacting dynamics associated with a composite scale instead of an elementary field. This composite scale is above the weak scale but not far away from it. If the Higgs boson is realized as a pNGB of a enlarged global symmetry of strong dynamics, it can be naturally light [22] compared to the scale of compositeness. For example, in order to construct a composite pNGB Higgs, there are two conditions needed to be satisfied. First, assume $\mathcal{G}$ is global symmetry, the SM electroweak group $G_{SM} = SU(2)_L \times U(1)_Y$ must be embedded in an unbroken group, $H_1$. $\mathcal{G} \to H_1 \supset G_{SM}$. As global symmetry breaking $\mathcal{G} \to H_1$ implies that there are $n = dim(\mathcal{G}) - dim(H_1)$ Goldstone bosons. $n_0 = dim(H_0) - dim(H_1)$ of Goldstone boson are "eaten" to give mass to vector boson with $H_0 = G_{SM}$. Secondly, $\mathcal{G}/H_1$ contains at least one $SU(2)_L$ doublet that is recognized as a Higgs doublet. When those two conditions

are satisfied, $G_{SM}$ is unbroken at tree level. The global symmetry $\mathcal{G}$ is explicitly broken by the couplings of the SM to the strong field that is not invariant under $\mathcal{G}$. More details can be found at [23]. In models of PNGB, the strong dynamics scale is near TeV scale. Thus, we need a UV completion immediately if we hope to explain other problems. Supersymmetry (SUSY) is often more preferred theoretically than the shift symmetry because it solves the quadratic divergent issue in a weakly coupled manner up to the Planck scale.

## 1.2 A brief introduction of Supersymmetry

Before discussing SUSY in detail, let's consider a toy model to understand how the hierarchy problem could be solved in a weakly coupled theory. If a Higgs field couples to a fermion $f$ via a term in $\mathcal{L}$ by $-\lambda_f H\bar{f}f$, the 1-loop correction to the Higgs mass (see Fig.1(a)) is given by

$$\Delta m_H^2 = -\frac{|\lambda_f|^2}{8\pi^2}\Lambda^2 + ... \tag{1.2}$$

where $\Lambda$ is a cut-off scale [1]. Suppose there is a complex scalar particle $S$ coupled to the Higgs field by $-\lambda_S|H|^2|S|^2$. Its 1-loop correction to the Higgs mass (see Fig.1(b)) is given by

$$\Delta m_H^2 = \frac{2\lambda_S}{16\pi^2} \times (\Lambda^2 - 2m_S^2 \ln(\Lambda/m_S) + ...) \tag{1.3}$$

where $m_S$ is the mass of scalar $S$. Note that the sign of fermionic 1-loop contribution and bosnoic 1-loop contribution are opposite. If one assumes $\lambda_S = |\lambda_f|^2$, this quadratic divergence

can be exactly cancelled. Even if the cut off scale $\Lambda$ is the Planck scale, total contributions to the Higgs mass from fermion and boson are very small because $\frac{2\lambda_S}{16\pi^2}\ln(\Lambda_{Planck}/m_S)$ could be smaller than 1.

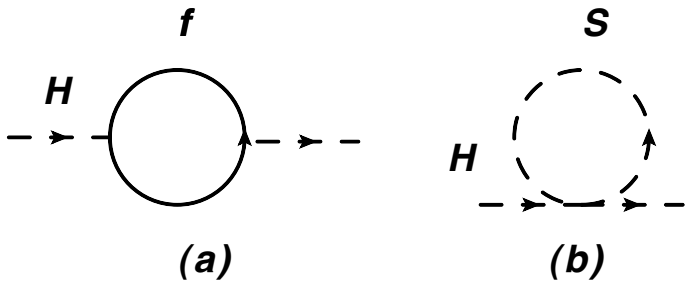


Figure 1: Higgs mass quantum corrections in 1-loop level in a toy model. (a) fermion correction, $-\lambda_f H\bar{f}f$ (b) complex scalar correction, $-\lambda_S|H|^2|S|^2$.

Supersymmetry provides those conditions which make the cancellation of the quadratic divergence happen to all orders. The $\mathcal{N}=1$ supersymmetry algebra, assuming $Q$ is a supersymmtry generator and $P^\mu$ is a four-momentum, is the following:

$$\{Q, Q^\dagger\} = P^\mu \tag{1.4}$$

$$\{Q, Q\} = \{Q^\dagger, Q^\dagger\} = 0 \tag{1.5}$$

$$[P^\mu, Q] = [P^\mu, Q^\dagger] = 0 \tag{1.6}$$

$\mathcal{N}$ denotes the number of supersymmetry generators. There are other SUSY models but only $\mathcal{N}=1$ leads to the chiral theories such as the SM.

$Q$ and $Q^\dagger$ are fermionic operators with spin angular momentum 1/2. They transform bosonic state to fermionic state and vice versa. A number operator $N$ is proportional to

$Q^\dagger Q$ and $QQ^\dagger$. It can be defined as $N = (-1)^{2s}\{Q, Q^\dagger\}$ with spin s. Taking trace of states of operator $N$ implies $n_F = n_B$. In addition, $Q$ and $Q^\dagger$ commute with gauge generators. It implies that both a particle and its superpartner have the same gauge quantum numbers. Also, $[P^2, Q] = [P^2, Q^\dagger] = 0$ guarantees that both particle and its superpartner share the same mass.

The single-particle states of $\mathcal{N} = 1$ SUSY can be described by irreducible representations of supersymmetry algebra, called superfields. For this purpose, there are two kinds of superfields. One is a chiral superfield. The other is a vector superfield. In Tables 1 and 2, the chiral and vector superfields that make up the particle content of the Minimal Supersymmetric Standard Model(MSSM) are shown. Every superfield includes both fermionic and bosonic states. In order to explain the corresponding relation of $\lambda_S = |\lambda_f|^2$ in the MSSM, let's understand the interactions in the MSSM. $\mathcal{L}_{SUSY}$ consists of three parts in the following. The superpotential is responsible for the non-gauge interactions. It must be holomorphic. The definition that the superpotential is holomorphic means the superpotential depends on $\phi$ only or $\phi^*$ only instead of dependence both on $\phi$ and $\phi^*$. The Kähler potential explains the gauge interaction parts as well the kinetic terms for the matter fields. The others are gauge kinetic terms. The superpotential in the MSSM is

$$W_{MSSM} = \bar{u}\mathbf{y_u}QH_u - \bar{d}\mathbf{y_d}QH_d - \bar{e}\mathbf{y_e}LH_d + \mu H_u H_d. \tag{1.7}$$

where $H_u$, $H_d$, $\bar{u}$, $\bar{d}$, $\bar{e}$, Q and L are chiral superfields. $\mathbf{y_u}$, $\mathbf{y_d}$ and $\mathbf{y_e}$ are dimensionaless Yukawa couplings and they are a $3 \times 3$ matrix in family space. $W_{MSSM}$ can describe the

Yukawa interaction using F-term $F_k = -W_k^*$ and $W^k = \partial W/\partial\phi_k$ ($\phi_k$ is a scalar part in a superfield.). F-term can generate the interaction between sfermion and the Higgs boson. For example, $\partial W/\partial\tilde{u} \sim y_u\tilde{Q}H_u$. $W^kW_k$ contains $y^2$ which corresponds to $\lambda_S$ in the toy model. On the other hand, $\int d^2\theta \times W$ results in the SM Yukawa couplings $\bar{u}y_uQH_u$. Thus, $y$ corresponds to $\lambda_f$ in the toy model. Therefore, the relation of $\lambda_S = |\lambda_f|^2$ in the toy model is realized in the MSSM.

Furthermore, the terminologies in the MSSM are discussed in the following. For fermion's superpartner, we call it $sfermion$. On the other hand, for gauge boson's superpartner, we call it *gaugino*. In Table 1, $Q$, $\bar{u}$, $\bar{d}$, $L$, $\bar{e}$, $H_u$ and $H_d$ are chiral superfields. The spin-0 fields are complex scalars and spin-1/2 fields are left-handed Weyl ferminos. In Table 2, (gluino, gluon), (wino, W bosons) and (bino, B boson) are vector superfields. The spin-1/2 is gaugino; the spin-1 is gauge boson. In $SU(3)_C$ QCD interaction, gluon(spin-1) and gluino(spin-1/2). The electroweak interaction $SU(2)_L \times U(1)_Y$ contains gauge bosons, $W^\pm$, $W^0$ and $B^0$. In addition, their superpartners, wino and bino, are $\tilde{W}^\pm$ and $\tilde{B}^0$. After electroweak symmetry breaking, $W^0$ and $B^0$ are mixed to generate mass eigenstates, $Z^0$ and $\gamma$. Similarly, $\tilde{W}^0$ and $\tilde{B}^0$ result in $\tilde{Z}^0$(zino) and $\tilde{\gamma}$(photino).

The particle content of MSSM contains two Higgs superfields. There are two reasons why we need two Higgs superfields instead of one. First, if we only have one Higgs superfield, there is one fermion (Higgsino) in this superfield. As we know the SM is gauge anomaly free, this additional fermion (Higgsino) can generate a gauge anomaly through a triangle loop. Second, in order to keep superpotential holomorphic, we need two different Higgs superfields $H_u$ and $H_d$ which are responsible for mass of up-type and down-type fermion respectively.

| | | spin-0 | spin-1/2 | $SU(3)_C$,$SU(2)_L$,$U(1)_Y$ |
|---|---|---|---|---|
| (s)quark | $Q$ | $(\tilde{u}_L,\tilde{d}_L)$ | $(u_L,d_L)$ | $(\mathbf{3},\ \mathbf{2},\ \frac{1}{6})$ |
| | $\bar{u}$ | $\tilde{u}_R^*$ | $u_R^\dagger$ | $(\bar{\mathbf{3}},\ \mathbf{1},\ -\frac{2}{3})$ |
| | $\bar{d}$ | $\tilde{d}_R^*$ | $d_R^\dagger$ | $(\bar{\mathbf{3}},\ \mathbf{1},\ \frac{1}{3})$ |
| (s)lepton | $L$ | $(\tilde{\nu},\tilde{e}_L)$ | $(\nu,e_L)$ | $(\mathbf{1},\ \mathbf{2},\ -\frac{1}{2})$ |
| | $\bar{e}$ | $\tilde{e}_R^*$ | $e_R^\dagger$ | $(\mathbf{1},\ \mathbf{1},\ 1)$ |
| Higgs,Higgsino | $H_u$ | $(H_u^+,H_u^0)$ | $(\tilde{H}_u^+,\tilde{H}_u^0)$ | $(\mathbf{1},\ \mathbf{2},\ \frac{1}{2})$ |
| | $H_d$ | $(H_d^0,H_d^-)$ | $(\tilde{H}_d^0,\tilde{H}_d^-)$ | $(\mathbf{1},\ \mathbf{2},\ -\frac{1}{2})$ |

Table 1: Chiral superfields in the MSSM. Spin-0: complex scalars. Spin-1/2: left-handed two-component Weyl fermions. We uses the same notations as in [1].

| | spin-1/2 | spin-1 | $SU(3)_C$,$SU(2)_L$,$U(1)_Y$ |
|---|---|---|---|
| gluino, gluon | $\tilde{g}$ | $g$ | $(\mathbf{8},\mathbf{1},0)$ |
| Wino, W boson | $(\tilde{W}^\pm,\tilde{W}^0)$ | $(W^\pm,W^0)$ | $(\mathbf{1},\ \mathbf{3},\ 0)$ |
| Bino, B boson | $\tilde{B}^0$ | $B^0$ | $(\mathbf{1},\ \mathbf{1},\ 0)$ |

Table 2: Vector superfields in the MSSM. Spin-1: gauge boson. Spin-1/2: gauginos, two-component Weyl fermion. We uses the same notations as in [1].

In the SM, $\phi$ is responsible for down-type fermion mass, $\lambda_d\bar{Q}\phi d_R$. On the other hand, $\phi^\dagger$ is used to construct up-type fermion mass, $\lambda_u\epsilon\bar{Q}\phi^\dagger u_R$. In other word, $\phi$ plays a role likes $H_d$ in the MSSM. The role of $\phi^\dagger$ corresponds to $H_u$ in the MSSM. Therefore, to avoid gauge anomaly and to keep the superpotential holomorphic, two Higgs superfields are necessary.

In the MSSM, there are some terms resulting in baryon or lepton number violation even if they are constructed by gauge invariance and supersymmetry. Those terms look like

$$LL\bar{e}, LQ\bar{d}, LH_u, \bar{u}\bar{d}\bar{d} \tag{1.8}$$

with $B = 1/3$ for $Q$, $B = -1/3$ for $\bar{u}, \bar{d}$ and $L = 1$ for $L$, $L = -1$ for $\bar{e}$. Those terms allow a proton decay (see Fig. 2). If these terms are unsurppressed, the coupling constants between quarks and squark must be small because of the proton life time $\tau_{proton} > 10^{31}$ year [92]. We can remove those terms by imposing so-called R-parity. For SM particles, they have even R-parity ($R = +1$). Their superpartners have odd R-parity ($R = -1$). Those states in the same superfield do not have the same R-parity. Therefore, if R-parity is preserved, the coupling of quark-quark-squark is not allowed. Furthermore, the lightest sparticles with R-parity$= -1$ are called LSP, lightest supersymmetric particles and it is a stable particle. If it is electrically neutral, it can become a good dark matter candidate because of its weak interaction with ordinary particles. Every non-LSP supersymmetric particles eventually decays into a final state having an odd number of LSPs. If R-parity is preserved and the LSP is electrically neutral, this has important implications for experimental searches. For example, in the pair production of SUSY particles, the final states includes LSPs contributing to missing energy and it provides a guidance to how to search for physics beyond the SM. With experimental data from LHC and dark matter search, physicists can impose constraints on LSP mass that will be discussed in more detail in this dissertation. In addition, SUSY does not require the presence of R parity because the coefficient in front of those R-parity violations can be very small and they generate different phenomenologies in the colliders.

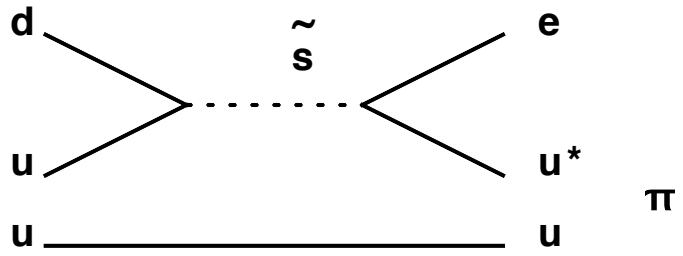


Figure 2: Proton decay: $p \to e^+\pi^0$

## 1.3 Supersymmetry breaking

In SUSY, both $\tilde{e}_L$ and $\tilde{e}_R$ have the same mass as $e$, 0.511 MeV. It implies that SUSY must be broken because we do not find any sparticles with the same mass as their superpartners in experiments. But, even when SUSY is broken, we would like to hold the advantages SUSY provides, vanishing quadratically divergence in $\Delta m_H^2$, to solve the hierarchy problem. Thus, the soft supersymmetric breaking terms are introduced, $\mathcal{L}_{soft}$ and it has been shown that they are consistent with the cancellation of quadratic divergence up to all orders [2]. It contains only mass terms and coupling parameters with positive mass dimension. For example, $M_1$, $M_2$ and $M_3$ are Bino, Wino and Gluino mass terms respectively and they can be complex scalars. The a-term is a $3 \times 3$ complex matrix in family space. The $\mathbf{m^2}$ is a soft mass and a Hermitian matrix. The $b$ term can be a complex scalar. The dimensions of $\mathbf{m^2}$ and $b$ are 2. The other parameters are dimension 1. It keeps the necessary relation between $\lambda_S$ and $\lambda_f$ which are held even if SUSY is broken. Thus, the Lagrangian of the MSSM can be written as

$$\mathcal{L} = \mathcal{L}_{SUSY} + \mathcal{L}_{soft} \tag{1.9}$$

Explicitly, the soft SUSY breaking terms below follow the notation of Ref. [1]. $\mathcal{L}_{soft}$ provides around 105 masses and phases. Those parameters are good sources to CP violating phases. They also contribute to electric dipole moments and rare decays. The soft SUSY breaking terms are

$$\begin{aligned}
\mathcal{L}_{soft} = & - \frac{1}{2}(M_3\tilde{g}\tilde{g} + M_2\tilde{W}\tilde{W} + M_1\tilde{B}\tilde{B} + c.c) \\
& - (\tilde{\bar{u}}\mathbf{a_u}\tilde{Q}H_u - \tilde{\bar{d}}\mathbf{a_d}\tilde{Q}H_d - \tilde{\bar{e}}\mathbf{a_e}\tilde{L}H_d + c.c) \\
& - \tilde{Q}^\dagger\mathbf{m_Q^2}\tilde{Q} - \tilde{L}^\dagger\mathbf{m_L^2}\tilde{L} - \tilde{\bar{u}}\mathbf{m_{\bar{u}}^2}\tilde{\bar{u}}^\dagger - \tilde{\bar{d}}\mathbf{m_{\bar{d}}^2}\tilde{\bar{d}}^\dagger - \tilde{\bar{e}}\mathbf{m_{\bar{e}}^2}\tilde{\bar{e}}^\dagger \\
& - m_{H_u}^2 H_u^* H_u - m_{H_d}^2 H_d^* H_d - (bH_u H_d + c.c).
\end{aligned} \tag{1.10}$$

There are several reasons to separate the SUSY breaking sector and the SUSY preserving sector. In order to spontaneously break SUSY, it would be a problem to generate gaugino mass terms. For example, there are no supersymmetric terms, scalar-gaugino-gaugino, which can give rise to gaugino mass when the scalar gets a VEV. Moreover, the spontaneous breaking in the MSSM implies vanishing of supertrace [3]. The supertrace describes the relation of mass square between the SM particles and its superpartner. Take electron/selectron for an example.

$$\begin{aligned}
STr(m^2) & \equiv \sum_j (-1)^j (2j+1) Tr(m_j^2) \\
m_{\tilde{e}_1}^2 & + m_{\tilde{e}_2}^2 - 2m_e^2 = 0
\end{aligned} \tag{1.11}$$

$m_{\tilde{e}_{1,2}}$ are selectron mass and $m_e$ is electron mass. This implies that there is one selectron having a mass lighter than electron mass. It should have been seen in experiment already. For these reasons, we expect that the soft terms in the MSSM are generated radiatively rather than generated at tree level. Supersymmetry breaking happens in a "hidden sector" and the chiral superfields in the MSSM occur in a "visible sector" (see Fig.3). If there is a mediation between these two sectors, the square mass sum rules are not necessarily held. Thus, the particle spectrum become acceptable. In addition, if this mediating interaction is flavor-blind, the soft terms in $\mathcal{L}_{soft}$ can be reduced into the following,

$$\mathbf{m_Q^2} = m_Q^2\mathbf{1},\ \mathbf{m_{\bar{u}}^2} = m_{\bar{u}}^2\mathbf{1},\ \mathbf{m_{\bar{d}}^2} = m_{\bar{d}}^2\mathbf{1},\ \mathbf{m_{\bar{e}}^2} = m_{\bar{e}}^2\mathbf{1} \tag{1.12}$$

$$\mathbf{a_u} = A_{u0}\mathbf{y_u},\ \mathbf{a_d} = A_{d0}\mathbf{y_d},\ \mathbf{a_e} = A_{e0}\mathbf{y_e}$$

$$Im(M_{1,2,3}) = Im(A_{u0}) = Im(A_{d0}) = Im(A_{e0}) = 0$$

Gauge-mediated supersymmetry breaking (GMSB) scenario is one of many mediation models describing the mechanism of separation between a hidden sector and a visible sector. Messengers are introduced to be responsible for the interaction shared by the hidden sector and the visible sector. These messengers are chiral superfields with gauge interactions, $SU(3)_c \times SU(2)_L \times U(1)_Y$. Thus, it is automatically flavor-blinded. When SUSY is broken and get a VEV, the messenger particles generate soft mass terms through loop contributions. For example, they generate gaugino mass by 1-loop contributions and sfermion mass by 2-loop contributions. a-terms are assumed to be zero. In minimal GMSB, the gaugino mass

and sfermsion mass can be determined by two parameters only. There are many other mediation mechanisms, for example anomaly mediation [4, 5]. They each provide their own patterns of soft terms.

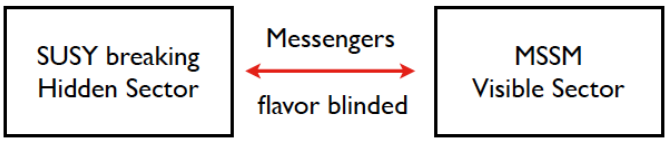


Figure 3: A separation between a SUSY breaking sector and a MSSM sector.

## 1.4 Electroweak Symmetry Breaking

Electroweak symmetry breaking (EWSB) in the MSSM is slightly different from SM because of the presence of two Higgs doublets. After electroweak symmetry is broken and both $H_u$ and $H_d$ get VEV, the mixture of $\mathcal{L}_{SUSY}$ and $\mathcal{L}_{soft}$ make those sparticles massive. After $H_u$ and $H_d$ get VEV and $H_u^+ = H_d^- = 0$, the scalar potential in the MSSM becomes:

$$\begin{aligned} V &= (|\mu|^2 + m_{H_u}^2)|H_u^0|^2 + (|\mu|^2 + m_{H_d}^2)|H_d^0|^2 - (bH_u^0 H_d^0 + c.c) \\ &+ \frac{1}{8}(g^2 + g'^2)(|H_u^0|^2 - |H_d^0|^2)^2. \end{aligned} \tag{1.13}$$

where only $\mu$-term is a SUSY term and other terms are from $\mathcal{L}_{soft}$. There are two complex $SU(2)_L$ Higgs doublets implying eight real scalars. When EWSB happens, three of eight scalars are Goldstone bosons contributing to the longitudinal components of $Z$ and $W^{\pm}$

bosons. There are remaining five Higgs scalar mass eigenstates. Two CP-even neutral scalars $h^0$ and $H^0$, one CP-odd neutral scalar $A^0$, and two charged scalars $H^{\pm}$.

In order to bound V from below and ensure EWSB, two inequalities need to be satisfied.

$$2b < 2|\mu|^2 + m_{H_u}^2 + m_{H_d}^2 \tag{1.14}$$

$$b^2 > (|\mu|^2 + m_{H_u}^2)(|\mu|^2 + m_{H_d}^2) \tag{1.15}$$

To relate to particle phenomenology, the VEVs $v_u$ and $v_d$ are related to the Z-boson mass,

$$v_u^2 + v_d^2 = v^2 = 2m_Z^2/(g^2 + g'^2) \tag{1.16}$$

The ratio of VEVs is written as $\tan\beta = v_u/v_d$. Thus, we can write $m_Z$ in terms of $m_{H_u}^2$, $m_{H_d}^2$, $\mu$ and $\sin 2\beta$.

$$m_Z^2 = \frac{|m_{H_d}^2 - m_{H_u}^2|}{\sqrt{1 - \sin^2(2\beta)}} - m_{H_u}^2 - m_{H_d}^2 - 2|\mu|^2 \tag{1.17}$$

$m_{H_u}^2$ and $m_{H_d}^2$ are SUSY soft breaking parameters. The requirements of EWSB and naturalness also require light EW states, for example Higgsino (see Eq. 1.17). $\mu$, $m_{H_u}^2$ and $m_{H_d}^2$ are all similar. In order to get correct Z-bson mass, $\mu$ must be around $\sim m_{soft}$. There is one

method to achieve it, called spurion. $\mu$ can be promoted to a field. Once SUSY is broken, this field gets a VEV, $\mu$.

From the Higgs potential $V$, Eq. 1.13, we can obtain the lighter Higgs mass $m_{h^0}$ in tree-level. The tree-level Higgs mass is:

$$m_{h^0} = m_Z |\cos 2\beta|. \tag{1.18}$$

Given that the Higgs mass has been measured to be around 125 GeV, the tree-level contribution to the Higgs mass is not enough to get the correct mass. The next leading contribution comes from stop contributions in 1-loop level.

$$m_{h^0}^2 = m_Z^2 |\cos 2\beta|^2 + \frac{3m_t^4}{4\pi^2 v^2}\{\ln(\frac{M_S^2}{m_t^2}) + \frac{X_t^2}{M_S^2}(1 - \frac{X_t^2}{12M_S^2})\} \tag{1.19}$$

where $m_t$ is top quark mass. $M_S^2 = m_{\tilde{t}_1} m_{\tilde{t}_2}$ and $X_t = A_t - \mu \cot\beta$. There is no quadratic divergence in the Higgs mass correction as we expect in SUSY model. A 125 GeV Higgs mass naively requires stops above a TeV. This can easily be accommodated within the MSSM but somewhat counteracts the supersymmetric solution to the hierarchy problem, since the same particles which give radiative contributions to the quartic term in the Higgs potential also cancel its quadratic divergences. This tension, with heavy stops required for a heavy Higgs but light stops required for naturalness, is the so-called "little hierarchy

problem" of the MSSM. There are many model building solutions to the little hierarchy problem within SUSY. Two important examples of theories which generate new Higgs quartic contributions without heavy stops are the NMSSM/$\lambda$SUSY [31, 32] and additional D-term contributions [33]. In these models, SUSY can in principle be fully natural, solving the hierarchy problem without fine-tuning, provided that the stops are sufficiently light. This has motivated an extensive LHC program at both ATLAS and CMS in an attempt to cover all possibilities to search for light stops [34, 35, 40, 45–47]. This logic also extends to other BSM models that solve the hierarchy problem, with both major LHC collaborations [48] working to pin down generic top partners [49, 50]. Despite these efforts, no 3$^{\text{rd}}$ generation partners of SM particles have been found, and lower limits on the masses of particles potentially responsible for naturalness are becoming uncomfortably stringent [34, 35, 40, 45–48].

The MSSM provides a method for breaking radiatively the electroweak symmetry (REWSB). REWSB relies on the renormalization group evolution (RGE) from a grand unification scale $\Lambda_{GUT}$ to weak scale. This is a contrast to the SM, which does not explain why EWSB occurs. At $\Lambda_{GUT}$, there is a simple input of a boundary condition and electroweak symmetry is unbroken. For example, at $\Lambda_{GUT}$, $m^2_{H_u} = m^2_{H_d}$ is held in tree level of GMSB. The RGEs of $m^2_{H_u}$ and $m^2_{H_d}$ are driven by $|y_t|^2$ and $|y_b|^2$ respectively. $m^2_{H_u}$ naturally has a smaller value than $m^2_{H_d}$ at electroweak scale. Therefore, it helps the Higgs fields obtain nonzero VEV and EWSB is achieved.

Gauge unification is an attractive consequence in the MSSM. The 1-loop RG equations for gauge couplings $g_1$, $g_2$, $g_3$ are

$$\beta_{g_a} = \frac{d}{dt} g_a = \frac{1}{16\pi^2} b_a g_a^3 \tag{1.20}$$

$$(b_1, b_2, b_3) = \begin{cases} (41/10, -19/6, -7) & \text{Standard Model;} \\ (33/5, 1, -3) & \text{MSSM.} \end{cases}$$

where $t = ln(Q/Q_0)$, Q is RG scale. The conventional electroweak gauge couplings $g$ and $g'$ satisfy $e = g \sin\theta_w = g' \cos\theta_w$. The normalization for $g_1$ is $g_1 = \sqrt{5/3} g'$ and $g_2 = g$. Consider $\alpha_a = g_a^2/4\pi$

$$\frac{d}{dt} \alpha_a^{-1} = -\frac{b_a}{2\pi} \tag{1.21}$$

In Fig.4, compared to the evolutions of gauge couplings in the SM, the gauge unification in the MSSM is much better than that in the SM.

SUSY can also be a potentially promising solution to the matter-antimatter symmetry in our universe. The cause of the matter-antimatter asymmetry in our universe (Baryon Asymmetry of the Universe, BAU [6]) is still an open fundamental question in particle physics. The Sakharov conditions [6] for baryogenesis are CP violation, baryon number violation and non-equilibrium processes. Many models, for instance, electroweak baryogenesis [7–9] (EWBG), leptogenesis [10] and Affleck-Dine baryogenesis [11], can potentially explain the BAU. But, the common thing among these models is the need of more CP violation phases because CP violation phases in the Standard Model (SM) are not enough to explain the BAU because SM only provides two CP violation phases, $\theta_{QCD}$ and Kobayashi-Maskawa(KM) phase. It is also quite generic in any model of Beyond Standard Model (BSM) physics to have new

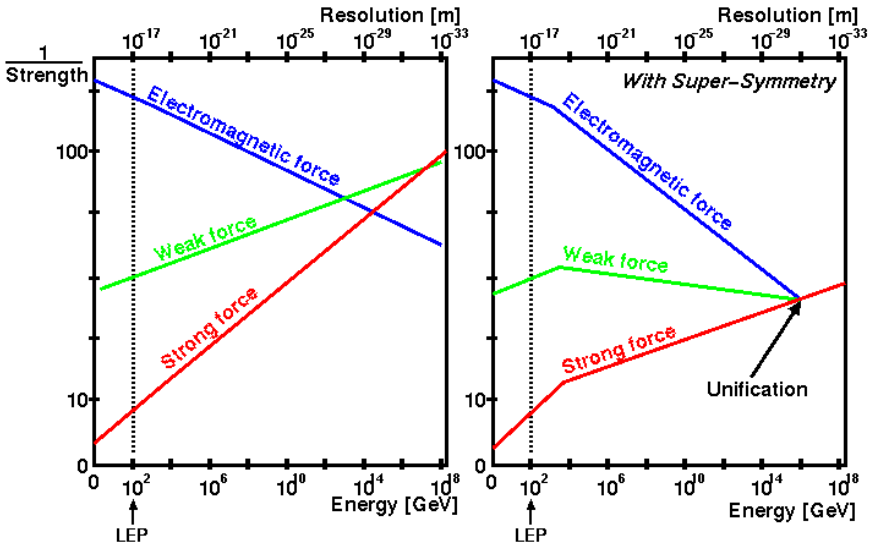


Figure 4: Gauge coupling evolutions in Standard Model and MSSM. Left: gauge coupling evolutions in Standard Model. Those three gauge couplings are not unified at GUT scale. Right: gauge coupling evolutions in the MSSM. Those three gauge couplings are unified at GUT [12].

sources of CP violation even without having a particular explanation for BAU. Supersymmetry is an example of where additional sources of CP violation arise in a motivated model. Electroweak baryogenesis is more compelling than other kind of baryogenesis because it is weak scale physics and testable. The Light Stop scenario (LSS) in the MSSM is required to achieve successful EWBG. But, Higgs decay and production channels performed by ATLAS and CMS excluded LSS above 90% confidence level [13]. It is possible that the extended-MSSM can release this tension.

## 1.5 Experimental Search for SUSY in LHC

Experimental physicists have been looking for new physics hints at the Tevatron and the LHC for many years. The impressive performance of the LHC has thrust theoretical physics into a state of some confusion. The discovery by ATLAS and CMS of the Higgs boson [14], or something very much like it, is an unparalleled triumph. That being said, it also brings the naturalness and hierarchy problems to the fore. We now have to directly confront the possibility that a fundamental scalar has been discovered in nature. In general, any weakly coupled solution of the hierarchy problem should feature new states below the TeV scale. Unfortunately, no such new states have been discovered so far by either ATLAS or CMS [18, 19].

Although SUSY is a calculable solution to the hierarchy problem, it is this very calculability which naively places it under stronger tension than most other potential solutions. This is because MSSM predicts the Higgs quartic coupling solely within the IR sector of the theory. While this predictive nature of the MSSM is one of its more desirable features, accounting for the exact mass of the Higgs discovered by ATLAS and CMS requires radiative corrections to the quartic coupling from particles within the MSSM.

Fig.5 presents SUSY searches performed by ATLAS and CMS [15]. They included the current mass constraints on squark, electroweak gaugino, slepton and gluinio searches. LHC pushed these mass bounds toward to higher energy scale. For example, in stop searches, they show stop mass limit at different kinds of decay channels, $\tilde{t} \to t\tilde{\chi}^0$ and $\tilde{t} \to b(\tilde{\chi}^{\pm} \to W\tilde{\chi}^0)$. The stop mass limit is pushed to around $\sim 500$ GeV. Those mass bounds vary for different

search channels. In Fig.6, both CMS and ATLAS performed stop pair productions with $20/4.7fb^{-1}$ and 8/7 TeV. They presented 95% exclusion regions for stop decay via t/c quark or W boson. For example, they searched 1-lepton,0-lepton, monjet stop or hadronic stop in $\tilde{t} \to t\tilde{\chi}_1^0/c\tilde{\chi}_1^0$ and considered the stop decay 100%. The observed limits are quite similar to the expected limits. Moreover, those searches almost rule out stop mass from 200 GeV to 700 GeV and there are still some regions allowing stop living around 200 GeV.

In addition, they also performed those searches for the electroweak production of charginos and neutralinos based on $20.3fb^{-1}$ and 8 TeV. In Fig.7, they presented 95% exclusion region in LSP-neutralino/chargino mass plane. The chargino decay channels included the decay via H/W/Z or slepton, for example, $\tilde{\chi}_2^0\tilde{\chi}_1^\pm \to (H/Z\tilde{\chi}_1^0)(W\tilde{\chi}_1^0)$, $\tilde{\chi}_1^\pm \to \tilde{l}\nu_l$ and $\tilde{\chi}_2^0 \to \tilde{l}l$ with Br($\tilde{\chi}_2^0 \to \tilde{l}l$)=0.5,1. With these decay models, they searched for these events with final states having multi-leptons. In general, as neutralino/chargino mass smaller than 700 GeV, they ruled out the possibility of the case that LSP has a mass smaller than 100 GeV. In most cases, expected limits are similar to observed limits except $\tilde{\chi}_1^\pm\tilde{\chi}_2^0$ via WZ. The observed limit has less stringent than the expected limits because the data exceed the expectation in three-lepton regions [75, 76]. Besides SUSY searches, ATLAS and CMS have also been working on exotics searches [17], for example, extra dimension, W'/Z', vector-like quark and leptoquarks. For exotics results in Fig.8, the new physics masses are pushed to around 1 TeV.

However, because of lack of any new physics evidence, not even the most promising theory, SUSY, physicists question about SUSY itself. For example, "Does SUSY really exist?", "Does SUSY exist in much higher scale because there is nothing interesting happened below

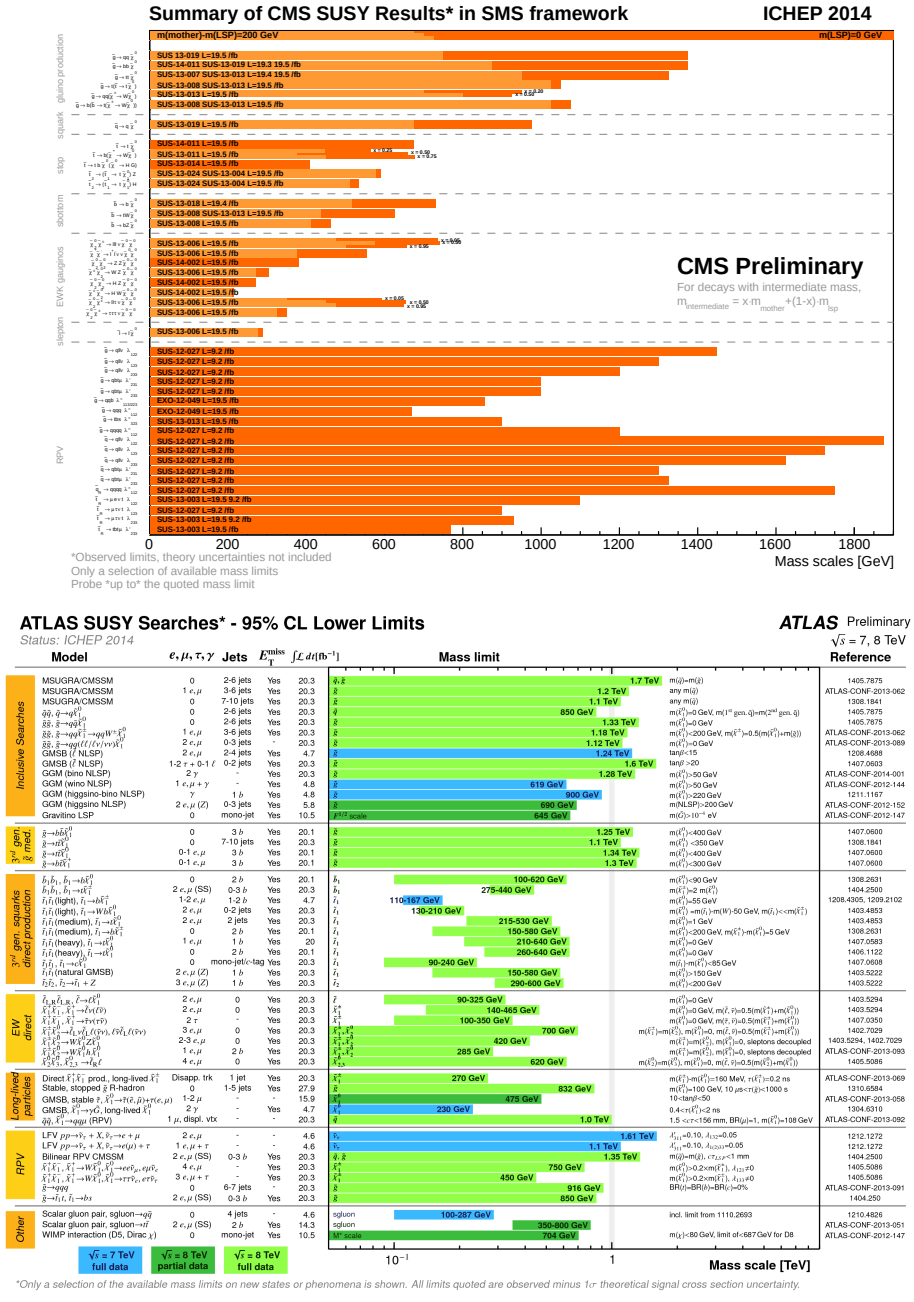





Figure 5: SUSY Search in CMS and ATLAS [15]. Both of them included squark, electroweak gaugino, slepton and gluino search. Up: SUSY searches in CMS. Down: SUSY searches in ATLAS.

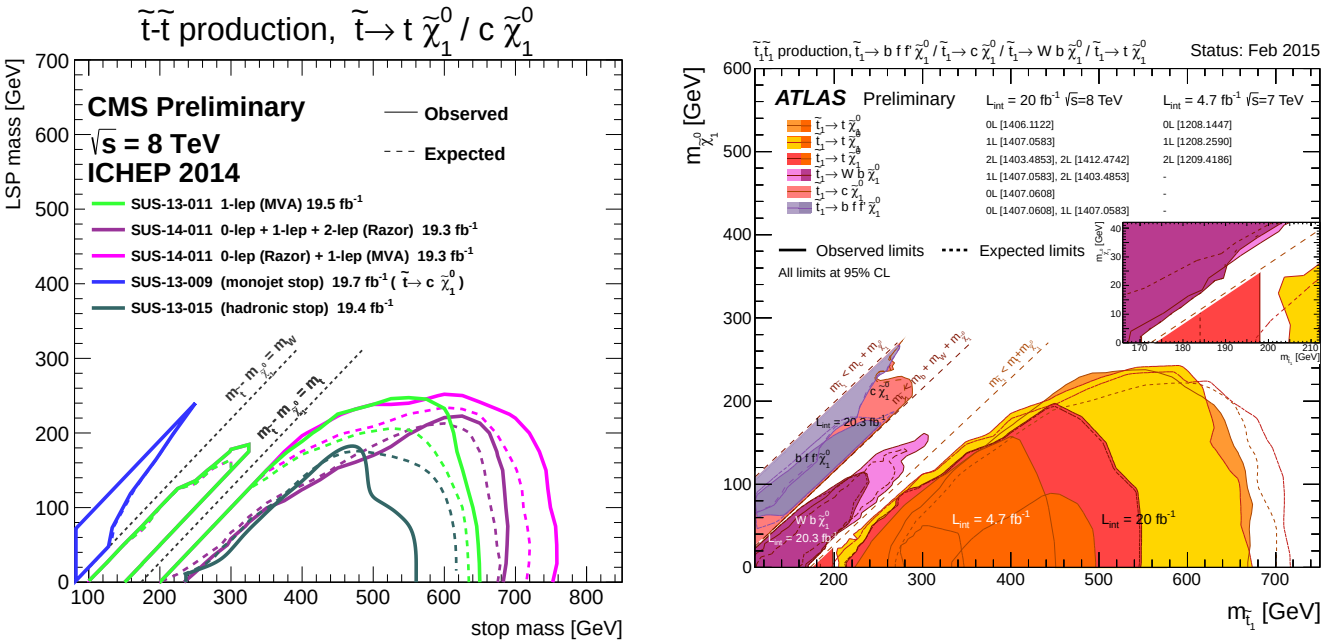


Figure 6: Stop Searches in CMS and ATLAS [15]. The stop mass from 200 GeVto 700 GeVare excluded. However, there are still some regions allowing the stop living around 200 GeV. Left: Stop searches in CMS. It includes $\tilde{t} \to t/c\tilde{\chi}_1^0$ with varied final states having zero or multiple leptons. Right: Stop searches in ATLAS. In addition to $\tilde{t} \to t/c\tilde{\chi}_1^0$, $\tilde{t} \to bff'\tilde{\chi}_1^0$ and $\tilde{t} \to Wb\tilde{\chi}_1^0$ are included.

TeV scale except Higgs?", "Are physicists in the right direction to detect SUSY?", "Does SUSY sit around the corner but somehow we miss it?". Large background has been a serious issue that might make SUSY hints invisible. In general, in order to shed light on the non-SUSY situation, there are several directions to deal with this huge background issue. First, in the SM side, people can work to calculate higher order QCD corrections and try to find whether the high-order QCD corrections are able to arise sufficient large deviations away from the data. At the same time, people may need to consider whether our understanding of QCD calculations is good enough. Second, creating and applying jet analysis, for example jet substructure [24], on QCD backgrounds, may be able to distinguish signal from the SM

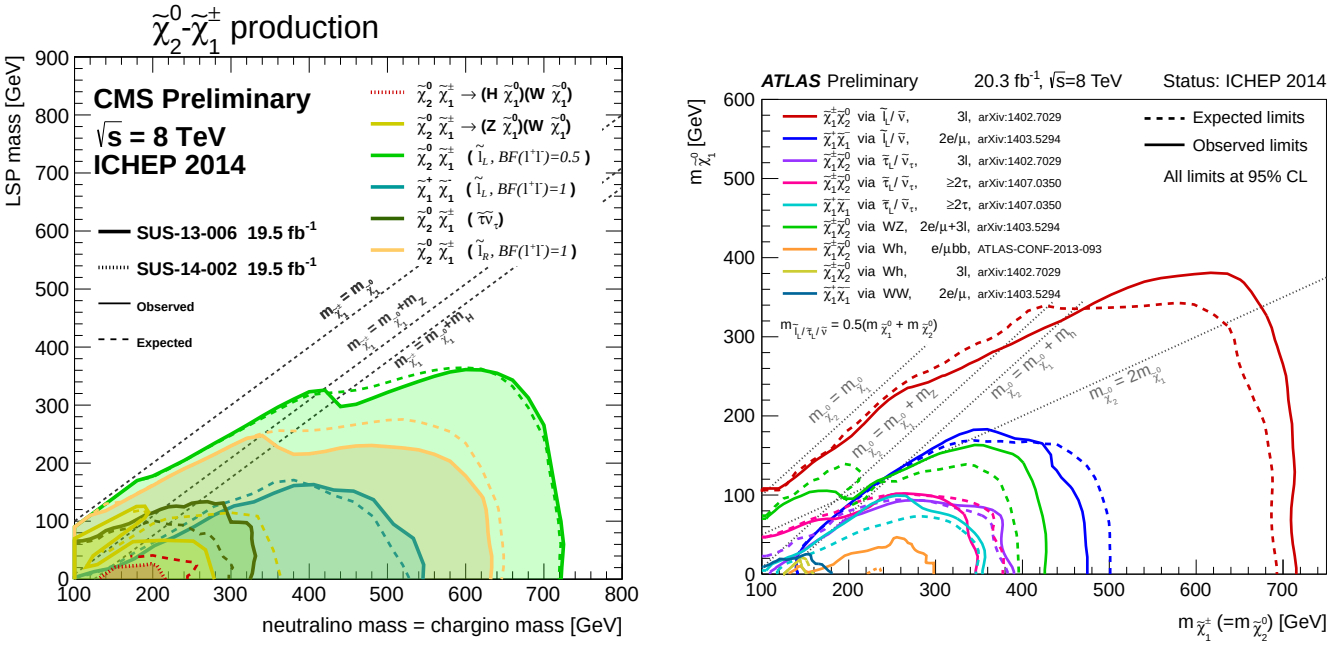


Figure 7: Electroweak gaugino Search in CMS and ATLAS [16] with 8TeV and $20 fb^{-1}$. Left: $\tilde{\chi}_2^0\tilde{\chi}_1^\pm$ pair production. LSP - neutralino/chargino mass plane in CMS. It includes $\tilde{\chi}_2^0 \to \tilde{\chi}_1^0 H/Z$ and $\tilde{\chi}_1^\pm \to W^\pm\tilde{\chi}_1^0$. Right: Beside $\tilde{\chi}_2^0\tilde{\chi}_1^\pm$, it also includes $\tilde{\chi}_1^\pm\tilde{\chi}_1^\mp$. LSP - neutralino/chargino mass plane in ATLAS.

background robustly. Third, given the present data, even if they are all negative results, those channels with a small deviation from the SM predictions may be a new physics hint [26]. So far, we see only one possible SUSY hint, which has a three sigma deviation from the SM. As good physicists, we should put much more attentions on investigating these small deviations.

The LHC has made amazing strides forward in understanding the SM at the TeV scale, and what could possibly lie beyond the SM. However, the LHC as with all hadron colliders, produces colored states with much larger cross sections than Electroweak (EW) states of the same mass. For more than a decade the results of the LEP experiments have generally set the most stringent constraints on new EW states beyond the SM despite the full run of

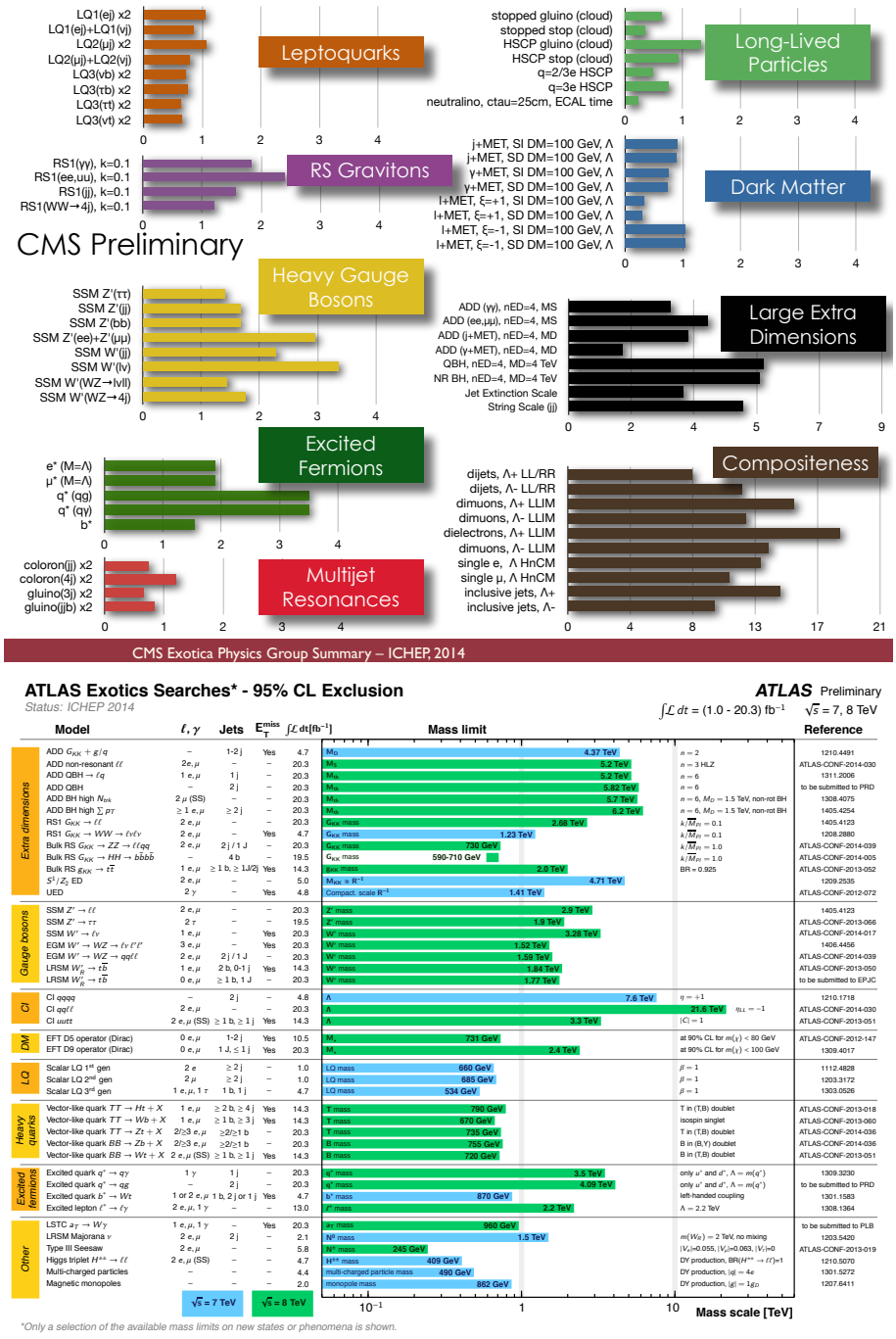


Figure 8: Exotics Searches in CMS and ATLAS [17]. Both of them included squark, electroweak gaugino, slepton and gluino search. Up: Exotics search in CMS. Down: Exotics search in ATLAS.

the Tevatron physics program. However, with the large energy and luminosity of the LHC, ATLAS and CMS have started to probe and set constraints beyond LEP for very generic EW final states [25].

Despite the impressive achievements of the LHC, we are still relatively insensitive to new EW physics with mass $\mathcal{O}(100)$ GeV. It is always possible that new particles are "just around the corner" at higher mass scales, but naturalness prompts us to look for lower-lying hiding places. A remarkable possibility is that new physics could still be very close to the electroweak scale. Searches are typically based on being able to maximally separate new physics from SM backgrounds. However, if new physics is very close to the EW scale it becomes difficult to disentangle and searches lose their sensitivity. Related to this is the even more interesting possibility that new physics already contaminates measurements of SM processes. At this energy range, backgrounds for new physics are dominated by SM gauge boson processes, and thus kinematical handles that searches rely on to separate signal from background are much less powerful. This typically results in a gap in searches/exclusions between LEP [27, 92] and the new ATLAS and CMS bounds [29, 30].

The idea of capturing all possible new physics hints is to investigate all channels presented both by ATLAS [29] and CMS [30] and to pay more attentions on those experimental measurements that are slightly deviated from the SM prediction, see Fig.11 and Fig.12. For example, electroweak gauge boson productions are $WW$, $WZ$ and $ZZ$. Electroweak theory has been understood very well. In most of electroweak channels, the SM predictions are consistent to the experimental measurements. Both $ZZ$ and $WZ$ can be explained by the SM predictions very well (within $1\sigma$ deviation). However, $WW$ deviated from the

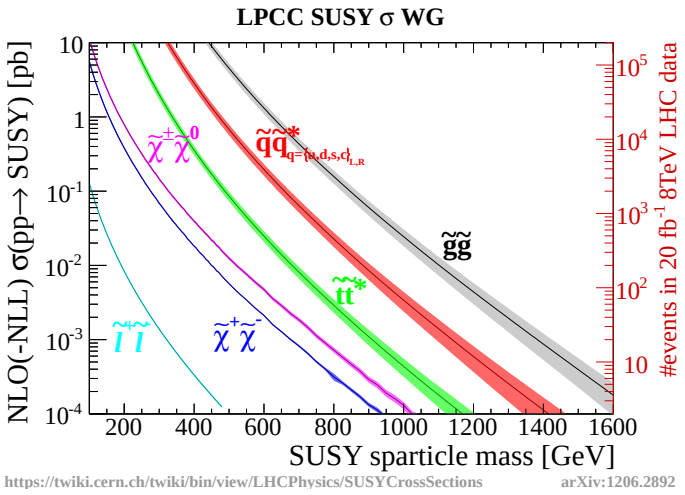


Figure 9: SUSY theoretical cross sections at 8 TeV [28] with $20 fb^{-1}$. Colored sparticles have much larger pair production cross section than other sparticles. For example, stop pair production cross section is larger than slepton cross section by greater than three order.

SM next-leading-order (NLO) calculation in all experimental measurements and at all energies. This $WW$ deviation becomes even larger in 8 TeV than one in 7 TeV. Recently, CMS updated WW cross section at 8 TeV result by considering next-to-next-leading-order (NNLO)calculations [39]. The deviation between the data and prediction becomes smaller than 1 sigma. But, for WZ and ZZ, they can be explained very well by the SM NLO predictions within one sigma. Furthermore, Ref. [97] also performed QCD higher order calculation up to NNLO which can reduce the WW deviation by around 10%. In these cases, the SM NNLO effects may bring up disagreements on WZ and ZZ channels. In the following about the WW discrepancy, they are all based on the comparison to the SM NLO calculations. In Fig.12, it shows the ratios of data to the theoretical predictions. Blue bar is the result of 7 TeV. Red bar is the result of 8 TeV. The combined sigma deviation from 7 TeV and 8 TeV in the $WW$ channel is about $3\sigma$. Because we did not see any new physics yet, this deviation is

definitely worth being explored in detail. In [52–54], we pointed out that not only could new physics be hiding in searches, but based on existing LHC measurements it could in certain cases *improve* the fit to the data, compared to the SM alone. In other channels involving colored particles, for example, $H_{ggF}$, $t\bar{t}W$ ...etc, those error bars are larger compared to electroweak productions, more data or background analysis technique are needed to reduce those error bars. It will become more clear whether the difference between their measurement and predictions are large or not. Here, we focus on electroweak processes. Searching for $W^+W^-$ events is looking for those events with final states having opposite sign diplepton and missing energy.

The dominant $W^+W^-$ cross section, see Fig.10, comes from quark-antiquark annihilation (both s- and t-channels, $q\bar{q} \to W^{\pm}W^{\mp}$). These quark-antiquark cross sections are $\sim 90\%$ of $W^+W^-$ total cross section. Beside, there are gluon fusion contributions via a quark loop (both $gg \to W^{\pm}W^{\mp}$ and $gg \to H \to W^{\pm}W^{\mp}$). This describes measurements of $W^+W^-$ total cross section as well as the fiducial cross section in pp collisions. The measurement of fiducial cross section is using $l^{\pm}\nu l^{\mp}\bar{\nu}$ with jet-veto in the final states. The main backgrounds are Drell-Yan, top quark, other diboson productions ($WZ$, $ZZ$ and $W\gamma^*$) and W production associated with a jet. These productions have dilepton and missing energy that are the same as $W^+W^-$ final states when jets are misidentified as a lepton or photons as a lepton. Those selection requirements are used to achieve a high $W^+W^-$ signal efficiency and reduce those backgrounds. For example, in order to prevent $WZ$ contamination from $WW$ signal (multiple leptons in the final state), those events are rejected if they have additional isolated leptons with $p_T > 7$ GeV. In addition, Drell-Yan events are suppressed by requiring an

invariant dilepton mass that does not lie within 15 GeV of the Z-boson mass. This means $|m_{ll} - m_Z| > 15$ GeV. Furthermore, Drell-Yan process can be suppressed by requiring large $E_T^{miss}$, large $p_T^{miss}$ and small $\Delta\phi$. $\Delta\phi$ is the azimuthal angular difference between $\vec{E}_T^{miss}$ and the closest selected jet or lepton in the event. Other top events with jets in the final state can be rejected by requiring zero number of jet (jet-veto requirement). Therefore, the total measured WW production cross section is given by:

$$\sigma(pp \to WW) = \frac{N_{data} - N_{bg}}{A_{WW} \times C_{WW} \times \mathcal{L} \times BR^2} \tag{1.22}$$

where $N_{data}$ and $N_{bg}$ are the numbers of observed data events and estimated background events respectively. $\mathcal{L}$ is the integrated luminosity. BR is the branching ratio of W leptonic decay, $BR(W \to l\nu) = 0.108$. $C_{WW}$ is the correction factor, defined as the ratio of the number of reconstructed WW events in the fiducial region with electrons and/or muons in the final state over the number of WW events generated in the fiducial region and including only prompt electrons and muons. $A_{WW}$ is the acceptance factor defined as the ratio of MC signal event yield passing the fiducial selection at generator particle level to the total number of generated signal MC events.

In order to come up with possible SUSY solutions [52–54, 61, 62] about this $W^+W^-$ anomaly, understanding cross section of pair production of SUSY particle and how they decay play an important role in this study. Fig. 9 demonstrates that colored sparticles have larger cross section than electroweak gaugino. The cross section for electroweak gaugino pair production is larger than for slepton. In general, the new physics contributions are

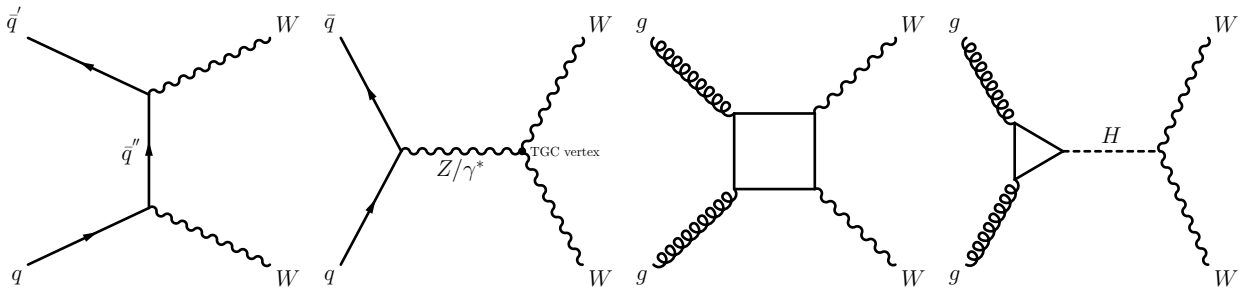


Figure 10: Standard Model $W^+W^-$ total cross section. Left: t-channel quark-antiquark annihilation. Middle left: s-channel quark-antiquark annihilation. Middle right: gluon fusion via a quark loop. Right: gluon fusion via a quark loop, which includes virtual Higgs production decaying into two W bosons.

proportional to $r \times \sigma \times \mathcal{L} \times BR$, where $r$ is the rate of new physics events passing experimental requirement. To find suitable SUSY contributions to explain WW anomaly, we can tune both $\sigma$ and $BR$. Thus, smaller cross section (slepton) having $BR \sim 1$ can have as similar contribution as large cross section(stop) having smaller $BR$.

In summary, it is possible that colored SUSY particles are hiding even though their production cross section is large. Hiding stops at low masses has been investigated by many groups in the past [51]. Particular attention has been paid to the idea that stops could be at the same mass as the top quarks, or that they could decay via R-parity violation into a jet-rich final state. In both of these scenarios the stop is very difficult to find. The absence of any anomalies means bounds are set by living within the error bars of current measurements.

The works of [52–54] were based on the $W^+W^-$ cross section as measured by both ATLAS [56] and CMS [57] at 7 TeV and with low luminosity at 8 TeV by CMS [58]. Both experiments observed a total cross section $\sim 15-20\%$ above the SM expectation, disagreeing with the SM at the $1-2\sigma$ level individually, with a combined significance of about $3\sigma$. Fur-

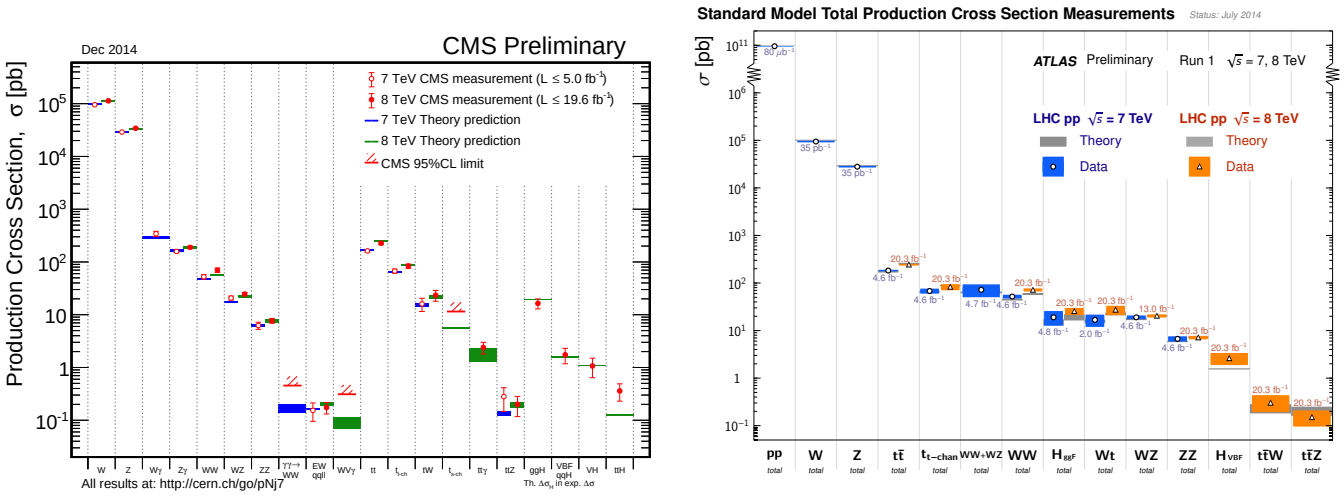


Figure 11: Standard Model total cross section both in 7 and 8 TeVpresented by CMS and ATLAS. Right: SM production cross sections in ATLAS. Left: SM production cross sections in CMS.

thermore, the excess seems to be concentrated near the center of the kinematic distributions at moderate $p_T$ and invariant masses, while the tails are very well modeled by the SM. These shape differences, apart from raising the significance of the excess, could be suggestive of an additional kinematically distinct contribution to the $\ell\ell + \text{MET}$ final state in which the $W^+W^-$ cross section is measured.

In addition to the anomalies in the SM measurements, the control region for $h \to W^+W^-$ with 0-jets is also higher than expected for run I [59]. In order to improve $W^+W^-$ SM differential distributions, there are two directions to construct SUSY solutions. One is that SUSY particles, chargino or stop, can produce a real W boson. The other is the SUSY particle, slepton, generates a pair of dilepton and missing energy in the final state directly instead of producing a real W. Although slepton has smaller cross section, it have larger $BR$ than the other two.

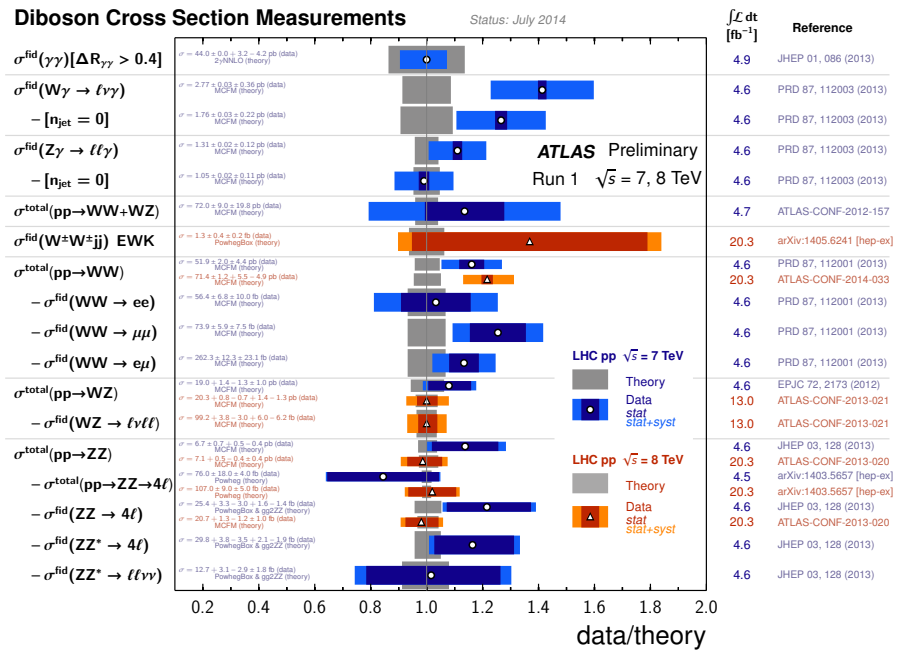


Figure 12: ATLAS diboson cross section measurements. It is the ratio of data to theoretical prediction. Blue bar is the result of 7 TeV. Red bar is the result of 8TeV. Both $WZ$ and $ZZ$ pair productions can be explained well by SM prediction within $1\sigma$ level. However, $WW$ pair production cross section is away from SM prediction by more than $1\sigma$ level. This deviation becomes robust at 8TeV.

The simplest new physics explanation of the $W^+W^-$ cross section increase is to introduce a new source of $W$ gauge bosons. The challenge lies in avoiding additional particle production, since the jet veto and strict OS (opposite sign) dilepton cut used in the $W^+W^-$ measurements basically requires the new physics to produce nothing but $l^+l^- + \text{MET}$ in the final state. This avenue was explored in [52], where chargino pair production followed by the subsequent decay to $W$ gauge bosons and MET was studied, for example, $\chi^{\pm} \to W^{\pm} + \chi^0$. Another direction based on stop production was explored in [54, 61], where it was demonstrated that the process $pp \to \tilde{t}\tilde{t}^* \to b\bar{b}\chi^+\chi^- \to b\bar{b}W^+W^-\chi^0\chi^0$ can contribute to the $W^+W^-$

cross section provided that the $b$ jets are soft enough.

Ref [52,54] proposed one possible explanation for this anomaly. It was shown that certain Electroweakinos could improve the $\chi^2$ of the $W^+W^-$ differential distributions significantly compared to the SM, while evading all other direct searches at the time. Subsequent to this, it was also shown that scenarios involving a single squeezed stop [54,61] or light sleptons [53] could also fit the data. This of course is not a smoking gun for new physics, but it was shown that new physics can significantly improve the $\chi^2$ for all differential measurements of these cross sections.

In our stop research [54], we show that there are several more scenarios involving stops than proposed in [61] that can also fit the $W^+W^-$ anomaly. In particular we show that there are scenarios where the third generation alone plays the role of generating the signal, rather than relying upon a particular squeezing between a stop and chargino as in [61]. Additionally, we also show that *both* stop eigenstates can be light and explain the $W^+W^-$ signal, thereby satisfying all naturalness constraints in the most important sector of SUSY models. Finally it is also possible, in principle, to combine these results with sleptons in [53], where the $g-2$ anomaly and the relic density of DM in the universe are also explained.

In considering these light stop scenarios we do not address the Higgs mass within SUSY, implicitly relying on one of the above-mentioned mechanisms for generating additional contributions needed to account for the observed value of $\approx 125\,\text{GeV}$. More explicitly speaking, the MSSM with two light stops $\approx 200\,\text{GeV}$ can not explain Higgs mass $\approx 125\,\text{GeV}$ unless there is a new sector beyond the MSSM which can save Higgs mass. This puts the discussion of naturalness within SUSY on equal footing with, for instance, many composite Higgs

models [63]. In principle the spectra and types of particles investigated here do not have to be realized within a supersymmetric framework, and an alternative model with top partners could also explain the $W^+W^-$ excess with low mass particles.

Even putting aside the Higgs mass, there are other measurements that can indirectly bound stops by their radiative contributions to Higgs couplings [68–70]. The introduction of light stop partners can significantly enhance the $h \to gg$ production process, constraining the mass scales we are interested in. However, these constraints rely on combined coupling fits, and the differences between ATLAS and CMS measurements significantly weaken constraints [69, 74].

Taking all this into account, along with other relevant bounds from direct searches, we demonstrate that stops can still be very light, allowing them to contribute their part of the naturalness puzzle while simultaneously fitting the LHC data better than the SM alone.

In the slepton scenario [53], we explored an alternate scenario for explaining the measured $W^+W^-$ cross section without producing actual $W$ gauge bosons. In a SUSY model where sleptons are light enough to be directly produced at the LHC, their subsequent decay $\tilde{l} \to l\chi^0$ can also contribute to the $l^+l^-$ + MET final state. Typically this spectrum will be harder than in scenarios with $W$ partners as previously described, since the MET will come from 2 missing particles rather than being spread amongst 4. However, as we will show there is a region of $m_{\tilde{l}} - m_{\chi^0}$ parameter space where similar to [52, 61] the $\chi^2$ of the SM $W^+W^-$ cross section can be significantly improved. There is an important quantitative and qualitative difference between slepton and chargino based models. In slepton models only the flavor diagonal contribution is realized in the $W^+W^-$ cross section measurement, whereas

charginos will contribute exactly as SM $W$'s with respect to flavor. At this point the (publicly available) data from the $W^+W^-$ cross section in the flavor separated measurements is not sufficient to favor either of these two possibilities over the other, but it will be an important phenomenological handle in the future.

Light sleptons can also cast light on several other important puzzles. In models with neutralino dark matter (DM) that is mostly Bino, light sleptons are required to achieve the correct relic density (unless the Bino is tuned to lie close to the Higgs resonance region or the sneutrino co-annihilation region). They are also favored as an explanation to the anomalous measurement of $(g-2)_\mu$ [92]. Finally, if the $h \to \gamma\gamma$ rate is higher than the SM rate as hinted at by the ATLAS measurement, then light $\tilde{\tau}$'s are a possible explanation.

We will show in the slepton-only scenario that, remarkably, the same region of slepton-bino parameter space preferred by the $W^+W^-$ cross section measurement also naturally accounts for the correct dark matter relic density and the g-2 anomaly. A slight increase in the $h \to \gamma\gamma$ rate can also be accommodated at the price of introducing violations of Lepton Flavor Universality (LFU) at a level well below experimental constraints on LFU violation, and dark matter direct detection cross sections are below current bounds set by XENON100 but would be discovered by the next generation of experiments.

Another important aspect of this thesis is how to search in regions around weak scale for new physics when the SM backgrounds become huge. In principle, even if these anomalies aren not due to new physics, the question remains, can new physics be right under our nose at the EW scale. We demonstrate that the WW channel can also be used to derive new exclusion limits which are more powerful than existing results using the same ATLAS

and CMS datasets. By examining the differential WW cross section we show that the gap between LHC and LEP exclusions can be start to be closed. We obtain these exclusions using two different methods. First, if the SM background is assumed to be correct, the sum of new physics contributions and the SM backgrounds can be used to define a powerful exclusion region. Second, if the overall rate of the SM background is assumed to be unsure, but the shape is robust, we renormalize the SM background and the additional new physics to be bounded by equal to the data to perform a more conservative exclusion. We call this method a shape-only exclusion. In the end it is informative to compare these two methods of exclusion. Beside using these exclusion methods on the WW cross section, they can also be applied on other SM channels. For example, the top pair production cross section can be used to obtain new stop exclusion limits [60].

The rest of this dissertation is organized as follows. Section 2 briefly introduce possible BSM candidates. For example, chargino, slepton and stop. One part is the scenario producing real W boson. The other is the scenario producing dilepton directly not through W decay. In Section 3 and Section 4, we present the detailed discussions about slepton and stop scenarios respectively. In Section 5, we summarize the possible solutions to the WW anomaly.

# 2 BSM Explanations for the $W^+W^-$ Excess

Both ATLAS and CMS measure the $W^+W^-$ cross section by counting the number of events in the $l^+l^- + \text{MET}$ final state, intending to capture mostly $W^+W^- \to l^+\nu l^-\bar{\nu}$ decays.

There are other SM contributions to this final state: the contribution of $t\bar{t}$ and other QCD final states is reduced with a jet veto, while $m_{ll}$ and $p_T$ cuts are used to reduce the Drell-Yan contribution and further isolate the $W^+W^-$ contribution. As has been demonstrated in [52–54,61], even with these cuts it is possible for BSM events to contaminate the $l^+l^- + \text{MET}$ final state. This leads to significant deviations in both the measured overall $W^+W^-$ cross section as well as the shape of the associated kinematic distributions. In this section we will explore the utility of the $W^+W^-$ measurement not as a Standard Model Standard Candle, but as a *search* for BSM physics. This has only become feasible at the LHC, both due to the high statistics of the measurement as well as the low theoretical errors on the modern $W^+W^-$ cross section prediction, which are now interpreted as a SM background.

The BSM scenarios in [52, 54, 61, 62] explained the observed $W^+W^-$ excess using real W production of new particles, while [53] discusses the possibility of generating a pseudo-W signal by new particles. In each case, the new particles decay to a $\ell\ell + \text{MET}$ observable final state and mimick the dileptonic $W^+W^-$ signal. Any such spectrum has to escape detection by a multitude of new physics searches for lepton-rich final states. Ultimately this led to a handful of viable scenarios to explain the $W^+W^-$ excess while remaining consistent with all other LHC data, which we review briefly below. We also outline the new light stop scenarios we study in this work.

## 2.1 Data Analysis Methods

We create a grid of SLHA spectrum files (for example, $m_X$-$m_Y$ parameter plane) with decay tables using `CPsuperH 2.3` [103] and `SUSY-HIT` [104] and simulate the pair productions of new physics particles. The showers of these new physics particles are generated using `Pythia 6.4/8.15` [105] and `FastJet 3.0.2` [106]. Additionally, the next-leading-order (NLO) normalizations are using `Prospino 2.1` [108]. These procedures generate various kinematic distributions shown in the $W^+W^-$ cross section measurements. We can obtain the chi-square

$$\chi^2(r_{SM}, r_{BSM}; m_Y, m_X) = \sum_{\text{all bins}} r_{SM} \times \text{SM} + r_{BSM} \times \text{New Physics} \tag{2.1}$$

by comparing to experimental data and the contributions from the SM and new physics in all kinematic distributions. Then, we can define a $\chi^2$ ratio

$$\frac{\chi^2(1,1; m_Y, m_X)}{\chi^2(1,0)} \tag{2.2}$$

to evaluate how much the stop contribution improved ($< 1$) or degraded ($> 1$) agreement with data compared to the SM at each mass point. The analysis of exclusion were obtained from the $W^+W^-$ measurements in two ways. To be conservative, one could decide not to trust the SM prediction for the total $W^+W^-$ cross section. In this case, we defined the

best-fit $\chi^2$ for each point by minimizing with respect to $r_{SM}$:

$$\chi^2_{\text{float}}(m_Y, m_X) \equiv \min_{r_{SM}} \chi^2(r_{SM}, 1; m_Y, m_X). \tag{2.3}$$

Stronger exclusions can be obtained by trusting the normalization of the SM contribtions. In that case we simply define

$$\chi^2_{\text{fixed}}(m_Y, m_X) \equiv \chi^2(1, 1; m_Y, m_X). \tag{2.4}$$

Contours where $\chi^2_{\text{float}}(m_Y, m_X)$ and $\chi^2_{\text{fixed}}(m_Y, m_X)$ gave a $p$-value of 0.05 are given as 95% CL exclusions. The bound obtained with floating SM contribution should be very robust even in light of possible future corrections to the SM $W^+W^-$ cross section calculation, unless they significantly change the expected shape of kinematic distributions. The exclusions regions obtained by using these methods are more powerful than the exist searches at ATLAS and CMS. Moreover, we use `micrOMEGAs 2.4.5` [90] to perform dark matter analysis and `CPsuperH 2.3` [103] to the anomalous $(g-2)_\mu$ measurement.

## 2.2 Pseudo-W scenario: slepton

Sleptons have low production cross sections and are difficult to study at the LHC. That makes them a natural test bed for our methods. The typical mass scale for slepton bounds prior to the LHC was set by LEP-II at approximately 100 GeV [27], with some variation depending on the particular flavor of the slepton. Most of the early LHC bounds on slep-

tons were based on producing them in cascade decays from new EW states. These bounds typically constrained heavier mass sleptons, but depended crucially on other parts of the BSM spectrum. Recently, however, CMS has set a bound on *direct* LH (left-handed) slepton production [30] which complements LEP in a different region of the neutralino-slepton mass plane (assuming degenerate LH selectrons and smuons). This is done by exploring the difference in kinematics between SM $W^+W^-$ and sleptons using the $M_{CT\perp}$ variable, which essentially encodes the mass scale separation of the mother particles that produce the charged leptons and the particles that make up the MET in the event. In the case of direct slepton production and decay to $l^{\pm}\tilde{\chi}_1^0$, if there is a larger mass splitting than the background which is dominated by SM $W$'s, then strong bounds can be set on the slepton mass. However, in the region where the slepton-neutralino mass scale separation becomes more similar to $m_W$, the bounds disappear because of the large SM backgrounds.

In summary, slepton bounds from LEP are relatively insensitive to $m_{\tilde{\chi}_1^0}$ but only go as high as 100 GeV, while slepton searches at the LHC probe higher masses but loose sensitivity for $m_{\tilde{l}} - m_{\tilde{\chi}_1^0} \lesssim m_W$. However, it is exactly in this "$WW$-like funnel" that the $W^+W^-$ cross section measurement would be most sensitive to contamination by slepton decay products. This motivates using the cross section measurement to set bounds in order cover the entire slepton-neutralino mass plane.

In [53] we showed that $\sim 130\,\text{GeV}$ sleptons decaying to dileptons and $\sim 75\,\text{GeV}$ Binos also have the correct cross section and kinematics to account for the $W^+W^-$ anomaly.[1] The

[1] $\tilde{\ell} \to W\tilde{\nu}$ is not suitable. $m_{\tilde{\ell}_L} - m_{\tilde{\nu}_L}$ is too small for LH slepton production to give correct kinematics for the $\ell\ell$ + MET final state, but large enough for it to be excluded by LEP searches if the RH slepton is on top of the spectrum to explain the $W^+W^-$ excess.

light slepton scenario is compelling, since the spectrum preferred by $W^+W^-$ also generates the correct dark matter relic density by providing a sufficiently large $t$-channel annihilation process for the Bino, and explains the anomalous $(g-2)_\mu$ measurement. The smoking gun of this possibility is a predicted flavor-diagonal excess in $W^+W^-$ . Ref. [53] also sets new constraints on slepton scenarios by using the $W^+W^-$ measurement as a new physics search. The observation that diboson measurements can provide new BSM constraints orthogonal to traditional high-MET SUSY searches (which cut away diboson background) is a general one, and should apply to other scenarios as well.[2]

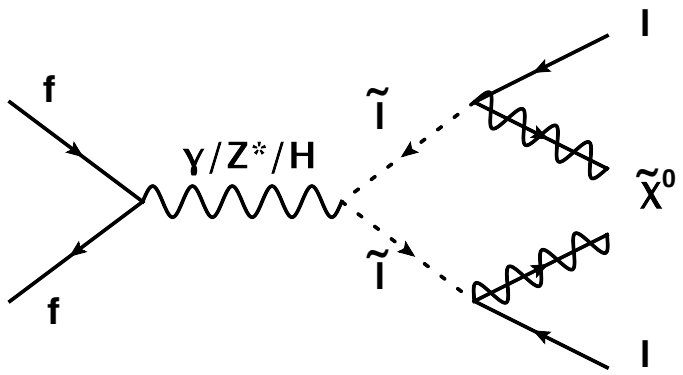


Figure 13: Slepton scenario for producing $W^+W^-$ signal. every slepton decay to lepton and neurtalino. Neutralino contribute to MET. Final states are OS dilepton and MET without jets.

[2]We checked whether the $W^+W^-$ measurements provide new constraints on chargino pair production scenarios, but the low cross section and *preference* of $W^+W^-$ data for light charginos means that in this case no new constraints can be derived. Ref. [80] directly searched for $\tilde{\chi}_1^\pm \to W + \tilde{\chi}_1^0$ and also specifically the Chargino model presented in [52], but does not have sensitivity to cross sections relevant for SUSY.

## 2.3 Real-W scenario: chargino

Ref. [52] pointed out that not only could new physics be hiding in searches, but based on existing LHC measurements it could in certain cases *improve* the fit to the data, compared to the SM alone. The work of [52] was based on the $W^+W^-$ cross section as measured by both ATLAS [56] and CMS [57] at 7 TeV and with low luminosity at 8 TeV by CMS [58]. Both experiments observed a total cross section $\sim 15-20\%$ above the SM expectation, disagreeing with the SM at the $1-2\sigma$ level individually, with a combined significance of about $3\sigma$. The authors in [52] considered gauge-mediated scenario. Charginos can be as light as $\sim 100$ GeV and the neutralino can be massless. These mass range are allowed by experiement [55]. The cross sections of $\tilde{\chi}^{\pm}\tilde{\chi}^{\mp}$ and $\tilde{\chi}^0\tilde{\chi}^0$ are $\mathcal{O}(1-10)$pb. In that letter, they performed $\chi^2$ fit of SM + EWino in $W^+W^-$ differential cross section. The combined $\chi^2$ fit of SM+EWino is better than SM-only. In addition to $W^+W^-$ signal, $\tilde{\chi}^{\pm}\tilde{\chi}^0$ can generate $Wh$, $WZ$ and $W\gamma$ signals. However, the trilepton searches, $Wh$ and $WZ$, have a strong constraint. Only some cases of $\tilde{\chi}^{\pm}$ and $\tilde{\chi}^0$ can pass this constraint.

In the gauge-mediated model with gravitino LSP($\tilde{G}$), $\tilde{\chi}_1^{\pm}$ can decay to $W^{\pm}+\tilde{G}$ and $\tilde{\chi}_1^0 \to \tilde{\chi}_1^{\pm}+W^{\mp}$ in Fig.14. The small mass difference between $\tilde{\chi}^{\pm}$ and $\tilde{\chi}^0$ emit off-shell W. It results in same-sign(SS) dilepton signal in final state. This SS dilepton in this model is in a great tension with experimental data. To get most preferred benchmark by $W^+W^-$ , it is chargino-NLSP scenario, $m_{\tilde{\chi}_1^{\pm}} \approx 110$GeV, $m_{\tilde{\chi}_1^0} \approx 113$GeV and $m_{\tilde{\chi}_2^0} \approx 130$GeV. Low $\tan\beta$ and a large higgsino components make $m_{\tilde{\chi}_{1,2}^0} > m_{\tilde{\chi}_1^{\pm}}$.

On the other hand, in gravity-mediated model with neutralino LSP ($\tilde{\chi}_1^0$), we would have

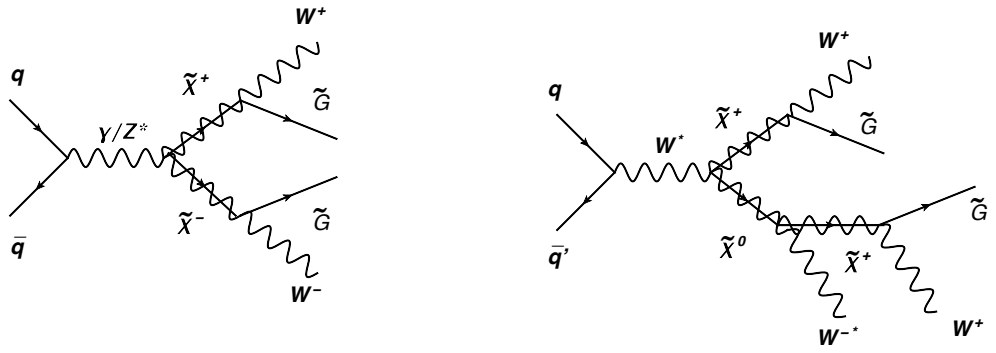


Figure 14: Electroweakino pair production with gravitino LSP. Left: $\tilde{\chi}^{\pm}\tilde{\chi}^{\mp}$ cross section. $\tilde{\chi}_1^{\pm} \to W^{\pm} + \tilde{G}$. It corresponds to OS (opposite sign) lepton+MET in the final state. Right: $\tilde{\chi}_1^{\pm}\tilde{\chi}_1^0$ cross section. This result include one off-shell W. It has same-sign dilepton signals in the final state [52].

$\tilde{\chi}_1^{\pm} \to W^{\pm} + \tilde{\chi}_1^0$. This contributes to $W^+W^-$ signals, OS (opposite sign) dilepton+MET, as in Fig.15. But, $\tilde{\chi}_1^{\pm}\tilde{\chi}_2^0$ pair production results in tri-lepton final states that can be bounded by $Wh$ and $WZ$ searches. In this case, $\tilde{\chi}_2^0 \to \tilde{\chi}_1^0 + Z/h$. The tri-lepton searches $WZ$ [75, 76] ruled out this neutralino wino-LSP possibility. While Higgsino-like LSP are not ruled out by [77, 78], their cross sections are too small to make a significant contribution to improve $\chi^2$ fit of $W^+W^-$ .

Although this chargino scenario has some issues with experimental measurement, it is still an interesting idea to know which parameter space in $\tilde{\chi}_1^{\pm} - \tilde{\chi}_1^0$ can improve the chi-square fit of $W^+W^-$ or have an exclusion power. In Fig 16, we present the chargino-neutralino plane. Both ATLAS 7 and CMS 8 prefer $\tilde{\chi}_1^{\pm} \sim 120$GeV and $\tilde{\chi}_1^0 \sim 20$GeV. However, $W^+W^-$ does not have any exclusion power here.

For example, in CMS 8 TeV of Fig.16, in neutralino-LSP scenario, $\tilde{\chi}_1^{\pm} \to W^*\tilde{\chi}_1^0$. The $W^+W^-$ preferred region is $\tilde{\chi}_1^0 \sim 20$GeV,$\tilde{\chi}_1^{\pm} \sim 110$GeV. In order to understand the behavior

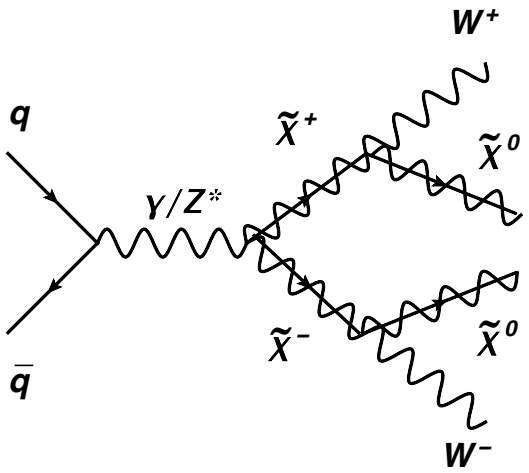


Figure 15: Electroweakino pair production with neutralino LSP. $\tilde{\chi}_1^{\pm} \to W^{\pm} + \tilde{\chi}_1^0$.

of this plot, keeping the same $\tilde{\chi}_1^0$ mass, as $\tilde{\chi}_1^{\pm}$ becomes lighter, $\sigma(\tilde{\chi}_1^{\pm}\tilde{\chi}_1^{\mp})$ becomes larger but the $p_T$ of lepton from $W^*$ is softer because the kinematic region becomes narrower. Thus, only few lepton pass lepton isolation condition. For fixed $\tilde{\chi}_1^0$, as $\tilde{\chi}_1^{\pm}$ becomes heavier, the cross section becomes lighter. The contributions to WW become smaller as $\tilde{\chi}_1^{\pm}$ becomes heavier. On the other hand, as $\tilde{\chi}_1^{\pm}$ become heavier, the chargino pair production cross section becomes smaller and its contribution to $W^+W^-$ is not sufficient. Therefore, the heavier $\tilde{\chi}^{\pm}$ is not preferred by $W^+W^-$ that much. If $\tilde{\chi}_1^0$ has larger mass, the allowed kinematic region becomes more narrow. Furthermore, the shape of preferred region(Blue contour line) follows the line of $m_{\tilde{\chi}_1^{\pm}} - m_{\tilde{\chi}_1^0} \sim m_W$. However, $W^+W^-$ does not have any interesting exclusion power in the plane of $\tilde{\chi}_1^{\pm}$ and $\tilde{\chi}_1^0$ and all p-values in chargino-neutralino plane are greater than 0.05.

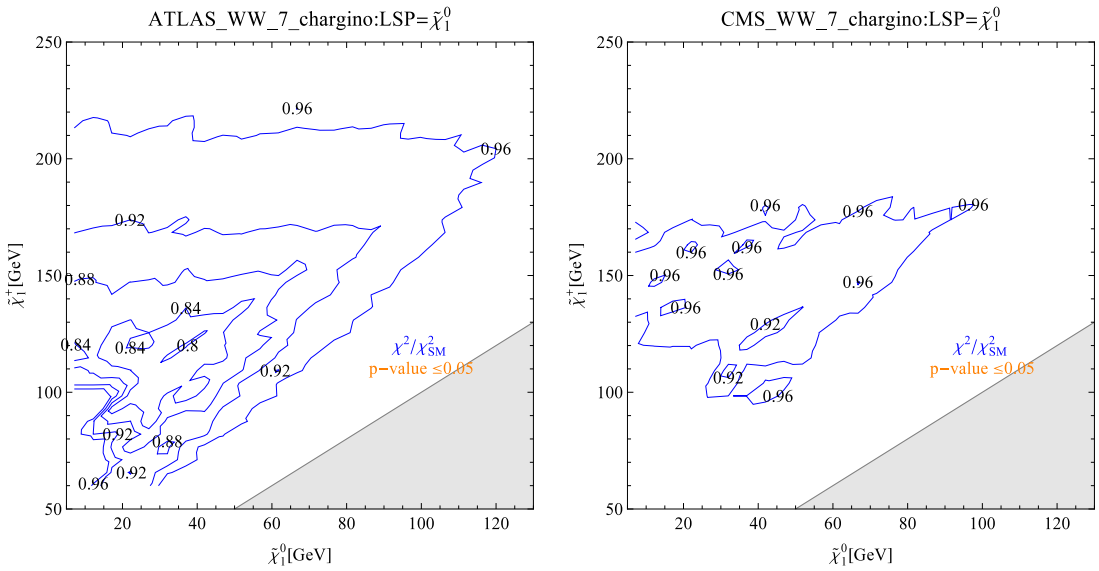


ATLAS 7TeV CMS 7TeV

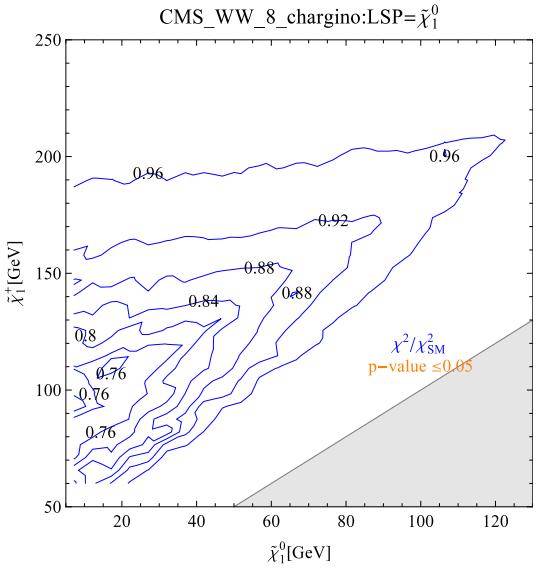


CMS 8TeV

Figure 16: In the chargino-neutralino plane, we calculate the chi-square ratio of the SM and chargino to the SM. The smaller chi-square ratio implies the WW preferred region. At the result of ATLAS 7 TeV and CMS 8 TeV, the WW preferred region is $\tilde{\chi}_1^{\pm} \sim 120$ GeV and $\tilde{\chi}_1^0 \sim 20$ GeV. However, $W^+W^-$ does not have any interesting exclusion power because all p-values in the chargino-neutralino plane are greater than 0.05.

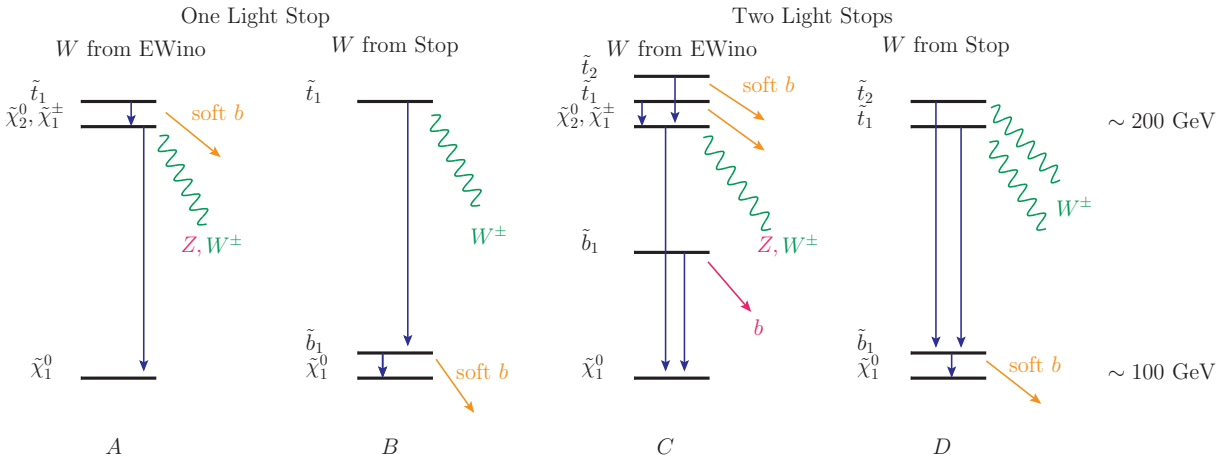


Figure 17: The four types of stop spectra which could account for the $W^+W^-$ excess via stop pair production, labelled Scenarios A - D. The top and bottom of the spectrum are at $\sim 200\,\text{GeV}$ and $\sim 100\,\text{GeV}$, with $W$'s (green) being produced when decaying across the big gap in the spectrum. Small gaps are $\lesssim 10\,\text{GeV}$. The 2-body decays of each state are shown as blue vertical arrows, with SM decay products on the right of each spectrum. The red color for $Z$ and $b$ indicates that these are not produced from stop pair production but from a different processes (direct $\tilde{\chi}_2^0\tilde{\chi}_1^\pm$ and $\tilde{b}_1\tilde{b}_1^*$ production). The soft $b$'s (orange) should be practically undetectable.

## 2.4 Real-W scenario: stop

The above two possibilities involve relatively simple spectra, but the scale of new physics has to be lower than about 150 GeV, otherwise the electroweak production cross sections are too low to account for the $W^+W^-$ excess. This restriction can be avoided if the BSM states decaying to $W$'s (or dileptons + MET) are colored. As mentioned in Section 1, [61] proposed a squeezed stop scenario where a relatively light stop decays to a chargino (and a soft, presumed undetectable $b$) with a mass gap of $m_{\tilde{t}_1} - m_{\tilde{\chi}_1^\pm} \lesssim 10\,\text{GeV}$. In Fig. 17 this is called Scenario A. It effectively gives the chargino a strong production cross section, allowing it to be as heavy as $\sim 250\,\text{GeV}$ while still providing enough events in the $W^+W^-$ signal region to potentially explain the excess. The authors of [61] performed no differential

analysis within the signal region, but to replicate the kinematic shape fit of our original chargino scenario [52], the mass difference between the chargino and neutralino LSP would have to be about $m_W$.

Ref. [52] explored electroweak production of charginos decaying into $W+\text{LSP}$. At a mass of $\sim 110\,\text{GeV}$, a wino-like chargino has the required direct production cross section of a few pb to explain the $W^+W^-$ excess. However, this possibility is ruled out in simple gravity-mediated scenarios, since $\tilde{\chi}_2^0\tilde{\chi}_1^\pm$ associated production yields a large $WZ$ signal which is thoroughly excluded at that mass scale [75,76]. While Higgsino-like scenarios above the LEP limit are not yet excluded [77, 78], their chargino pair production cross section is too small to explain the $W^+W^-$ excess. This led Ref. [52] to consider a gauge-mediated scenario [79] with a $\approx 110\,\text{GeV}$ chargino NLSP decaying to a massless gravitino. Neutralinos $\tilde{\chi}_{1,2}^0$ at $\approx 113$ and $130\,\text{GeV}$ decay to charginos via off-shell $W^\pm$ emission, which is mostly too soft to be detected. This further enhances the chargino signal. Adding the chargino contribution to the $W^+W^-$ signal expectation in [56–58] greatly improves fit to data, both in terms of overall cross section and shape agreement in all differential distributions. Strikingly, the signal bins in which the SM correctly accounts for the data are not modifed, while the chargino contribution is concentrated in exactly those bins where the SM expectation is below the data. A side-effect of this spectrum is a sizable same-sign dilepton signature, which serves as a smoking gun of the chargino NLSP scenario.

In this work we suggest a qualitatively different mechanism for accounting for the $W^+W^-$ excess via QCD production as well as two other extended scenarios. Rather than using stops to produce electroweakinos, $W$'s can be produced directly from electroweak stop decay to a

light sbottom, which then has to be close in mass to a neutralino LSP to be undetectable. This is Scenario B in Fig. 17. In Section 4 we perform a fully differential fit of both single stop scenarios to the $W^+W^-$ data, identifying the regions in the stop-neutralino mass-plane that are preferred (or excluded) by the $W^+W^-$ measurement while escaping stop and sbottom direct search constraints. The best-fit point for both single stop scenarios is near $(m_{\tilde{t}_1}, m_{\tilde{\chi}_1^0}) \sim (220, 130)\,\text{GeV}$.

While Scenarios A and B in Fig. 17 are intriguing in providing ways to describe the $W^+W^-$ excess using colored particles, ultimately light stops are theoretically motivated for reasons of naturalness. The single light stop scenarios are certainly interesting in this regard, but in both cases the rest of the third generation squarks have to generically be heavy (near a TeV) to avoid direct stop and sbottom searches [34, 81]. Therefore, in those cases naturalness in the stop sector is only partially accommodated. This motivates us to explore the possibility of not just one stop, but both stops and at least one sbottom below $\sim 250\,\text{GeV}$, shown in Fig. 17 as Scenarios C and D. In both cases the stops are close in mass and decay either to charginos or to $W$ directly, generalizing the above single-stop scenarios. As we will see below, both of these scenarios are viable, meaning the $W^+W^-$ excess could already be pointing towards a completely natural light SUSY spectrum.

Going beyond $W^+W^-$ and naturalness, the new stop scenarios we propose could also replicate some of the phenomenological success of the slepton scenarios in [53]. Firstly, the presence of light sbottoms could generate a thermal Bino DM particle. Secondly, in the absence of a chargino (Scenarios B and D), sleptons could sit between the LSP and the stop(s). This slepton could then account for the $(g-2)_\mu$ anomaly without being excluded

by direct searches. A plethora of new particles may await discovery below 250 GeV.

# 3 Slepton scenario

Fig. 18 shows our results. We derived slepton mass bounds for selectrons and smuons at the same mass decaying into a neutralino, for each of the performed LHC $W^+W^-$ measurements and all of them combined. To do this we create a grid of SLHA spectrum files with decay tables using `CPsuperH 2.3` [103] and simulate direct slepton production[1] using `Pythia 6.4/8.15` [105] (hard process/shower), normalized to the NLO cross section calculated using `Prospino 2.1` [108]. Since the source of the observed $W^+W^-$ excess is unclear, we obtained slepton limits in two ways. The solid lines indicate bounds obtained by analyzing only the *shape* of the various kinematic distributions in the $W^+W^-$ measurements, normalizing the SM theoretical expectation so that the SM + BSM overall expected event count matched the measurement. This bound should be very robust, even in light of possible future corrections to the SM $W^+W^-$ cross section calculation (unless they significantly change the expected shape of kinematic distributions). On the other had, the dashed lines show bounds obtained by comparing kinematic distributions of expected SM + BSM to the data, without renormalizing the SM prediction. These bounds can be significantly more powerful, but might be less robust. Comparing the two bounds can be instructive.

We show those bounds along-side LEP and CMS bounds[2], and the complementarity of

[1] Our `FastJet 3.0.2` [106] based analysis code took into account lepton isolation requirements and geometrical acceptances but did not simulate detector effects. Given the nature of our final state this will not invalidate our results.

[2] The explicit cross section bounds in [30] are not of high enough resolution in the slepton-neutralino mass plane to compute a useful mass exclusion curve for the LH + RH slepton case. (It is enough to show,

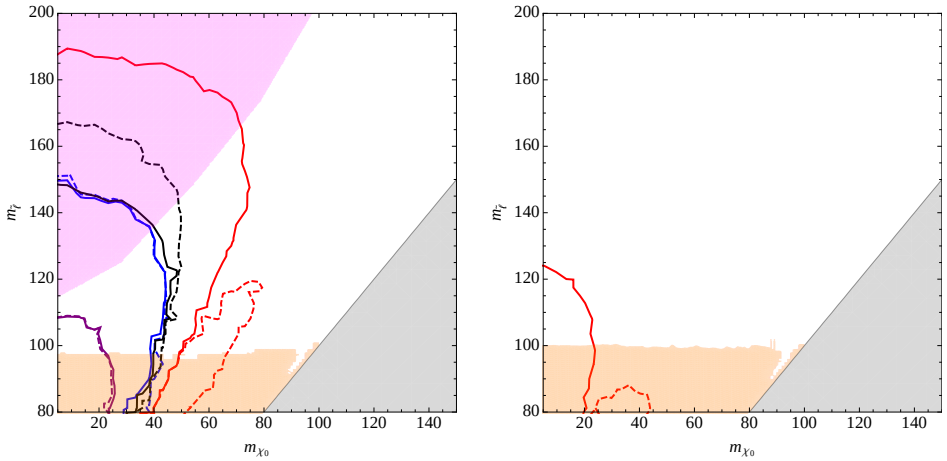


LH $\tilde{e}/\tilde{\mu} \to \ell + \tilde{\chi}_1^0$




RH $\tilde{e}/\tilde{\mu} \to \ell + \tilde{\chi}_1^0$

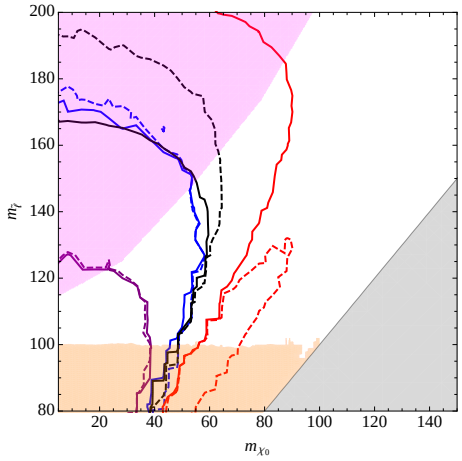


LH + RH $\tilde{e}/\tilde{\mu} \to \ell + \tilde{\chi}_1^0$

Figure 18: 95% Exclusions in the neutralino-slepton mass plane for degenerate $\tilde{e}, \tilde{\mu}$ decaying to $e/\mu + \tilde{\chi}_1^0$. Magenta regions are excluded by the CMS 9fb$^{-1}$ LHC8 slepton search [30] (see text footnote). Orange regions are excluded by LEP [27]. The regions below the Purple (ATLAS LHC7 [36], Blue (CMS LHC7 [37]), Red (CMS LHC8 [38]) and Black (combined) lines are new exclusions we obtained from the respective $W^+W^-$ measurements. Solid (dashed) lines represent limits obtained by (not) renormalizing the SM expectation in all kinematic distributions to match the SM + BSM normalization to data. The CMS8 $W^+W^-$ measurement was so high that only the region *inside* the red dashed line is not 'excluded' when normalization is taken into account.

our $WW$-derived bounds is clear – they help fill in the $WW$-like funnel, inaccessible to both LEP and CMS dedicated slepton searches. We can see that the gap between the LEP measurement and the LHC can now start to be closed. Our bounds also represent the first LHC bounds on direct RH-only slepton production for degenerate selectrons and smuons, but the LHC still cannot set any bounds for just a single RH slepton generation.

For the 7 TeV ATLAS and CMS measurements, the bounds obtained by our two analysis methods are almost identical. This is due to the relatively small size of the $WW$-excess in those measurements, compared to the slepton cross section dependence on slepton mass. The situation is very different for the 8 TeV CMS measurement: while the shape-only bound looks as one might expect, the bound obtained without renormalizing the SM expectation seems to 'exclude' the entire slepton mass plane with the exception of a small island centered around $m_{\tilde{\ell}} \sim 100\,\text{GeV}, m_{\tilde{\chi}_1^0} \sim 60\,\text{GeV}$. This is not due to any extraordinary exclusion power of the CMS8 measurement, but rather because the measurement of the $W^+W^-$ cross section is so high that, under the assumptions of the un-renormalized analysis, the Standard Model itself is excluded at better than 95% CL. Only within the small island is the slepton contribution so large as to push the $p$-value of the kinematic fit above 0.05.

This result underscores the utility of setting bounds conservatively, using the shape of kinematic distributions only, but also serves as motivation for going one step further: using the $W^+W^-$ measurement not just for exclusion, but for *discovery* of a possible BSM signal.

however, that CMS sets no bounds on RH sleptons only.) Therefore we use the CMS supplied LH slepton mass bound in the LH + RH plot as well, which makes it slightly conservative: the magenta region should be roughly $\mathcal{O}(5\,\text{GeV})$ 'larger' in every direction than shown.

## 3.1 Hint of New Physics

We will now consider a simplified model with light sleptons and bino dark matter, realized within the MSSM, that can improve agreement with the $W^+W^-$ measurement while also accounting for a range of other anomalies.

The basic parameter space of our scenario is the $(M_{\text{bino}}, M_{\text{slepton}})$-plane, where $M_{bino} \equiv M_{\tilde{\chi}_1^0}$ and $M_{slepton} \equiv M_{\tilde{e}_R} \approx M_{\tilde{e}_L} \approx M_{\tilde{\mu}_R} \approx M_{\tilde{\mu}_L}$ (all within about a GeV of each other) for universal slepton soft masses, which we will mean to also imply $m_{\tilde{\ell}_L} = m_{\tilde{\ell}_R}$ unless otherwise stated. Assuming the squarks and gluinos to be above $\sim 500\,\text{GeV}$ or so along with the heavy higgs scalars (decoupling limit), the remaining relevant parameters are $\mu, \tan\beta, M_2$ and $A_\tau$.

We first show in Section 3.2 that all the $W^+W^-$ measurements prefer a particular region of the $(M_{\text{bino}}, M_{\text{slepton}})$-plane. This is completely independent of $\mu, \tan\beta, M_2$ and $A_\tau$, and depends only on the kinematics of selectron and smuon decay. However, since very light sleptons are preferred, slepton soft mass universality and LEP bounds on the stau mass prefer $A_\tau \sim 0$.

Bino-like dark-matter can have sufficient annihilation cross section through $t$-channel slepton exchange to obtain the correct relic density, while higgs-mediated direct detection is automatically below current bounds but within reach of the next generation of experiments. In Section 3.3 we show that, for wide ranges of the other parameters, the $W^+W^-$ -preferred region and the region of correct relic density intersect in the $(M_{\text{bino}}, M_{\text{slepton}})$-plane. The most important parameters here are $\mu$ and $\tan\beta$, since $A_\tau$ is preferred to be small (see above) and $M_2$ has little effect on the properties of a bino-like LSP. We also explore the

departures from slepton soft mass universality to achieve light highly mixed staus and raise $\mathrm{Br}(h \to \gamma\gamma)$, but we find that a tension between the diphoton rate and the dark matter relic density limits the size of the enhancement to about $\sim 15\%$.

In Section 3.4 we demonstrate how smuon-bino loops can account for the 3 $\sigma$ deviation between observation and SM expectation of the muon anomalous $(g-2)$. This contribution depends, apart from $(M_{\mathrm{bino}}, M_{\mathrm{slepton}})$, mostly on $\mu$ and $\tan\beta$, and we find that our scenario naturally generates a correct size contribution.

We explore the consequences of the slepton soft mass non-universality that is required to moderately enhance $\mathrm{Br}(h \to \gamma\gamma)$ while achieving the correct dark matter relic density in Section 3.5. The resulting lepton-flavor violating operators are tightly constrained, and we show that our scenario would still be well within bounds.

The main success of our scenario is that light sleptons and bino dark matter explain the $W^+W^-$ excess as well as the measured deviation in the muon anomalous $(g-2)$ while producing the correct dark matte relic density. This is shown in Section 3.2.

## 3.2 Sleptons in $W^+W^-$

Sleptons have a much lower pair production cross section than Charginos [52] or Stops [54, 61]. As a result, even with their higher acceptance in the ATLAS and CMS searches and their 100% dileptonic branching fraction, they have to be very light in order to meaningfully contribute to the $W^+W^-$ cross section. To make this statement more quantitative it is instructive to revisit the slepton bounds we derived in Section 2.

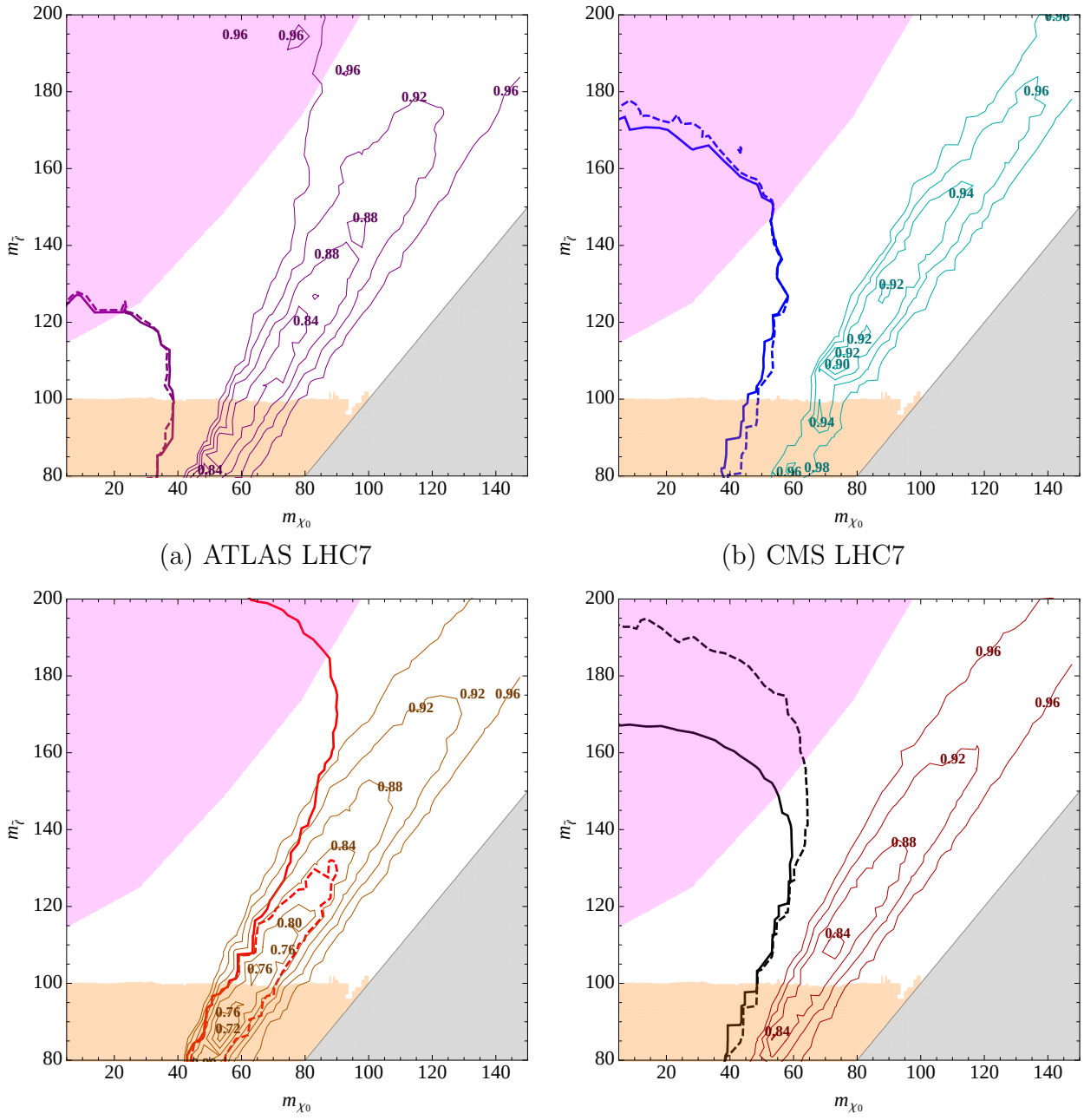


(a) ATLAS LHC7

(b) CMS LHC7

(c) CMS LHC8

(d) Combined

Figure 19: 95% Exclusions in the neutralino-slepton mass plane for degenerate $\tilde{e}_L, \tilde{e}_R, \tilde{\mu}_L, \tilde{\mu}_R$ decaying to $e/\mu + \tilde{\chi}_1^0$. Same color coding as Fig. 18, but now we also show contours of $r_{\chi^2} = \chi^2_{\text{SM+sleptons}}/\chi^2_{SM}$ where $r_{\chi^2} < 1$, i.e. the slepton contribution improves the fit to data. The overall most preferred point is $m_{\tilde{\ell}} \approx 120\,\text{GeV}$, $m_{\tilde{\chi}_1^0} \approx 80\,\text{GeV}$.

Fig. 19 shows the bounds for the RH+LH slepton scenario for each experiment. In addition to the mass bounds, we also show regions where sleptons *improve* the fit to data, as indicated by contours of $r_{\chi^2} = \chi^2_{\text{SM+sleptons}}/\chi^2_{SM}$ where $r_{\chi^2} < 1$. In those regions the $W^+W^-$ measurement obviously cannot set a bound. Note that *all* the measurements separately or combined prefer the same region in the bino-slepton mass plane, defined roughly by $m_{\tilde{\ell}} - m_{\tilde{\chi}_1^0} \approx m_W/2$ and $m_{\tilde{\ell}} \lesssim 150\,\text{GeV}$, with the most improvement achieved for $m_{\tilde{\ell}} \lesssim 120\,\text{GeV}$. This is squarely in the $WW$-like funnel and invisible to dedicated slepton searches.

Some kinematic distributions from the ATLAS7, CMS7 and CMS8 $W^+W^-$ measurements are shown in Fig. 20. The slepton contribution for one of the most preferred points, $m_{\tilde{\ell}} \approx 110\,\text{GeV}$ and $m_{\tilde{\chi}_1^0} \approx 70\,\text{GeV}$, is added. Note how the BSM contribution affects the bulk of the distributions where the experimental excess lies, and not the hard tail where the SM is in good agreement with data (and anomalous triple gauge couplings would contribute). This is contrary to one possible naive expectation, namely that the two-body decay of sleptons to a lepton + MET would produce a much harder spectrum than $WW$ or charginos. The improvement is particularly stark for the CMS8 measurement: the $p$-value of the SM expected kinematic distributions fitting the observed data is $\sim 10^{-3}$, improved to 0.13, 0.15 or 0.57 by adding sleptons, a 125 GeV SM higgs, or both respectively.

It is important to point out that these conclusions do not depend on all the variables of our scenario. In fact, they *only* depend on the slepton and neutralino masses (and the assumption that $m_{\tilde{e}_L} \approx m_{\tilde{e}_R} \approx m_{\tilde{\mu}_L} \approx m_{\tilde{\mu}_R}$, and that all $\tilde{e}/\tilde{\mu}$ decay to $e/\mu + \tilde{\chi}_1^0$). This is because slepton production at the LHC is through an $s$-channel $\gamma^*/Z^*$ with fixed gauge couplings (unlike at LEP where $t$-channel neutralino contributions are important for selectrons). Staus are also

unimportant — they give almost no contribution to the $W^+W^-$ measurement since two taus have a low dileptonic branching fraction of $\sim 10\%$, and the leptons resulting from that three-body decay are so soft (in our regime of interest) that they do not pass the lepton $p_T$ triggers and cuts of the $W^+W^-$ analysis. The tau three-body decay follows $\tau \to f\bar{\nu}_f\nu_\tau$ with $f = e, \mu$. However, under the assumption of slepton soft mass universality, the light first and second generation sleptons preferred by the $W^+W^-$ measurement prohibit large stau mixing to avoid LEP bounds on $m_{\tilde{\tau}_1}$ [27]. This implies moderately-sized $|A_\tau - \mu \tan\beta| \lesssim 3\,\text{TeV}$, pointing to $\tan\beta \sim 5, \mu \sim 500\,\text{GeV}$ for $A_\tau \sim 0$.

## 3.3 Dark Matter

Dark Matter has long been one of the motivations for physics at the TeV scale, and in particular for Supersymmetry. While the LHC has ruled out a great deal of SUSY DM parameter space, this is always obliquely through an assumption about charged states, since after all there was a longstanding possibility of heavy Higgsino DM alone which gave both the right relic density and improved unification [71] [1]. The real tension for generic WIMP dark matter is the consistently strong limits placed by direct detection on EW-scale candidates, up to the occasional claims for discovery or odd events. In particular, if a WIMP carries $SU(2)$ quantum numbers and can interact with nucleons through a $Z$ boson directly it is generally in significant tension with direct detection experiments. This statement is model-independent and does not depend on supersymmetry.

In the context of the MSSM, one candidate for DM with a small interaction cross section

[1] This has most recently been ruled out by the HESS measurements [72].

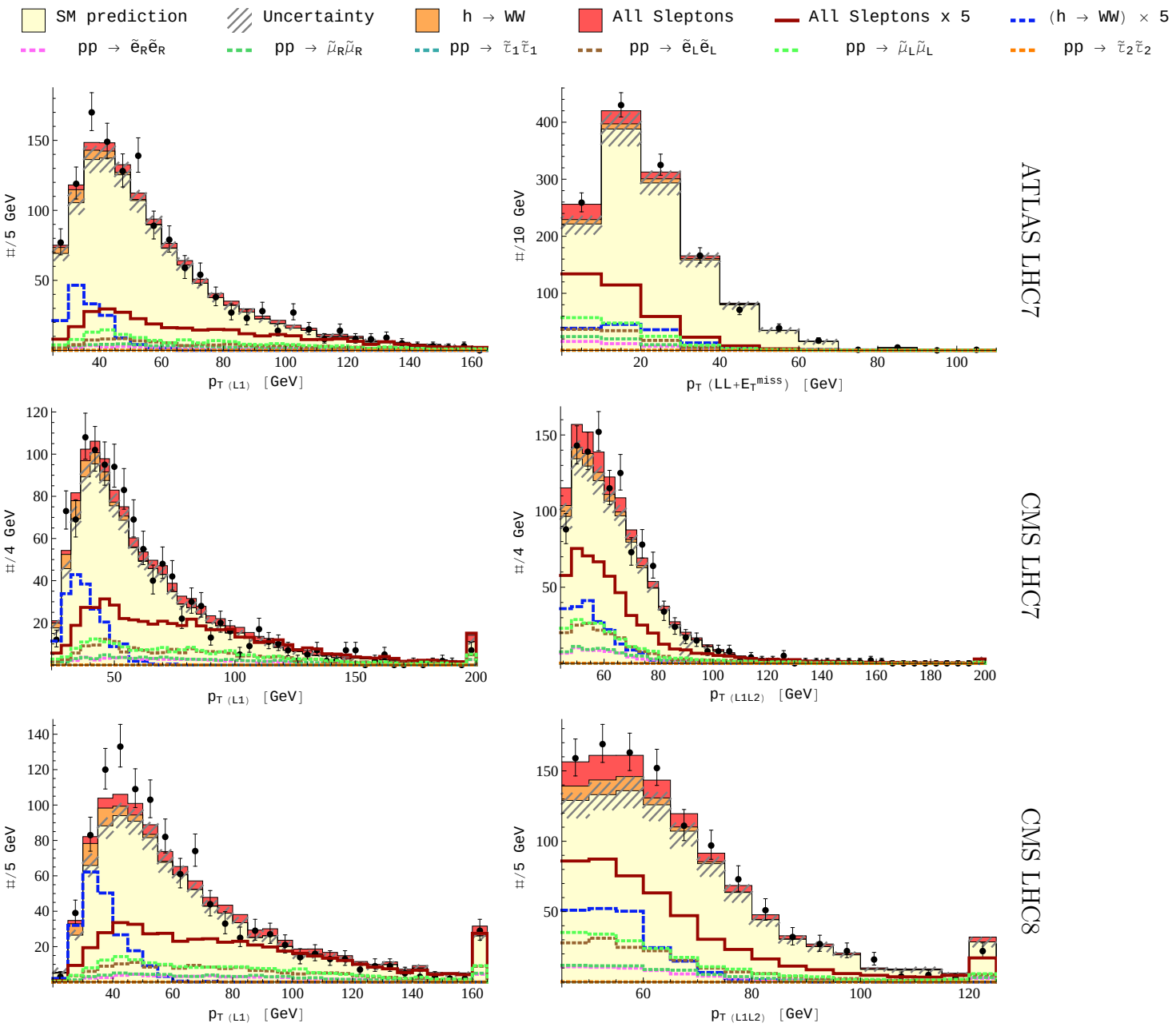


Figure 20: Some kinematic Distributions from the $W^+W^-$ measurements done by ATLAS [36] and CMS [37, 38] with slepton contributions for $M_{\text{slepton}} \approx 110\,\text{GeV}$, $M_{\text{bino}} \approx 70\,\text{GeV}$ overlaid. The uncertainty refers to the SM prediction. We have also included the effect of a 125 GeV SM higgs, which is a small but non-negligible contribution.

for direct detection experiments is a neutralino that is mostly Bino-like. This is a double-edged sword however, since suppressing the direct-detection cross section can also render the annihilation or co-annihilation cross section very small. This in turn leads to a relic density that is much too high compared to the very precisely measured value given by the Planck satellite [89]:

$$\Omega_{\rm CDM}h^2 = 0.1196 \pm 0.0031. \tag{3.1}$$

To generate the correct relic density for a bino-like neutralino, it has been long known that other super partner states are needed to increase the annihilation cross section and achieve the correct relic density (see e.g. [1] for a review). However, it has been pointed out that the window for this is relatively small when resonant annihilation or coannhilation are not relied upon [88]. In particular, by analyzing the t-channel annihilation contribution (see Fig.21) from a single RH slepton (which has the largest coupling to the Bino) the relic density away from those special regions is well described by [88]:

$$\Omega_{\tilde{B}}h^2 \approx 1.3 \times 10^{-2} \left(\frac{m_{\tilde{e}_R}}{100\,\text{GeV}}\right)^2 \frac{(1+r)^4}{r(1+r^2)} \left(1 + 0.07 \log \frac{\sqrt{r}100\,\text{GeV}}{m_{\tilde{e}_R}}\right), \tag{3.2}$$

where $r = M_1^2/m_{\tilde{e}_R}^2$. Without relying upon coannihilation $r \sim 1$ or a particular resonance such as $Z$ or $h$, what naively appears to be a very constrained acceptable region given in (3.2) is precisely the region favored by the $W^+W^-$ cross section measurements which improves the fit to the data.

We start by considering the case of $A_\tau = 0$ and $M_2 = 600$ GeV. Fig. 22 and Fig. 23 show

the DM abundance in the ($M_{bino}$, $M_{slepton}$)-plane for $\mu = 400$ GeVor 600 GeVand $\tan\beta = 4$ or 6. To understand the dark matter constraints on our scenario we make the following remarks:

- Increasing $\tan\beta$ from 4 to 12 decreases the relic density by a factor of $\sim 2$ away from the s-channel annihilation regions, and while the neutralino is still the NLSP. This is mostly due to the increased $\tilde{\tau}$-mixing decreasing the mass of $\tilde{\tau}_1$, which increases the annihilation cross section. Increasing $\tan\beta$ also decreases the prominence of the higgs resonance region while it increases the prominence of the $Z$ resonance region. Ignoring the small and unchanging wino component, this behavior can be understood from the structure of the neutralino couplings. The coupling to the $Z$ is doubly suppressed by the higgsino-component of the bino-like neutralino, which couple with opposite sign since their $T_3$ charge is $\pm\frac{1}{2}$. The $\tilde{H}_u^0$, $\tilde{H}_d^0$ components of $\tilde{\chi}_1^0$ are proportional to $\sin\beta$, $-\cos\beta$, yielding

$$g_{\chi_1^0\chi_1^0 Z} \propto \frac{g}{c_W}(\sin^2\beta - \cos^2\beta) \times \left[\frac{s_W m_Z}{\mu M_1}\right]^2 \sim \tan^2\beta \qquad \text{for sizable } \tan\beta. \quad (3.3)$$

The term in square brackets is the double mixing suppression of the small higgsino fraction. On the other hand, the coupling to the scalar higgs vanishes in the decoupling limit, with the lowest order term in $m_A$ being

$$g_{\chi_1^0\chi_1^0 h} \propto \frac{m_h^2 + m_Z^2}{M_A^2}\frac{1}{\tan\beta}\left[\frac{s_W m_Z}{\mu M_1}\right] + \mathcal{O}\left(\frac{1}{m_A^4}, \frac{1}{\tan^3\beta}\right) \quad (3.4)$$

This term, while only singly-suppressed by higgsino mixing, decreases with $\tan\beta$.

- Increasing $\mu$ from 400 to 1000 GeV will also decrease the relic density by an $\mathcal{O}(1)$ factor. This is partially due to decreasing $m_{\tilde{\tau}_1}$, but also from decreasing the higgsino fraction of $\tilde{\chi}_1^0$. (The higgsino fraction reduces the neutralino-slepton coupling since it destructively interferes with the dominant hypercharge contribution.) Increasing $\mu$ also decreases the prominence of the higgs- and especially the $Z$-resonance regions, as expected due to the neutralino-mixing suppression in the respective couplings.

- The value of $M_2$ has minimal effect on the dark matter properties so long as it remains dominantly bino to comply with direct detection constraints which forbid significant $Z$-mediated WIMP-nucleon interactions. Changing $M_2$ can affect the prominence of the resonant annihilation regions due to a wino contribution to the relevant couplings, but the qualitative picture does not change, with $t$-channel slepton exchange dominating the annihilation of the bino-like dark matter.

- Switching on an $A_\tau$ term would have no effect other than to increase $\tilde{\tau}$-mixing and decrease $m_{\tilde{\tau}_1}$. This would make the $\tilde{\nu}_\tau$ or $\tilde{\tau}_1$ the LSP for higher values of $M_{\text{slepton}}$ while decreasing the dark matter density, pushing the best-fit region beyond $M_{\text{slepton}} \gtrsim 130\,\text{GeV}$ for $M_{\text{bino}} \gtrsim m_h/2$. As we saw, this would reduce the overlap with the $WW$-preferred region.

- For similar reasons, values of $\mu, \tan\beta$ significantly higher than those shown in Fig. 22 are disfavored by $WW$-data, since they also increase $\tilde{\tau}$-mixing.

The dark matter relic density in our scenario depends not just on the the slepton and bino masses but also on $\mu, M_2, \tan\beta$ and $A_\tau$. This of course just comes from the parametric dependencies of the $\tilde{\tau}$ mass/coupling, and the mixing of the Bino with the other neutralino gauge eigenstates. These parameters matter most when there is either a resonant annihilation region or when the $\tilde{\tau}_1$ (or $\tilde{\nu}_\tau$) becomes lighter and reaches a co-annihilation regime. Within the simple ansatz of our scenario, the dark matter is always predominantly bino and the $\tilde{\tau}_1$ mass is never too different from the first and second generation sleptons, the only splitting coming from mixing effects. This automatically leads to the overlap of the preferred $W^+W^-$ collider region with the correct relic abundance in the bino-slepton mass plane. We have also shown that for moderate ranges of $\mu, M_2, \tan\beta$ and $A_\tau$ our results are also unaffected and the preferred parameter spaces agree. Finally the spin-independent direct detection cross section in our parameter space is always a factor of a few to $\sim 10$ below the current bounds of $\sim 10^{-45}$cm [102] for dark matter masses $M_{\rm bino} \approx 20 - 200\,\text{GeV}$. Our scenario therefore avoids all bounds from direct detection, but interestingly enough does predict a potential signal for LUX or XENON1T.

In Fig. 22 we summarize the relation of the relic density and direct detection limits to our collider parameter space by showing two representative examples of how different $\mu$ and $\tan\beta$ change the DM constraints in our slepton-bino mass plane. The dark matter relic density and direct detection cross section was computed using `micrOMEGAs 2.4.5` [90]. It is amusing to note that the resonant annihilation regions that once could be used to accommodate the correct relic density for Bino DM are the same regions that are ruled out by the collider bounds. This is even more obvious in Fig. 18, where the $m_{\tilde{\chi}_1^0} \approx m_h/2$ and $m_Z/2$ bands are

almost completely excluded by LEP limits and our new slepton exclusion from the CMS8 $WW$ measurement.

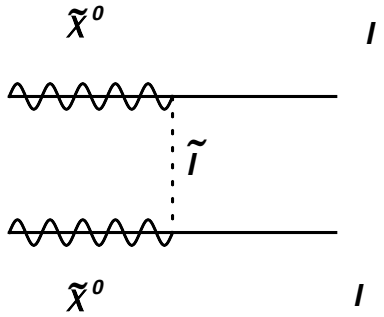


Figure 21: Dark matter t-channel annihilation. Here, the neutralino is a dark matter candidate. With a light slepton, it can reduce dark matter relic density to a range allowable by experiment.

## 3.4 $(g-2)_\mu$

As it appears in the muon magnetic moment $\vec{M} = g_\mu \frac{e}{2m_\mu}\vec{S}$, the gyromagnetic ratio $g_\mu$ is 2 classically. Since that value receives quantum corrections, the anomalous magnetic moment is defined as $a_\mu \equiv \frac{g_\mu - 2}{2}$. This quantity has been the subject of intense theoretical and experimental scrutiny in the last few decades, and the measurement is persistently about $3\sigma$ higher than the SM prediction [92]:

$$\delta a_\mu = a_\mu^{exp} - a_\mu^{SM} = (28.7 \pm 7.98) \times 10^{-10} \tag{3.5}$$

The muon anomalous magnetic moment is very sensitive to the existence of BSM charged states that couple to the muon, making it an interesting probe of low-energy supersymmetry.

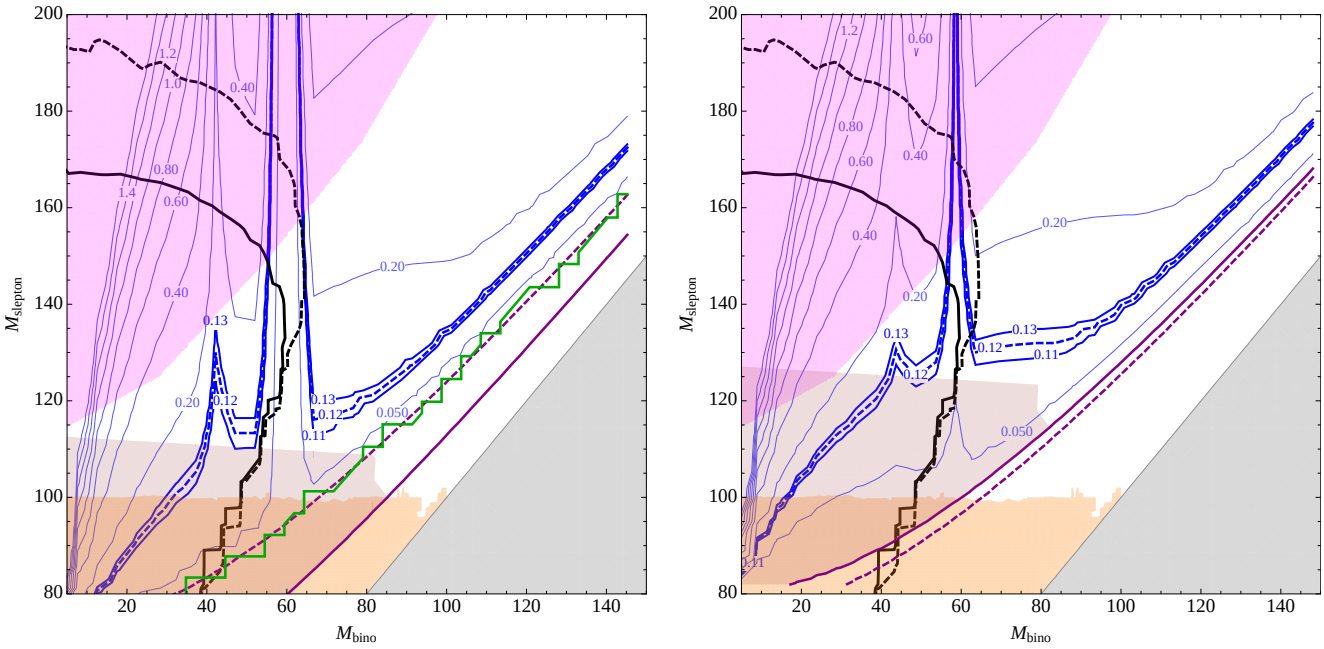


(a) $\tan\beta = 4, \mu = 400\,\text{GeV}$ (b) $\tan\beta = 6, \mu = 600\,\text{GeV}$

Figure 22: The dark matter relic density $\Omega_{\rm CDM}h^2$ in the $(M_{\rm bino}, M_{\rm slepton})$-plane with universal slepton soft masses ($m_{\tilde{\ell}_L} = m_{\tilde{\ell}_R}$). The thick dashed and solid lines indicate the best-fit value $\Omega_{\rm CDM}h^2 = 0.1196$ and the $\pm 3 \times 0.0031$ values. Grey (Orange) shaded regions are excluded by the LEP bound on $m_{\tilde{\tau}_1}$ ($m_{\tilde{e},\tilde{\mu}}$) [27]. The magenta region is excluded by the CMS slepton search [30], while the black lines indicate our combined slepton bounds from the $W^+W^-$ cross section measurement, see Fig. 18. Regions below the solid (dashed) purple line have a stau (sneutrino) LSP. Regions below the green line are excluded by the XENON100 direct detection bound [102] on the WIMP-nucleon cross section of $\sim 10^{-45}\text{cm}^2$ for $M_{\rm bino} \approx 20 - 200\,\text{GeV}$. $M_2 = 600\,\text{GeV}$ and $A_\tau = 0$ in this plot.

Our scenario features light smuons and binos which, as has been long known, can contribute to $a_\mu$ at one-loop level, see Fig. 24. (The corresponding two-loop contributions are small.) It therefore offers a possible explanation for the observed value of $\delta a_\mu$, with the one-loop

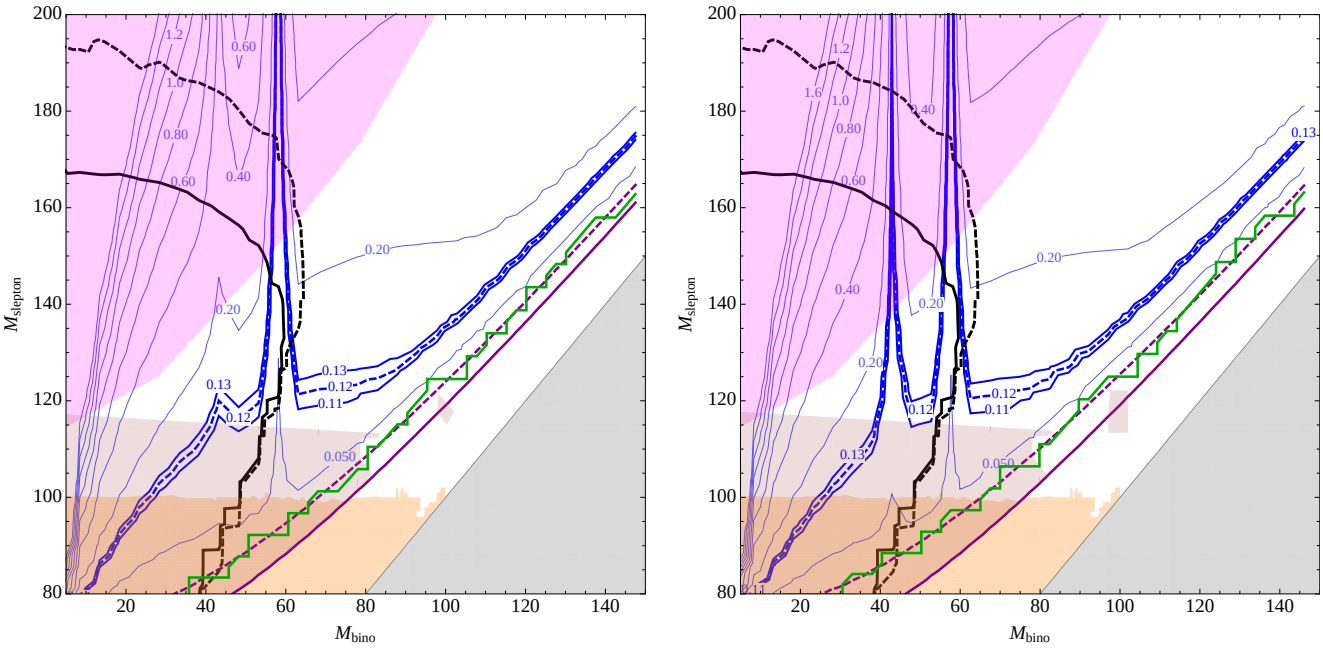


(c) $\tan\beta = 4, \mu = 600\,\text{GeV}$ (d) $\tan\beta = 6, \mu = 400\,\text{GeV}$

Figure 23: The dark matter relic density $\Omega_{\rm CDM}h^2$ in the $(M_{\rm bino}, M_{\rm slepton})$-plane with universal slepton soft masses ($m_{\tilde{\ell}_L} = m_{\tilde{\ell}_R}$). This caption is the same as Fig. 22.

contributions explicitly given by [73]:

$$
\begin{aligned}
a_\mu\left(\tilde{\chi}^0\right) &= \frac{-1}{8\pi^2}\sum_{i=1}^{2}\sum_{j=1}^{4}\frac{m_\mu}{m_{\tilde{\mu}_i}}\left\{\left(|g_L^{\tilde{\chi}_j^0\mu\tilde{\mu}_i}|^2+|g_R^{\tilde{\chi}_j^0\mu\tilde{\mu}_i}|^2\right)\frac{m_\mu}{m_{\tilde{\mu}_i}}G_2\left(\frac{m^2_{\tilde{\chi}_j^0}}{m^2_{\tilde{\mu}_i}}\right)\right. \\
&+ \left. Re[\left(g_R^{\tilde{\chi}_j^0\mu\tilde{\mu}_i}\right)^* g_L^{\tilde{\chi}_j^0\mu\tilde{\mu}_i}]\frac{m_{\tilde{\chi}_j^0}}{m_{\tilde{\mu}_i}}G_4\left(\frac{m^2_{\tilde{\chi}_j^0}}{m^2_{\tilde{\mu}_i}}\right)\right\} \qquad (3.6)\\
a_\mu\left(\tilde{\chi}^-\right) &= \frac{1}{8\pi^2}\frac{m_\mu}{m_{\tilde{\nu}_\mu}}\sum_{i=1}^{2}\left\{\left(|g_L^{\tilde{\chi}_j^-\mu\tilde{\nu}_\mu}|^2+|g_R^{\tilde{\chi}_j^-\mu\tilde{\nu}_\mu}|^2\right)\frac{m_\mu}{m_{\tilde{\nu}_\mu}}G_1\left(\frac{m^2_{\tilde{\chi}_j^-}}{m^2_{\tilde{\nu}_\mu}}\right)\right. \\
&+ \left. Re[\left(g_R^{\tilde{\chi}_j^-\mu\tilde{\nu}_\mu}\right)^* g_L^{\tilde{\chi}_j^-\mu\tilde{\nu}_\mu}]\frac{m_{\tilde{\chi}_j^-}}{m_{\tilde{\nu}_\mu}}G_3\left(\frac{m^2_{\tilde{\chi}_j^-}}{m^2_{\tilde{\nu}_\mu}}\right)\right\} \qquad (3.7)
\end{aligned}
$$

The $G_i$ are loop integrals. This formula is convenient for computation but not very illuminating. It is more instructive to examine the contributions in the gauge-eigenstate

basis [73]:

$$a_\mu(\tilde{B}, \tilde{\mu}_L - \tilde{\mu}_R) = \frac{g_Y^2}{8\pi^2}\frac{m_\mu^2 \mu \tan\beta}{M_1^3} F_b\left(\frac{m_{\tilde{\mu}_L}^2}{M_1^2}, \frac{m_{\tilde{\mu}_R}^2}{M_1^2}\right) \tag{3.8}$$

$$a_\mu(\tilde{B} - \tilde{H}, \tilde{\mu}_L) = \frac{g_Y^2}{16\pi^2}\frac{m_\mu^2 M_1 \mu \tan\beta}{m_{\tilde{\mu}_L}^4} F_b\left(\frac{M_1^2}{m_{\tilde{\mu}_L}^2}, \frac{\mu^2}{m_{\tilde{\mu}_L}^2}\right) \tag{3.9}$$

$$a_\mu(\tilde{B} - \tilde{H}, \tilde{\mu}_R) = -\frac{g_Y^2}{8\pi^2}\frac{m_\mu^2 M_1 \mu \tan\beta}{m_{\tilde{\mu}_R}^4} F_b\left(\frac{M_1^2}{m_{\tilde{\mu}_R}^2}, \frac{\mu^2}{m_{\tilde{\mu}_R}^2}\right) \tag{3.10}$$

$$a_\mu(\tilde{W}^0 - \tilde{H}, \tilde{\mu}_L) = -\frac{g^2}{16\pi^2}\frac{m_\mu^2 M_2 \mu \tan\beta}{m_{\tilde{\mu}_L}^4} F_b\left(\frac{M_2^2}{m_{\tilde{\mu}_L}^2}, \frac{\mu^2}{m_{\tilde{\mu}_L}^2}\right) \tag{3.11}$$

$$a_\mu(\tilde{W}^\pm - \tilde{H}, \tilde{\nu}_\mu) = \frac{g^2}{8\pi^2}\frac{m_\mu^2 M_2 \mu \tan\beta}{m_{\tilde{\nu}}^4} F_a\left(\frac{M_2^2}{m_{\tilde{\nu}}^2}, \frac{\mu^2}{m_{\tilde{\nu}}^2}\right) \tag{3.12}$$

A dash, as in $\tilde{\mu}_L - \tilde{\mu}_R$, indicates a corresponding mixing insertion. First, notice that all contributions are proportional to $\mu \tan\beta$, which is due to smuon mixing[2]. (There is additional dependence on $\mu$ in the loop functions $F_{a,b}$ but this comes from higgsino mixing.) The neutralino contributions $(3.8 - 3.11)$ are all neutralino contributions corresponding to Eq. (3.6). These contributions dominate for bino dark matter and large $M_2$. While this may be intuitively obvious, the prefactor of $M_2$ in Eq. (3.12) might imply the contribution to grow with chargino mass. However, the loop functions $F_{a,b}(x,)$ decrease with increasing $x, y$, meaning for our realm of interest for our scenario ($M_2 \gtrsim 200\,\text{GeV}$) the chargino contribution is smaller than the bino contribution by a factor of $\sim 4 - 8$.

Fig. 25 shows the $\delta a_\mu$ in the $(M_{\text{bino}}, M_{\text{slepton}})$-plane for different $\mu, \tan\beta$, computed in `CPsuperH 2.3` [103]. Increasing the slepton mass decreases $\delta a_\mu$, but the dependence on $M_{\text{bino}}$ has two different regimes: for small $M_1$ Eq. (3.8) dominates and $\delta a_\mu$ increases with

[2] $A_\mu$ is assumed to be zero.

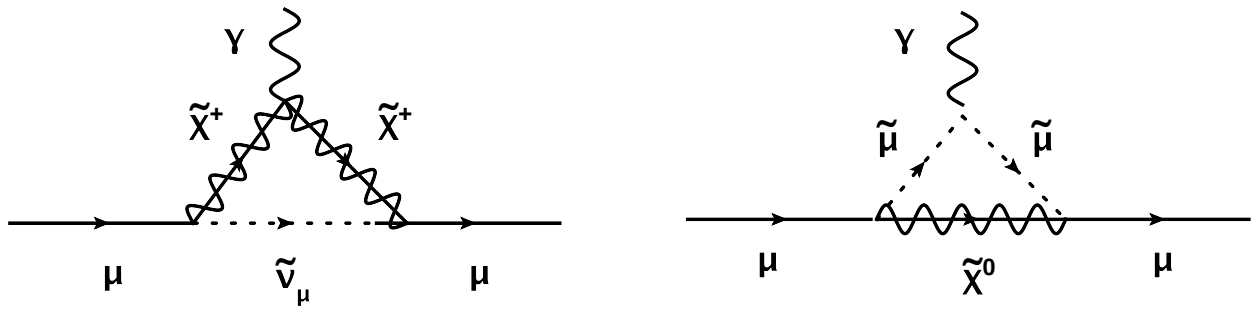


Figure 24: $a_\mu$ contributions from neutralinos and charginos in terms of mass eigenstates.

$M_1$; for large $M_1$, Eqns. (3.9), (3.10) give an overall negative contribution that grows with $M_1$ ($m_{\tilde{\mu}_L} = m_{\tilde{\mu}_R}$ in our scenario). This explains the maximum value of $\delta a_\mu$ when $M_{\rm bino} \sim M_{\rm slepton}$.

Within the regions not yet excluded by slepton bounds, $\delta a_\mu$ and $\Omega_{\rm DM}$ have very similar scaling with $\mu, \tan\beta$, and there are ranges of both parameters where the best-fit regions for both observables overlap to one sigma. Remarkably, that overlap region also lies in the region preferred by $W^+W^-$ measurements.

## 3.5 $h \to \gamma\gamma$ and LFU Violation

The LHC has recently discovered a $\approx 125\,\text{GeV}$ resonance [14], properties of which seem consistent with those of the SM Higgs boson at the $2\sigma$ level. A mild excess in the diphoton channel, $pp \to h \to \gamma\gamma$, has been reported by the ATLAS experiment [41] while a similar excess which had been reported by the CMS experiment earlier in 2012 [42] has considerably reduced after the new analysis in 2013 [43]. Though it is not immediately clear whether the diphoton excess will survive the test of time, it is nevertheless an interesting possibility that

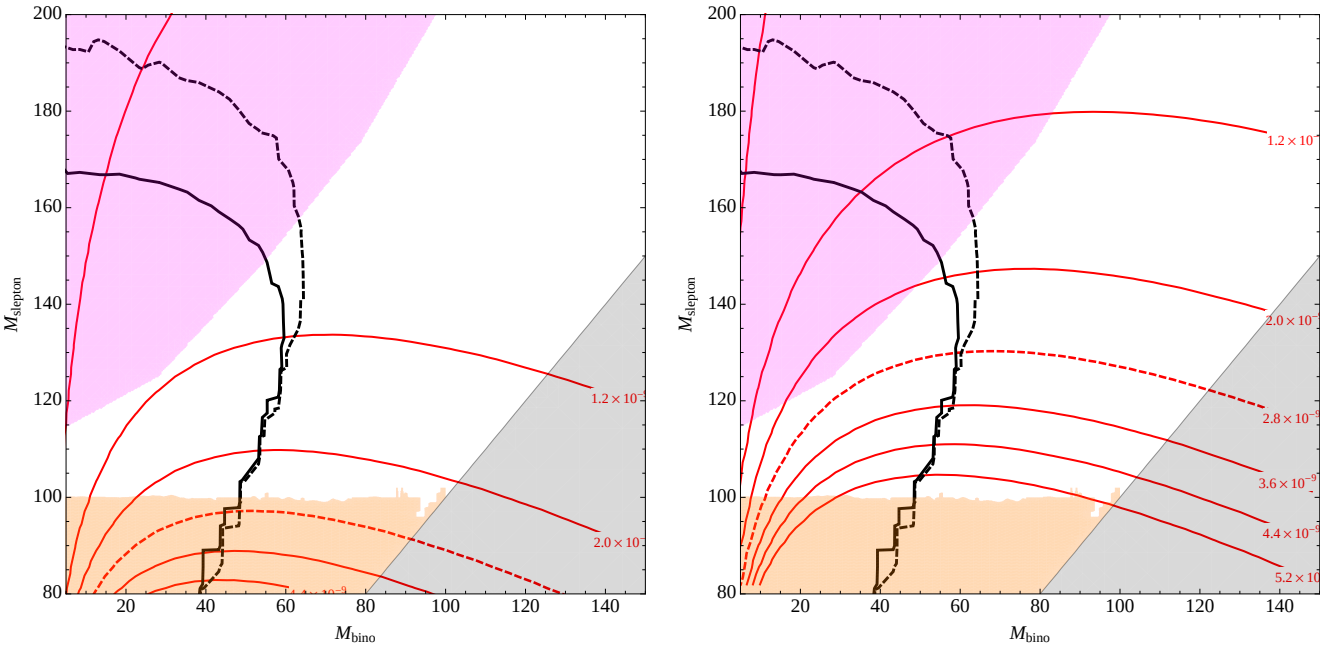


(a) $\tan\beta = 4, \mu = 400\,\text{GeV}$ (b) $\tan\beta = 6, \mu = 600\,\text{GeV}$

Figure 25: Variation of $\delta a_\mu$ in the $(M_{\text{bino}}, M_{\text{slepton}})$-plane with universal slepton soft masses ($m_{\tilde{\ell}_L} = m_{\tilde{\ell}_R}$). Red lines are contours of $\delta a_\mu$, with the dashed line indicating the experimentally preferred value of $2.87 \times 10^{-9}$ and each contour spacing corresponding to $0.8 \times 10^{-9}$ (one $\sigma$ of the experimental measurement). Grey (Orange) shaded regions are excluded by the LEP bound on $m_{\tilde{\tau}_1}$ ($m_{\tilde{e},\tilde{\mu}}$) [27]. The magenta region is excluded by the CMS slepton search [30], while the black lines indicate our combined slepton bounds from the $W^+W^-$ cross section measurement, see Fig. 18.

new physics at the electroweak scale can lead to deviations in the $h \to \gamma\gamma$ effective coupling through loop induced processes. In particular, the possibility of light staus enhancing the Higgs diphoton rate has been well-studied in the literature [44]. A diphoton rate enhancement of $\sim 50\%$ requires large stau-mixing with $|A_\tau - \mu \tan\beta| \gtrsim 18\,\text{TeV}$ and the lightest stau of mass $m_{\tilde{\tau}_1} \sim 90 - 100\,\text{GeV}$. This rather narrow *stau window* constrains the soft masses of the third generation sleptons to be $m^2_{L_3} \approx m^2_{E_3} \approx m_\tau(A_\tau - \mu\tan\beta)$. Therefore, a large mass-splitting between the stau eigenstates is induced by electroweak symmetry breaking (EWSB) in this scenario. It also explains why our simple MSSM scenario cannot improve

the $W^+W^-$ measurement while enhancing the higgs diphoton rate: under the assumption of slepton soft mass universality, the first and second generation sleptons would be too heavy to significantly influence the measured $W^+W^-$ cross section.

This motivates us to explore, within our MSSM scenario, a departure from slepton soft mass universality, allowing $m_{\tilde{\tau}_L} = m_{\tilde{\tau}_R}$ to differ from the first and second generation $m_{\tilde{\ell}} = m_{\tilde{\ell}_R}$[3]. Since the muon $(g-2)$ is not sensitive to the stau parameters, our task is to understand whether the correct bino relic density is compatible with enhancing $h \to \gamma\gamma$ by increasing both stau mixing and stau soft masses.

To answer this question, we investigated the three-dimensional parameter space $(\mu, \tan\beta, X_\tau)$, where $X_\tau = \frac{1}{m_\tau}\{M^2_{\tilde{\tau}}\}_{LR}$, which is $(A_\tau - \mu\tan\beta)$ at tree-level. (Using $X_\tau$ instead of $A_\tau$ disentangles stau mixing effects from bino-higgsino mixing effects.) We fixed $m_h \approx 125\,\text{GeV}$, as well as $M_{\text{bino}} \approx 80\,\text{GeV}$ and $M_{\text{slepton}} = 110\,\text{GeV}$ to minimize tension in the $WW$ measurements. To maximally increase the $h \to \gamma\gamma$ rate we fixed $m_{\tilde{\tau}_1} = 100\,\text{GeV}$ by choosing appropriate soft masses $m^2_{\tilde{\tau}_L} = m^2_{\tilde{\tau}_R}$ for a given $\mu, \tan\beta$ and $X_\tau$ (equivalently, $A_\tau$).

Examining the dependence of $\Omega_{\text{DM}}$, $\text{Br}(h \to \gamma\gamma)$ and $(g-2)_\mu$ across this parameter space, we found that the requirements of correct relic density and significantly enhanced $h \to \gamma\gamma$ are impossible to satisfy simultaneously. Increasing the diphoton rate requires large stau mixing, which introduces additional diagrammatic contributions to $t$-channel neutralino annihilation and reduces dark matter density. Since the presence of first and second generation sleptons at $\sim 110\,\text{GeV}$ (from $WW$ measurements) already guarantees a relic density close to $\Omega_{\text{DM}}h^2 \approx 0.1$, introducing mixed staus increases the annihilation cross section beyond

[3]The situation is not changed when allowing L and R soft masses to vary independently.

acceptable values. This is readily demonstrated in Fig. 26(a), which shows the opposite dependency of the relic density and diphoton rate on stau mixing in the above-described scenario for the $\tan\beta = 10$ slice. (With the $X_\tau$ parameterization of stau mixing, the remaining explicit $\tan\beta$ dependence of $\Omega_{\rm DM}$ and $\mathrm{Br}(h \to \gamma\gamma)$ is small.) In general, requiring correct dark matter relic density limits the maximum diphoton rate enhancement to about 15% for first and second generation sleptons lighter than 145 GeV. It also requires $\mu$ to be in the few hundred GeV range, as demonstrated by Fig. 26(b): increasing $\mu$ decreases the higgsino fraction of the neutralino, which as explained above significantly reduces relic density due to more efficient annihilation, even when stau mixing is kept constant.

This paints a very clear picture. If the $WW$ measurements are interpreted as implying light first and second generation sleptons near 110 GeV and a neutralino near 80 GeV, the resulting dark matter annihilation is so efficient that both $\mu$ and stau-mixing must be relatively small. The maximum higgs diphoton enhancement that can be achieved is about 15%, and requires stau soft masses of $\sim 300\,\mathrm{GeV}$ compared to first and second generation slepton soft masses of $\sim 100\,\mathrm{GeV}$, as well as first and second generation sleptons slightly heavier ($\sim 120 - 130\,\mathrm{GeV}$) than what is ideally preferred by $W^+W^-$ measurements.

While our scenario cannot explain a 50% enhancement, as the measurements of the higgs diphoton rate become more precise a smaller but nonzero enhancement may still be desirable. Since our scenario requires a departure from slepton soft mass universality to achieve a 15% enhancement, it is prudent to check that the bounds on LFU violation do not exclude this possibility. There are two sources violating lepton flavor universality (LFU) in this scenario : (i) the EWSB induced term proportional to tau Yukawa, $m_\tau(A_\tau - \mu\tan\beta)$, which is large in

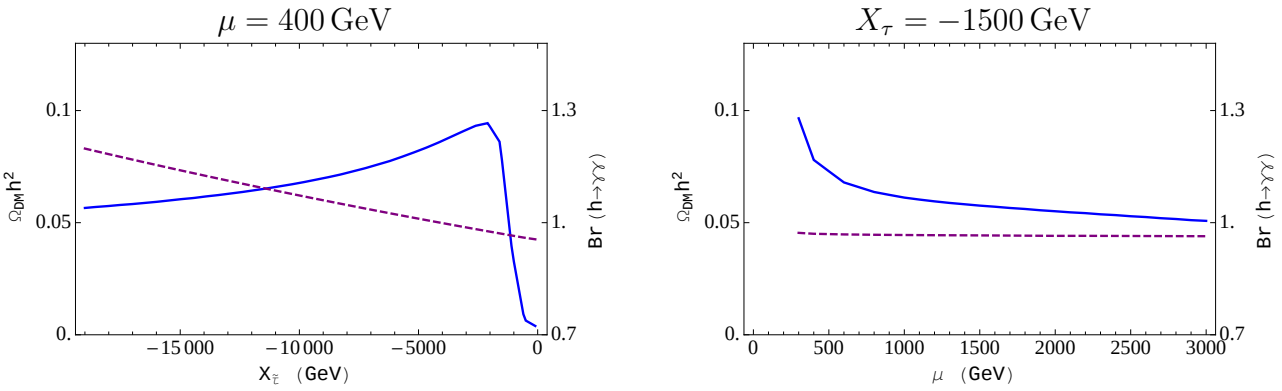


(a) (b)

Figure 26: The dark matter relic density (blue solid line) and Br($h \to \gamma\gamma$) (purple dashed line, normalized to SM) as functions of $X_\tau$ and $\mu$ in the $\tan\beta = 10$ slice. $X_\tau \equiv \frac{1}{m_\tau}\{M^2_{\tilde{\tau}}\}_{LR} = (A_\tau - \mu \tan\beta)$ at tree-level. $M_{\rm bino}, M_{\rm slepton}$ and $m_{\tilde{\tau}_1}$ were fixed at 80, 110 and 100 GeV. In (a) relic density increases with decreasing stau mixing. The sudden fall-off near $X_\tau = 0$ is from tau sneutrinos becoming light due to the small stau soft masses with minimal mixing, giving rise to stau-neutralino co-annihilation or even a stau LSP.

the region where the diphoton rate is enhanced and, (ii) non-degenrate soft SUSY parameters in the slepton sector, which is a necessary condition if both $W^+W^-$ and Higgs diphoton anomalies are to be reconciled. Even if one is agnostic about the diphoton excess, there are regions in the light slepton parameter space where LFU violation can be non-negiligible.[4]

Bounds on LFU violation can be parameterized by different effective Fermi constants for different leptons. Considering for example tau vs muon decay, we can define the quantity $\Delta r^{\mu/\tau}$ [65] as follows:

$$\begin{aligned}\Delta r^{\mu/\tau} &= \frac{(R_{\mu/\tau})}{(R_{\mu/\tau})_{\rm SM}} - 1 \\ &= \frac{\Gamma(\mu \to e\nu_\mu\overline{\nu}_e)/\Gamma(\tau \to e\nu_\tau\overline{\nu}_e)}{\Gamma(\mu \to e\nu_\mu\overline{\nu}_e)_{\rm SM}/\Gamma(\tau \to e\nu_\tau\overline{\nu}_e)_{\rm SM}} - 1 \\ &= \frac{G^2_\mu/G^2_\tau}{(G^2_\mu)_{\rm SM}/(G^2_\tau)_{\rm SM}} - 1\end{aligned} \tag{3.13}$$

[4]There is also a possibility of lepton flavour violation from flavour off-diagonal terms in the slepton mass matrix but we do not consider them here since they are known to be small [64].

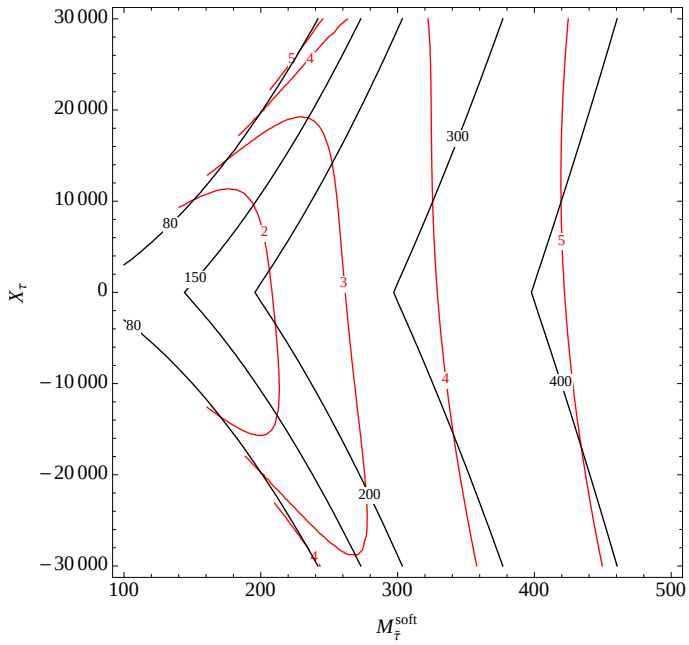


Figure 27: $\Delta r^{\mu/\tau} \times 10^5$ (red contours) as a function of $X_\tau = \frac{1}{m_\tau}\{M^2_{\tilde{\tau}}\}_{LR}$ (which is $(A_\tau - \mu \tan\beta)$ at tree-level) and $m^{\text{soft}}_{\tilde{\tau}}$, the common $\tilde{\tau}_L$, $\tilde{\tau}_R$ soft mass. The gray contours are the $\tilde{\tau}_1$ mass eigenvalue (all in GeV), and only regions where $m_{\tilde{\tau}_1} > 80\,\text{GeV}$ are of interest [27]. Across the entire range, $\Delta r^{\mu/\tau}$ is much smaller than the upper experimental bounds, which are $\mathcal{O}(10^{-3}) - \mathcal{O}(10^{-2})$ depending on the process [65]. For this plot, the first and second generation slepton soft mass is 100 GeV, $M_1 = 80\,\text{GeV}$, $\mu = 400\,\text{GeV}$, $\tan\beta = 4$, $M_2 = 600\,\text{GeV}$ and $A_\mu = 0$, but changing these parameters will not increase $\Delta r^{\mu/\tau}$ beyond experimental limits.

where $G_\tau(G_\mu)$ is the Fermi decay constant for tau (muon) decay. Depending on the process for which $\Delta r^{\mu/\tau}$ is evaluated, its absolute value is bounded to be smaller than $\mathcal{O}(10^{-3}) - \mathcal{O}(10^{-2})$. [65, 67].

To a good approximation, the theoretical prediction for $\Delta r^{\mu/\tau}$ is process-independent. The relation between the measured Fermi constant and the $W$ boson mass receives loop corrections depending on the process under consideration and is parametrized by $\Delta r^f$ (not

to be confused with $\Delta r^{\mu/\tau}$):

$$G_f = \frac{\pi\alpha}{\sqrt{2}M_W^2 s_w^2}(1+\Delta r^f)\,, \quad f=\mu,\tau \tag{3.14}$$

where $s_w$ is the sine of the weak mixing angle and $\alpha$ is the electromagnetic constant. Plugging this relation back in Eq. (3.13), we get

$$\begin{aligned}\Delta r^{\mu/\tau} &= \left|\frac{1+\Delta r^{\mu}}{1+\Delta r^{\mu}_{\rm SM}}\right|^2 \left|\frac{1+\Delta r^{\tau}_{\rm SM}}{1+\Delta r^{\tau}}\right|^2 - 1 \\ &\approx 2(\Delta r^{\mu}_{\rm SUSY} - \Delta r^{\tau}_{\rm SUSY})\end{aligned} \tag{3.15}$$

From the above expression, it is clear that any lepton-universal contributions to $\Delta r^{\mu/\tau}$ cancel out. Analytic expressions for supersymmetric contributions to $\Delta r$ are presented in [66] but are too lengthy to reproduce here. The most important input is the splitting between the stau soft masses and the first/second generation soft masses, and the stau mixing $X_\tau$, and includes both sources of LFU violation mentioned above. Fig. 27 shows $\Delta r^{\mu/\tau}$ for representative choices of parameters, and it is always orders of magnitude below experimental bounds for the relevant parameter ranges. Therefore, while our scenario does not naturally account for a $h \to \gamma\gamma$ enhancement, a moderate enhancement of $\sim 15\%$ may be accommodated.

# 4 Light Stop Scenarios

In this section we will show how each of the light stop scenarios in Fig. 17 could account for the $W^+W^-$ excess. In each case a $\chi^2$-fit over all kinematic distributions of the $W^+W^-$

cross section measurements [56–58] is performed, with preferred regions of the stop-neutralino mass plane identified by smaller values of $\chi^2_{\rm SM+stops}/\chi^2_{\rm SM}$. We include in our analysis the constraints from stop, sbottom and chargino direct searches, and find that they do not exclude one or two light stops as explanations for the $W^+W^-$ excess. In fact, as we outline below, chargino searches may already hint at an independent confirmation of certain types of spectra.

The presence of light sbottoms in Scenarios B-D allows the Bino to be a thermal DM candidate with correct relic density. The absence of charginos in Scenarios B & D also allows light sleptons to be included, which can account for the measured deviation in $(g-2)_\mu$. The corresponding treatment of these issues for Scenario B in Section 4.2.1 carries over to the subsequent scenarios. We also discuss Higgs coupling constraints on Scenario C & D with two light stops in Section 4.3.1. They are not prohibitive, but will be an interesting probe at the next run of the LHC.

## 4.1 Scenario A: One Light Stop, $W$ from EWino

This is Scenario A in Fig. 17, originally proposed by [61]. A single light stop is pair-produced and decays via soft $b$-jets to wino-like charginos, which then decay to a $W$ and a Bino LSP. The second stop could evade detection if it hides in the $t\bar{t}$ background with a mass of $m_{\tilde{t}_2} \approx m_t + m_{\tilde{\chi}^0_2}$, but then sbottom constraints would exclude this scenario, see Fig. 29. Therefore we assume the second stop to be heavier than $\sim 700\,\text{GeV}$ to evade $\bar{t}t + \text{MET}$ searches [34].

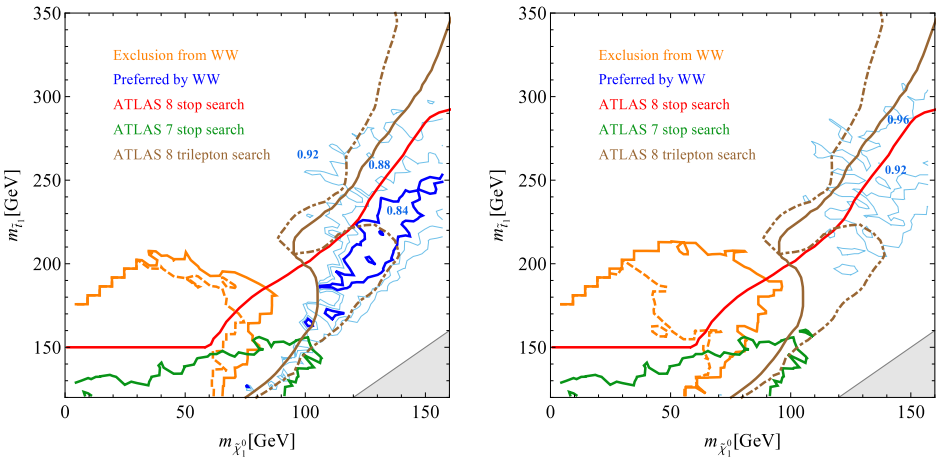


(a) ATLAS 7 TeV 5 fb$^{-1}$ [56]




(b) CMS 7 TeV 5 fb$^{-1}$ [57]

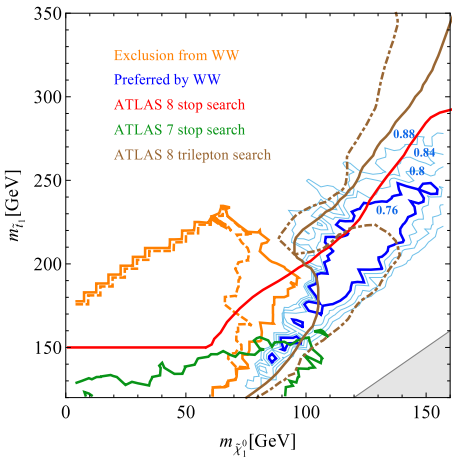


(c) CMS 8 TeV 3.5 fb$^{-1}$ [58]

Figure 28: Regions of the stop-neutralino mass plane excluded and preferred by the different $W^+W^-$ cross section measurements in Scenario A ("One Light Stop, $W$ from EWino"). We fix $\Delta m = \tilde{t}_1 - \chi_1^\pm \approx 10\,\text{GeV}$ to avoid hard b-jets. Solid (dashed) orange line: 95% exclusion from the $W^+W^-$ measurement with fixed (floating) normalization of SM contribution. Thin blue contours show values of $\chi^2_{\text{SM+stops}}/\chi^2_{\text{SM}}$, with the thick contour indicating the region most preferred by the $W^+W^-$ measurement. Exclusions from ATLAS stop searches shown in red [82] and green [47]. Observed (expected) exclusion from ATLAS trilepton $\chi_2^0\chi_1^\pm$ search [75] shown as solid (dot-dashed) brown line: note how an excess compatible with the $W^+W^-$ preferred region pushes the observed bounds down in Bino mass.

Fig. 28 shows the stop-neutralino mass plane, with $m_{\tilde{\chi}_1^\pm} \approx m_{\tilde{t}_1} - 10\,\text{GeV}$. (If the mass difference were much larger the stop events would fail the jet veto of the $W^+W^-$ measurements.) The region *above* the red contour is excluded by the 13 fb$^{-1}$ ATLAS 8 TeV low-MET $\tilde{t} \to b + \tilde{\chi}_1^\pm$ search.[1] Lighter stop masses $m_{\tilde{t}_1} < 150\,\text{GeV}$ are constrained by a 5 fb$^{-1}$ 7 TeV ATLAS search [47]. Applying the cuts from this search, and rescaling our efficiency by 0.5 to reproduce the acceptances quoted in [47], excludes the region below the green curve. Finally, the observed (expected) limits on $\chi_2^0\chi_1^\pm \to W + Z + 2\chi_1^0$ from the ATLAS 20fb$^{-1}$ 8 TeV trilepton search [75] are shown as a solid (dot-dashed) brown line. Note the deviation between observed and expected chargino limits, which is due to a $2\sigma$ excess in the SR0$\tau$a-bin01 of that search.

The solid (dashed) orange line shows the constraint obtained on this stop scenario by each of the published $W^+W^-$ measurements under the assumption of fixed (freely floating) SM contribution. The obtained limits close the gap between the two stop searches, but are superseded by the trilepton limits.

The thin blue lines are contours of $\chi^2_{\text{SM+stop}}/\chi^2_{SM}$ for the full shape fit across all published differential distributions in each $W^+W^-$ search. The actual value of this ratio is not very meaningful, since the public data does not allow us to take all correlations into account for the shape fit. Nevertheless, the result that some regions in the mass plane are preferred over others and improve the fit compared to the SM alone is robust, and we indicate the "most preferred regions" with a thick blue contour to guide the eye. Its vertical extent is mostly given by the stop production cross section. A stop-neutralino mass-difference of

[1] A recent 20 fb$^{-1}$ update [46] does not significantly change the limits in our mass region of interest.

$\sim m_W$ is preferred to give roughly at-rest $W$'s from chargino decay, improving agreement in all kinematic distributions of the $W^+W^-$ measurements. (If the kinematics were very different, the stop contribution would fill in the wrong bins and worsen the disagreement between expectation and data.) The best-fit point is near $(m_{\tilde{t}_1}, m_{\tilde{\chi}_1^0}) \approx (220, 130)\,\text{GeV}$.

The $WW$-preferred region is not excluded by either stop or chargino bounds. In fact, the ATLAS trilepton search [75] should be sensitive to the stop spectra in part of the preferred region, but the observed $2\sigma$ excess pushes the exclusion away from the preferred region. This might be interpreted as very tentative evidence for this light stop scenario, from a signal which is completely uncorrelated with the dilepton + MET final state in the $W^+W^-$ measurement.[2]

The pure Bino is a slightly problematic DM candidate within the MSSM, requiring non-standard cosmological history to have the correct relic density. This is discussed further in Section 4.2.1.

## 4.2 Scenario B: One Light Stop, $W$ from Stop

In contrast to the first example where charginos were required to produce the $W's$ in their decays, $W's$ can be produced with colored cross section simply via electroweak stop decay. This is Scenario B in Fig. 17.

For simplicity, $\tilde{t}_2$ is again assumed to be heavier than $\sim 700\,\text{GeV}$ to evade direct searches and demonstrate the minimal working parts necessary. The presence of a light sbottom decaying via $\tilde{b}_1 \to b + \tilde{\chi}_1^0$ is highly constrained, most importantly by a 12.8 $\text{fb}^{-1}$ ATLAS

[2]The CMS trilepton search [76] has no sensitivity in this mass region.

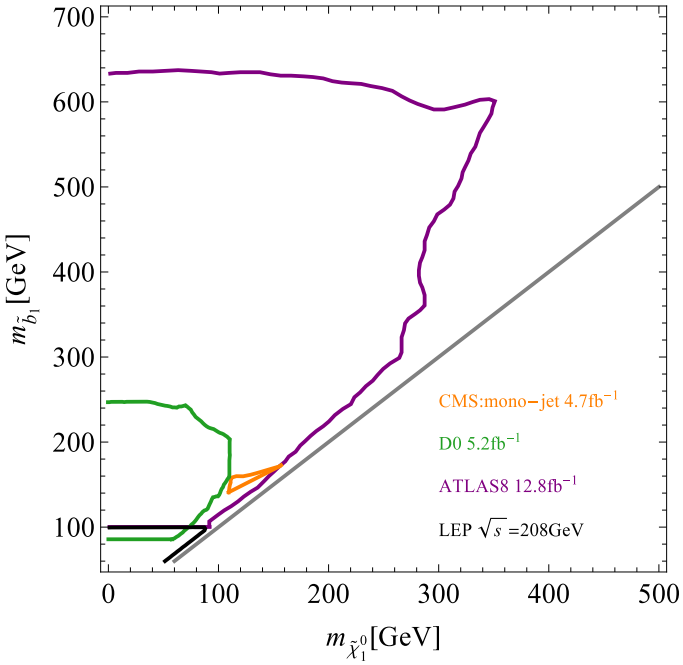


Figure 29: Bounds on a single sbottom decaying via $\tilde{b}_1 \to b + \tilde{\chi}_1^0$. Black: LEP $\sqrt{s} = 208\,\text{GeV}$ [83]. Purple: low-MET ATLAS 8TeV 12.8 $\text{fb}^{-1}$ search [81]. Green: D0 5.2 $\text{fb}^{-1}$ [85]. Orange: CMS 4.7 $\text{fb}^{-1}$ mono-jet recast by [86]. Gray: $m_{\tilde{b}_1} = m_{\tilde{\chi}_1^0}$ kinematic limit.

search [81], see Fig. 29. However, these bounds can be avoided if $m_{\tilde{b}_1} - m_{\chi_1^0} \lesssim 10\,\text{GeV}$, since for such small mass gaps sbottom decay is poorly understood, and it is possible for such spectra to evade searches by failing $b$-jet requirements or single-track vetoes.

Again for simplicity we assume mostly right-handed $\tilde{t}_1$ and $\tilde{b}_1$ to decouple $m_{\tilde{b}_1}$ from $m_{\tilde{t}_1}$ and easily allow for $m_{\tilde{b}_1} \sim m_{\chi_1^0}$. (Mixed sbottoms can also be accommodated by adjusting sbottom mixing, see Section 4.3.) Both states, $\tilde{t}_1$ and $\tilde{b}_1$, have to carry at least a small LH component to ensure $\text{Br}(\tilde{t}_1 \to \tilde{b}_1 + W^+) \approx 1$ and avoid a large $\tilde{t} \to c + \tilde{\chi}_1^0$ signal. Higgs coupling measurements are not yet sensitive to a single light stop [69], while deviations due to sbottoms are generically small, certainly so if the other sbottom is very heavy [87].

The kinematics of the BSM signal in the $W^+W^-$ measurement is very similar to Sce-

nario A, so most of Fig. 28 applies here as well. The same stop search limits apply, but there are no bounds from the ATLAS trilepton searches since there is no light wino-like chargino/neutralino pair. With $m_{\tilde{b}_1} - m_{\chi_1^0} \approx 10\,\text{GeV}$ there are no sbottom bounds, and a nearly identical region of the stop-neutralino mass plane is preferred/excluded by the $W^+W^-$ measurements. In the absence of a trilepton signal, these new bounds fill an important gap between the stop searches.

### 4.2.1 Thermal Bino Dark Matter and $(g-2)_\mu$

The pure Bino is a slightly problematic dark matter candidate within the MSSM. If it is the LSP, its annihilation cross section is typically very small, leading it to overclose the universe. (For a discussion see e.g. [88].) Scenario A can therefore not be realized within the standard MSSM, and some additional mechanisms to dilute the Bino density must be present.

Bino annihilation can be enhanced in three ways. Firstly, if the Bino-like LSP has a non-negligible Wino (Higgsino) fraction and its mass is near $m_Z/2$ ($m_h/2$), annihilation proceeds through an $s$-channel $Z$ ($h$) resonance. Secondly, if there is another sfermion close in mass it is possible to co-annihilate both LSP and NLSP particle populations. Thirdly, if there is a relatively light sfermion carrying hypercharge then it can mediate sizable annihilation via $t$-channel exchange. Scenarios B - D feature light sbottoms between LSP and stops in the spectrum. The presence of this additional degree of freedom makes it possible to enhance Bino annihilation to either make it a subdominant dark matter component, or to act as a thermal relic with the correct relic density $\Omega_{\text{CDM}}h^2 = 0.1196 \pm 0.0031$ [89].

To understand the impact of a light sbottom we computed the Bino DM relic density $\Omega_{\text{Bino}}$ using `micrOMEGAs 3.6.9.2` [90] for different $m_{\tilde{\chi}_1^0}, m_{\tilde{b}_1}$ assuming either $\tilde{b}_1 = \tilde{b}_R$ or $\tilde{b}_1 = \tilde{b}_L$.[3] In either case, we find that $t$-channel annihilation is insufficient to avoid overclosure, due to the small hypercharge of sbottoms compared to sleptons. The only way to satisfy $\Omega_{\text{Bino}} = \Omega_{\text{CDM}}$ with light sbottoms is via co-annihilation. For the Bino masses most of interest, $m_{\tilde{\chi}_1^0} \sim 130\,\text{GeV}$, this requires $m_{\tilde{b}_1} \approx m_{\tilde{\chi}_1^0} + 15\,\text{GeV}$ for both $\tilde{b}_L$ and $\tilde{b}_R$. This is just on the border of exclusion in the ATLAS sbottom search [81] (see Fig. 29), so this mechanism for generating the correct thermal relic density may be called marginally viable. At any rate, if the sbottom is closer in mass to the Bino than 15 GeV then the Bino makes up some fraction of the total DM density. This means the light sbottom scenarios are *not* excluded by cosmological considerations.

Regardless of cosmological history, if a Bino-like LSP constitutes a significant dark matter component then its higgsino fraction must be low enough to give a Higgs-mediated direct detection cross section below current bounds. We have checked that LUX direct detection bounds [91] are satisfied for $\mu \gtrsim 500\,\text{GeV}$.

Sbottom-Bino co-annihilation can make the LSP in Scenarios B - D a thermal relic in the $WW$-preferred region. There is, however, potential to address yet another anomaly which may hint at new physics. The absence of charginos in Scenarios B and D makes it possible to insert sleptons into the spectrum between the stop and the LSP without affecting the $W^+W^-$ signal from stop pair production. High-MET SUSY searches are not sensitive to

[3] We assume $m_h = 125\,\text{GeV}$ is generated by the heavy second stop or by some new physics beyond the MSSM for the scenarios with two light stops, so we fix the Higgs mass manually in the SLHA spectrum files.

sleptons in the "$WW$-funnel", $m_{\tilde{\ell}} - m_{\tilde{\chi}_1^0} \lesssim m_W$ [75]. In [53] we showed that such sleptons below $\sim 150\,\text{GeV}$ could account for the $W^+W^-$ anomaly while simultaneously providing a thermal Bino relic and serving as an explanation for the long-standing $3\sigma$ deviation in the measured value of the muon anomalous magnetic moment $(g-2)_\mu$ [92]. Inserting sleptons above $\sim 150\,\text{GeV}$ into the spectrum of Scenarios B and D would not significantly affect the $W^+W^-$ signal or the relic density (which is annihilated away by sbottom co-annihilation) but could still explain $(g-2)_\mu$.

In summary, light stop Scenario B can explain the $W^+W^-$ excess, while also generating the correct thermal Bino relic density and accounting for the venerable $(g-2)_\mu$ anomaly.

The conclusions of this subsection regarding relic density and direct detection can be applied verbatim to the next two scenarios as well, since they do not meaningfully depend on the stop spectrum or the composition of the lightest sbottom quark.

### 4.3 Scenario C: Two Light Stops, $W$ from EWino

In the context of naturalness, one light stop is good but two light stops are better. In this section and the next we will demonstrate that Scenarios A and B can be modified to have two light stops.

Scenario C in Fig. 17 represents a simple extension on Scenario A, making the second stop similarly light as the first one. The mass difference between the two stops has to be fairly small to ensure that $b$-jet from $\tilde{t}_2 \to \tilde{\chi}_1^\pm + b$ decay does not trigger the jet veto in the $W^+W^-$ measurements. This means the stops cannot have large mixing.

Making both unmixed stops near-degenerate will also introduce the left-handed sbottom into the spectrum. Using the notations of [93], setting stop mixing to zero ($X_t = 0$) via judicious choice of $A_t$ for a given $\mu$ and $\tan\beta$ fixes the left-handed 3$^{\text{rd}}$ generation squark soft mass at tree-level to be

$$M_Q^2 = m_{t_2}^2 - m_t^2 + \frac{1}{6} M_Z^2 (4\sin^2\theta_W - 3)\cos 2\beta, \tag{4.1}$$

where we take $m_{t_2}$ to be the LH stop mass. (In practice there will also be some small stop mixing and hence mass difference, to ensure both stops can decay to a chargino.) For zero sbottom mixing, this gives a LH sbottom mass

$$\begin{aligned} m_{b_L} &= \sqrt{m_{t_2}^2 + m_b^2 - m_t^2 + M_Z^2(\sin^2\theta_W - 1)\cos 2\beta} \\ &\approx 1.6 m_{t_2} - (200\,\text{GeV}), \end{aligned} \tag{4.2}$$

where the approximation in the second line holds to a few GeV in our stop mass range of interest $m_{\tilde{t}} \sim 180 - 260\,\text{GeV}$ when $\tan\beta \gtrsim 3$. Without sbottom mixing we therefore expect most of this Scenario's parameter space to be ruled out by sbottom searches. However, one can always lower the mass of the lightest sbottom by increasing mixing to satisfy $m_{\tilde{b}_1} - m_{\tilde{\chi}_1^0} \lesssim 10\,\text{GeV}$, which removes sbottom constraints as discussed for Scenario B in Section 4.2. The presence of light sbottoms could also help generate a thermal Bino DM relic (or annihilate away the primordeal Bino abundance so it is a subdominant dark matter component), see Section 4.2.1.

Two stops near 200 GeV would make the SUSY spectrum very natural, but within the MSSM they can not generate sufficient loop corrections to lift the Higgs mass to 125 GeV. There are, however, a myriad of extensions to the MSSM which introduce additional Higgs mass contributions. As outlined in Section 1 we will therefore assume some such contribution is present, and concentrate on direct consequences of these light stops.

Fig. 30 and Fig. 31 show the stop-neutralino mass plane for this scenario with $m_{\tilde{t}_2} \approx m_{\tilde{t}_1}$ and small sbottom mixing. The labeling is the same as Fig. 28, and the region preferred by each $W^+W^-$ measurement is shown by the thick blue contour. The purple line indicates the constraint from the ATLAS sbottom search [81]. For unmixed sbottoms it excludes much of the $WW$-preferred region, though some remains. However, increasing sbottom mixing can remove the this constraint. The fully natural scenario with $W^+W^-$ from electroweakinos is therefore viable, and the trilepton excess in [75] could still be taken as tentative corroboration of this spectrum.

### 4.3.1 Higgs Coupling Constraints

Two light stops can generate significant corrections to the loop-induced Higgs couplings (see e.g. [69, 87]). Higgs signal strength measurements in different channels can already give significant constraints on such deviations.

As discussed recently in [69], these measurements naively exclude two light unmixed stops near 200 GeV at the $3\sigma$ level. There are, however, important caveats to this conclusion. Firstly, [69] assumes no other light particles in the spectrum. The presence of other Higgs coupling modifications could loosen this constraint, especially considering that two light

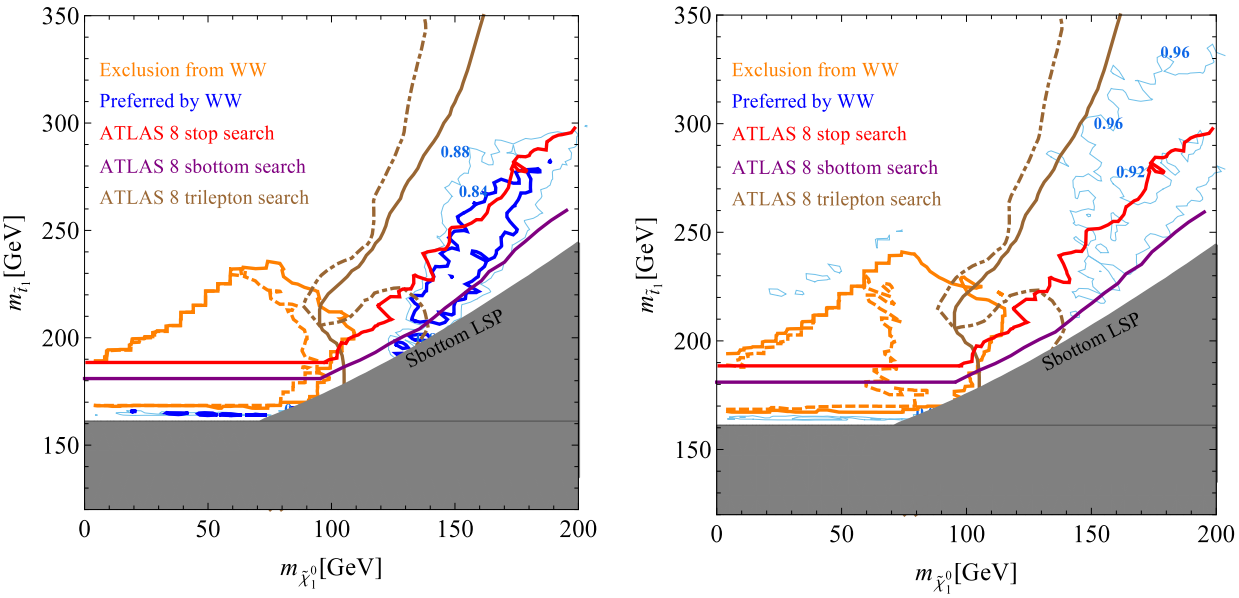


(a) ATLAS 7 TeV 5 fb$^{-1}$ [56] (b) CMS 7 TeV 5 fb$^{-1}$ [57]

Figure 30: Regions of the stop-neutralino mass plane excluded and preferred by the different $W^+W^-$ cross section measurements in Scenario C ("Two Light Stops, $W$ from EWino"). We fix $\Delta m = \tilde{t}_1 - \chi_1^\pm \approx 10\,\text{GeV}$ to avoid hard b-jets, and make the two stops degenerate $m_{\tilde{t}_1} \approx m_{\tilde{t}_2}$. There is no large sbottom mixing, so $m_{\tilde{b}_1}$ is given by Eq. (4.2). Solid (dashed) orange line: 95% exclusion from the $W^+W^-$ measurement with fixed (floating) normalization of SM contribution. Thin blue contours show values of $\chi^2_{\text{SM+stops}}/\chi^2_{\text{SM}}$, with the thick contour indicating the region most preferred by the $W^+W^-$ measurement. Exclusions from the ATLAS stop search shown in red [82]. Observed (expected) exclusion from ATLAS trilepton $\chi_2^0\chi_1^\pm$ search [75] shown as solid (dot-dashed) brown line. The purple line is the ATLAS sbottom search [81], but this constraint can be removed by increasing sbottom mixing.

stops already indicate the presence of additional new physics to raise the Higgs mass beyond the MSSM expectation. Secondly, and more importantly, the CMS [94] measurement of $h \to \gamma\gamma$ is about $2\sigma$ lower than ATLAS [95], which is somewhat above the SM expectation. When only ATLAS Higgs measurements are considered, two 200 GeV unmixed stops are not excluded [74].

The general lesson here is that constraints on SUSY spectra from Higgs coupling fits must be taken with a degree of caution until disagreement between the two experiments is resolved. Once the measurements converge they can be used to test Scenarios C and D.

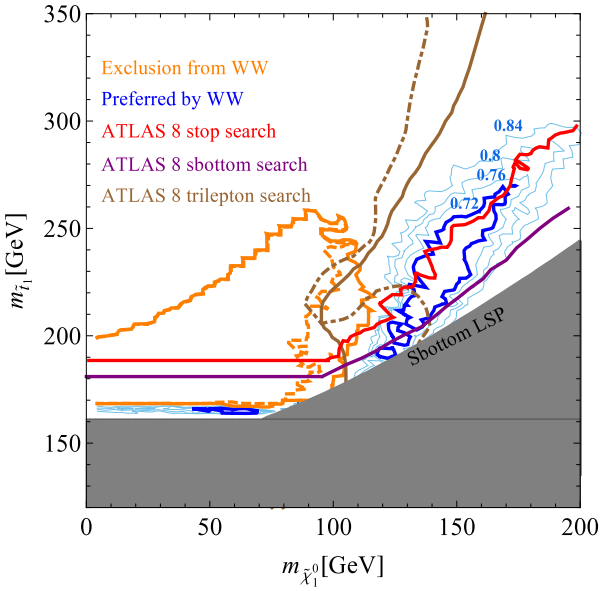


(c) CMS 8 TeV 3.5 fb$^{-1}$ [58]

Figure 31: This caption is the same as Fig. 30

Ignoring small sbottom corrections, the $WW$-preferred region of this scenario in Fig. 30 and Fig. 31 predicts a $hgg$ and $h\gamma\gamma$ coupling that is $20-35\%$ larger and $\approx 10\%$ smaller than the SM, respectively. The larger $hgg$ coupling results in $h \to VV^*$ signal strengths $\sim 40-60\%$ larger than SM, serving as an important prediction of these natural stop scenarios in the absence of other coupling corrections.

## 4.4 Scenario D: Two Light Stops, $W$ from Stop

Direct production of $W^+W^-$ from stop decay can be made fully natural in a similar fashion to $W^+W^-$ from EWinos. This is shown as Scenario D in Fig. 17. Similar to Section 4.3, the two stops are again near-degenerate with mixing that is small but nonzero, to allow both $\mathrm{Br}(\tilde{t}_{1,2} \to \tilde{\chi}_1^\pm b) \approx 1$. There is some mixing in the sbottom sector to guarantee $m_{\tilde{b}_1} - m_{\tilde{\chi}_1^0} \lesssim 10\,\mathrm{GeV}$ to escape sbottom searches, but the Higgs coupling correction of this mixed $\tilde{b}_1$ can always be made negligible with a heavy $\tilde{b}_2$ [87]. Other Higgs coupling

considerations are identical to Section 4.3.1 and do not exclude this scenario.

The preferred region of the stop-neutralino (or stop-sbottom) mass plane is very similar to that shown in Fig. 30 and Fig. 31, except by construction the sbottom bounds do not apply, and the absence of charginos means there are no trilepton bounds. As discussed in Section 4.2.1 it is possible for the Bino to be a thermal relic with correct abundance, and for sleptons inserted between the stops and the neutralino to account for the deviation in the measured $(g-2)_\mu$.

## 4.5 $W$ from Sbottom

One could imagine inverting the scenarios shown in Fig. 17: Producing sbottoms instead of stops, and possibly hiding stops by setting their mass very close to the neutralino LSP. However, this is either not viable or already excluded.

Scenarios A and C, with $W$ from EWino decay, cannot be inverted because the $\tilde{b} \to \tilde{\chi}_1^\pm t$ decay is 4-body and highly suppressed if the mass difference is small, and highly visible if it is not.

Inverted Scenarios $B$ and $D$, with one sbottom near $\sim 200\,\text{GeV}$ and one or two stops near the neutralino, could generate the required $W^+W^-$ signal. This requires a tuned sbottom mixing to ensure $\text{Br}(\tilde{b}_1 \to \tilde{\chi}_1^0 b) \ll \text{Br}(\tilde{b}_1 \to \tilde{t}_{1,2} W^-) \approx 1$, which is equivalent to tuning away the effective hypercharge of $\tilde{b}_1$. The light stops then decay via the loop-induced process $\tilde{t} \to c\tilde{\chi}_1^0$. However, such squeezed stops are the subject of dedicated ATLAS and CMS searches [45], which exclude $m_{\tilde{t}} < 250\,\text{GeV}$ for arbitrarily small $m_{\tilde{t}} - m_{\tilde{\chi}_1^0}$. Since the

bottom of the spectrum has to be below $\sim 150\,\text{GeV}$ to generate a suitable $W^+W^-$ signal, this eliminates the inverted Scenarios B and D as possibilities.

# 5 Conclusion

Naturalness prompts us to expect something beyond the SM near the electroweak scale. In light of this expectation, the absence of convincing new physics signals in all searches to date might be interpreted as painting a somewhat pessimistic picture. This has led to a degree of soul-searching within the field, questioning the basic assumptions on which these expectations are built [111–113] or to already plan for higher energy colliders. While this is a necessary exercise, it is important to understand that the possibilities for electroweak-scale new physics are far from exhausted.

By investigating just one SM standard candle, the $W^+W^-$ cross section, we have uncovered a wealth of possible information about new EW states at the LHC. In the search for new EW states at the LHC prior to this study, a gap had consistently remained between LEP and the LHC for low mass EW states. By examining the differential $W^+W^-$ cross section we have shown that this gap can be closed or new physics can hide in this gap when investigating simplified models based on supersymmetry particle productions. For example, chargino, slepton and stop can improve the agreement with the data both at ATLAS and CMS. In the slepton simplified model space we also discovered a region analogous to [52], where new EW states can fit the $W^+W^-$ differential cross section data *better* than the SM alone. Sleptons give significantly different predictions compared to the chargino [52] or

stop [61] explanations of the $W^+W^-$ cross section anomaly, most notably that the excess in $W^+W^-$ should be flavor-diagonal. They can also account for the correct relic density of dark matter in the universe, provide a signal for future direct detection experiments, and explain the longstanding $(g-2)_\mu$ discrepancy. Sleptons can also potentially explain some increase in the $h \to \gamma\gamma$ rate that may be slightly favored when combining both ATLAS and CMS results.

The excess in all $W^+W^-$ cross section measurements [56–58] can be interpreted as (i) a statistical fluctuation, (ii) an unexplained SM effect, or (iii) a genuine signal of new physics. The first possibility is, by definition, somewhat unlikely, with the combined significance of the excess being about $3\sigma$, more if shape differences in expected and observed distributions are taken into account. The second possibility would require those effects from QCD higher order corrections [39, 96, 97, 100, 101]. In fact recently, CMS updated WW cross section at 8 TeV result by considering NNLO calculations and NNLL $p_T$ resummation [39]. The deviation between the data and prediction becomes smaller than 1 sigma. But, for WZ and ZZ, they can be explained very well by the SM NLO predictions within one sigma. However, these SM NNLO effects may bring up disagreements on WZ and ZZ channels. The cross section for $ZZ$ production was first calculated at full NNLO in [98], the effects compared to NLO were found to be quite small provided that the $gg \to VV$ contribution to the cross section was included separately at NLO (which it is by both ATLAS and CMS in their $W^+W^-$ and $ZZ$ measurements). While this calculation is not the full NNLO $W^+W^-$ calculation, there is reason to believe they should be similar in size for these EW processes. Furthermore, if there were additional unexpected QCD behavior, it should manifest itself in the measurement of

$ZZ$ production, but both ATLAS and CMS measure that cross section to be in perfect agreement with the SM prediction [99]. Additionally, the $p_T$ resummation calculation [100] used in the most recent CMS study to model the jet veto [39] would also predict that the $p_T$ spectrums in other diboson channels should be different than their MC predictions.

In [52, 54] and [53] we showed that charginos or sleptons could account for the $W^+W^-$ excess, or, depending on one's interpretation, that such low-lying spectra below 150 GeV could not be excluded and remain open as possibilities. Producing $W$'s by decaying stops to charginos was first proposed in [61], realizing what we call Scenario A from Fig. 17. This suggested the intriguing possibility that natural SUSY spectra might be hiding in the $W^+W^-$ signal, or (again) at the very least are not excluded.

In stop scenarios, our work shows, in fact, several classes of spectra featuring one or two light stops can serve as viable explanations of the $W^+W^-$ excess without being excluded by other searches. These new possibilities are shown in Fig. 17, and their phenomenological consequences are summarized in Table 3. Scenario B introduces a qualitatively novel way of producing $W$'s from strong production via direct electroweak stop decay, while Scenarios C and D make both strong $W^+W^-$ production mechanisms fully natural. In each of these scenarios, the $W^+W^-$ signal is explained by one or two light stops with masses near $\sim 220\,\text{GeV}$ and a neutralino LSP near $\sim 130\,\text{GeV}$. All of these scenarios predict additional particles, charginos (A, C) and/or sbottoms (B, C, D) close in mass to the stops and neutralino respectively. The light sbottoms might allow the Bino DM to be a thermal relic by opening up a co-annihilation channel, and certainly remove overclosure bounds from the scenario, even for standard cosmological histories.

| Scenario | Explains $W^+W^-$ excess [56–58] | Explains trilepton excess [75] | Natural SUSY spectrum | thermal DM relic | $(g-2)_\mu$ |
|---|---|---|---|---|---|
| A | Yes | Yes | partial | No | No |
| B | Yes | No | partial | possible | possible |
| C | Yes | Yes | Yes | possible | No |
| D | Yes | No | Yes | possible | possible |

Table 3: Summarized phenomenological consequences of the four stop scenarios illustrated in Fig. 17. A thermal DM relic requires light sbottoms close to the Bino mass. Explaining $(g-2)_\mu$ requires sleptons to be inserted into the spectrum. See Section 4 for details.

Clearly any possible hints of new physics that SM standard candles shed light on should be investigated to the fullest. However, regardless of whether or not this particular anomalous region remains with larger luminosity or higher energy runs, the importance of using SM standard candles is clear. Current search strategies are typically based on looking in regions where the SM contributes a small number of events. To investigate the actual EW scale, where the only new particle discovered by the LHC lurks, we must confront these regions by understanding the SM in greater detail. Given that this prohibits the use of straightforward data-driven techniques it is important for experimentalists to measure these regions in as much detail as possible, while theorists must continue to improve their calculations of SM processes. Top physics has often been the hallmark of where to search for new physics, given that it couples so strongly to the Higgs. However, EW gauge bosons also couple strongly to the source of EWSB, and can provide just as important of window into the physics associated with EWSB. Both experimentalists and theorists need to explore the SM EW sector in exhaustive detail, otherwise we risk missing an important opportunity for discovering new physics, or understanding where it can and cannot exist.

# A Appendix

## A.1 Stop case in scenario B, D

In order to know the relation between $\Delta m(\tilde{t}_1 - \tilde{b}_1)$ and the preferred region, we performed two cases, $\Delta m(\tilde{t}_1 - \tilde{b}_1) \sim 85$GeV and $\Delta m(\tilde{t}_1 - \tilde{b}_1) \sim 100$GeV. we consider $\tilde{t}_1 \to \tilde{b}_1 W$ with $\Delta m(\tilde{t}_1 - \tilde{b}_1) \sim 100\,\text{GeV}$ in Fig.32. The preferred region(Blue) is $\tilde{t}_1 \sim 200\,\text{GeV}$ and $\tilde{\chi}_1^0 \sim 70\,\text{GeV}$ that is excluded LEP and ATLAS 8 TeV sbottom exclusion. WW exclusion region (orange line) is different from that in $\tilde{t}_1 \to \tilde{\chi}_1^{\pm} b$. For example, in CMS 8 TeV, as $\tilde{t}_1 \sim 180\,\text{GeV}$ and $\tilde{\chi}_1^0$ increases from 50 GeV to 80 GeV, the larger $\tilde{\chi}_1^0$ is ruled out by WW. As $\tilde{\chi}_1^0$ increases, b-jet becomes softer. There are too many events passing jet-veto and result in too many WW signal contributions and they are not preferred. In $\tilde{t}_1 \to \tilde{b}_1 W$ and $\tilde{b}_1 \to b\tilde{\chi}_1^0$, $\tilde{\chi}_1^0$ controls b-jet energy instead of lepton energy. However, in $\tilde{t}_1 \to \tilde{\chi}_1^{\pm} b$ and $\tilde{\chi}_1^{\pm} \to W^{(*)}\tilde{\chi}_1^0$, $\tilde{\chi}_1^0$ controls lepton energy instead of b-jet. Furthermore, as $\Delta m(\tilde{t}_1 - \tilde{b}_1) \sim 85\,\text{GeV}$ in Fig.33, the preferred region is in the allowed region. Compared to $\Delta m(\tilde{t}_1 - \tilde{b}_1) \sim 100\,\text{GeV}$, $\Delta m(\tilde{t}_1 - \tilde{b}_1) \sim 85\,\text{GeV}$ has heavier $\tilde{b}_1$ and b-jet is more energetic. Thus, jet-veto does not allow too many WW contributions.

In addition, with sbottom exclusion information, there is a narrow funnel among purple, black and gray line that are still allowed by collider searches. We would like to understand the WW preferred region when we consider two light stops and one sbottom that are all allowed by collider searches. In Fig.34, $\tilde{\chi}_1^0$ and $\tilde{b}_1$ are chosen 160 GeV and 175 GeV respectively. In this stop1-stop2 plane, both ATLAS 7 TeV and CMS 8 TeV have WW preferred region. The most preferred region (Blue contour) is $\tilde{t}_1 \sim \tilde{t}_2 \sim 260\,\text{GeV}$. This point is allowed by sbottom

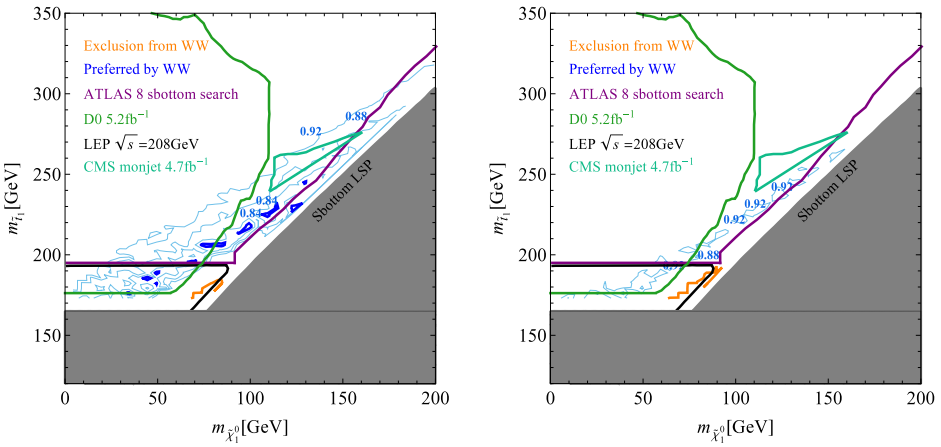


(a) ATLAS7 (b) CMS7

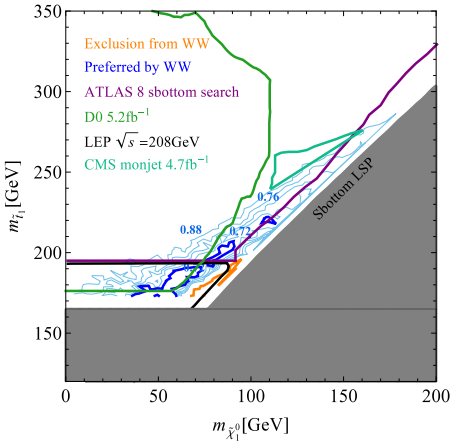


(c) CMS8

Figure 32: Stop scenario at $W^+W^-$ search. $\tilde{t}_1 \to \tilde{b}_1 W$ with $\tilde{t}_1 - \tilde{b}_1 \sim 100\,\text{GeV}$. All regions inside purple, green and black lines are excluded. The region below the gray line is excluded because sbottom is LSP. The most $W^+W^-$ preferred region are excluded by sbottom search. Both orange and blue are the same as previous plots. Purple line is ATLAS 8TeV $12.8 fb^{-1}$ [81]. Green is D0 $5.2 fb^{-1}$ [85]. Light green is CMS mono-jet search [84]. Black line is LEP $\sqrt{s} = 208\,\text{GeV}$ [83].

searches and WW search simultaneouly. For larger $\tilde{\chi}_1^0$ and $\tilde{b}_1$ that are allowed by sbottom searches, for example (200,218) GeVand (240,261) GeV, WW prefered region is not robust because stop pair production cross section is too small.

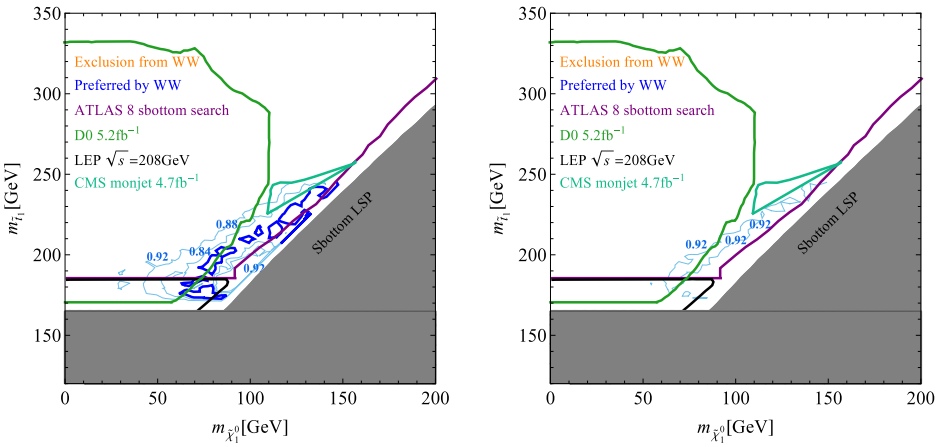


(a) ATLAS7 (b) CMS7

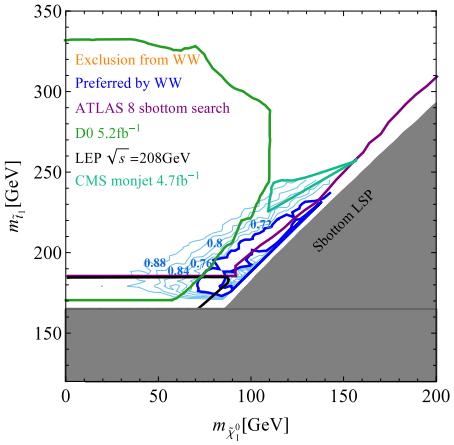


(c) CMS8

Figure 33: Stop scenario at $W^+W^-$ search. $\tilde{t}_1 \to \tilde{b}_1 W$ with $\tilde{t}_1 - \tilde{b}_1 \sim 85\,\text{GeV}$. All regions inside purple, green and black lines are excluded. The region below the gray line is excluded because sbottom is LSP. The most $W^+W^-$ preferred region are excluded by sbottom search. Both orange and blue are the same as previous plots. Purple line is ATLAS 8TeV $12.8 fb^{-1}$ [81]. Green is D0 $5.2 fb^{-1}$ [85]. Light green is CMS mono-jet search [84]. Black line is LEP $\sqrt{s} = 208\,\text{GeV}$ [83].

# References


[1] Stephen P. Martin, A Supersymmetry Primer, Adv. Ser. Direct. High Energy Phys. **21** (2010) 1-153

[2] L. Girardello and M. T. Grisaru, Soft Breaking of Supersymmetry, Nucl. Phys. B **1944** (1982) 65.

[3] S. Ferrara, L. Girardello and F. Palumbo, Phys. Rev. **D20** (1979) 403.

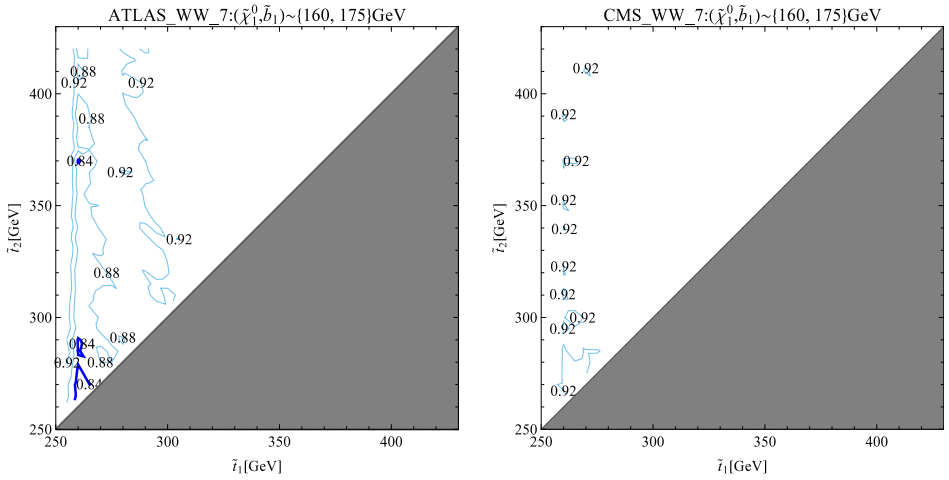


(a) ATLAS7 (b) CMS7

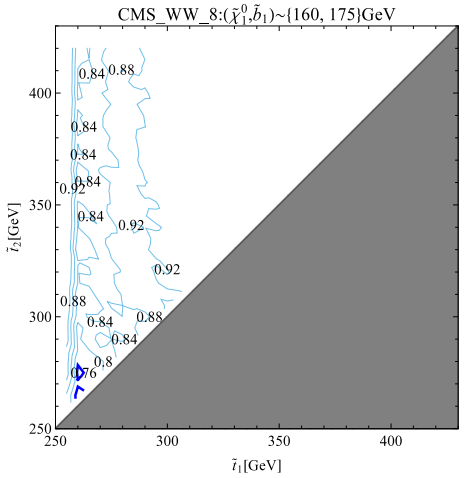


(c) CMS8

Figure 34: Stop scenario at $W^+W^-$ search. Two light stops with $\tilde{t}_{1,2} \to \tilde{b}_1 W$ and one sbottom allowed by collider search (Fig.29). Blue contours is $\chi^2/\chi^2_{SM}$. We consider $(\tilde{\chi}_1^0,\tilde{b}_1)$=(160,175) GeVat ATLAS7, CMS7 and CMS8. For both ATLAS7 and CMS8, $W^+W^-$ preferred region implies $\tilde{t}_{1,2} \sim 260\,\text{GeV}$.


[4] M. Dine and W. Fischler, Phys. Lett. B **110**, 227 (1982); C.R. Nappi and B.A. Ovrut, Phys. Lett. B **113**, 175 (1982); L. Alvarez-Gaume, M. Claudson and M. B. Wise, Nucl. Phys. B **207**, 96 (1982). M. Dine, A. E. Nelson, Phys. Rev. D **48**, 1277 (1993). M. Dine, A.E. Nelson, Y. Shirman, Phys. Rev. D **51**, 1362 (1995). M. Dine, A.E. Nelson, Y. Nir, Y. Shirman, Phys. Rev. D **53**, 2658 (1996).

[5] L. Randall and R. Sundrum, Out of this world supersymmetry breaking, Nucl. Phys. B **557** (1999) 79118. G. F. Giudice, M. A. Luty, H. Murayama, and R. Rattazzi, Gaugino mass without singlets, JHEP **9812** (1998) 027

[6] A. D. Sakharov, Pisma Zh. Eksp. Teor. Fiz., **5**, **32**, JETP Lett. 5, 24 (1967)

[7] Arnold, Peter and McLerran, Larry, Sphalerons, small fluctuations, and baryon-number violation in electroweak theory, Phys. Rev. D **36**, 581, 1987

[8] Arnold, Peter and McLerran, Larry, The sphaleron strikes back: A response to objections to the sphaleron approximation, Phys. Rev. D **37**, 1020, 1988

[9] S.Y. Khlebnikov, M.E. Shaposhnikov, Nucl. Phys. B **308**, 885, 1988

[10] M. Fukugita and T. Yanagida, Phys. Lett. B **174**, 45, 1986

[11] I. Affleck and M. Dine, Nucl. Phys. B **249**, 361, 1985

[12] CERN, European Organization for Nuclear Research, 2001. Via http://edu.pyhajoki.fi/.

[13] Curtin, David and Jaiswal, Prerit and Meade, Patrick, Excluding Electroweak Baryogenesis in the MSSM, JHEP **1208**, 005, [ARXIV:1203.2932]

[14] ATLAS-CONF-2013-034 (http://cds.cern.ch/record/1528170); G. Aad *et al.* [ATLAS Collaboration], Phys. Lett. B **716**, 1 (2012) [arXiv:1207.7214 [hep-ex]]; S. Chatrchyan *et al.* [CMS Collaboration], Phys. Lett. B **716**, 30 (2012) [arXiv:1207.7235 [hep-ex]].

[15] Summery plots of SUSY in ATLAS and CMS:"https://twiki.cern.ch/twiki/bin/view/CMSPublic/PhysicsResultsSUS","https://twiki.cern.ch/twiki/bin/view/AtlasPublic/SupersymmetryPublicResults"

[16] ATLAS, arXiv:1402.7029,1403.5294,1402.7029,1407.0350,1403.5294,1402.7029,1403.5294, ATLAS-CONF-2013-093; CMS, SUS-13-006,SUS-14-002.

[17] Summery plots of exotics in ATLAS and CMS."https://twiki.cern.ch/twiki/bin/view/AtlasPublic/ExoticsPublicResults","https://twiki.cern.ch/twiki/bin/view/CMSPublic/PhysicsResultsEXO"

[18] Talks given at March 2014 Electroweak Moriond Conference, specifically: "Strong SUSY production searches" (Pedrame Bargassa), "EW SUSY production searches at ATLAS and CMS" (Michael Flowerdew), "Multilepton and Multiphoton signatures of SUSY at the LHC" (Christoffer Petersson), "Dark Matter searches in LHC" (Philippe Calfayan), "Exotic Searches in LHC" (Thiago Rafael).

[19] Talks given at March 2014 QCD Moriond Conference, specifically: "Searches for BSM Higgs Bosons at the LHC" (Paolo Meridiani), "Third Generation SUSY Searches at the LHC" (Takashi Yamanaka), "Inclusive SUSY Searches at the LHC" (Sezen Sekmen), "Searches for Heavy Resonances at the LHC" (Tetiana Hryn'Ova), "Searches for dark matter and extra dimensions at the LHC" (Sarah Eno).

[20] K. Meissner, H. Nicolai (2006). "Conformal Symmetry and the Standard Model". Physics Letters B648: 312317. arXiv:hep-th/0612165

[21] H. Georgi and A. Pais, Phys. Rev. D **10**, 539 (1974); Phys. Rev. D **12**, 508 (1975).

[22] D. B. Kaplan and H. Georgi, Phys. Lett. B **136**, 183 (1984). D. B. Kaplan, H. Georgi and S. Dimopoulos, Phys. Lett. B **136**, 187 (1984).

[23] The Higgs as a Composite Nambu-Goldstone Boson, R. Contino, arXiv:hep-ph/1005.4269 **136**, 187 (1984).

[24] A. Abdesselam, E. B. Kuutmann, U. Bitenc, G. Brooijmans, J. Butterworth, et al., Boosted objects: A Probe of beyond the Standard Model physics, Eur.Phys.J. C71 (2011) 1661[[arXiv:1012.5412]. A. Altheimer, S. Arora, L. Asquith, G. Brooijmans, J. Butterworth, et al., Jet Substructure at the Tevatron and LHC: New results, new tools, new benchmarks, J.Phys. G39 (2012) 063001, [arXiv:1201.0008]. A Probe of beyond the Standard Model physics, Eur.Phys.J. C71 (2011) 1661 ATLAS-CONF-2011-073, CERN, Geneva, May, 2011. Tech. Rep. CMS-PAS-JME-10-013, CERN, Geneva, 2011. Tech. Rep. CMS-PAS-QCD-10-041, CERN, Geneva, 2010. ATLAS,Tech. Rep. ATL-PHYS-PROC-2011-142, 2011,JHEP 1205 (2012) 128. Larkoski, Andrew J. and Salam, Gavin P. and Thaler, JHEP,1306,108,10.1007/JHEP06(2013) 108.

[25] ATLAS-CONF-2013-028, ATLAS-CONF-2013-036, ATLAS-CONF-2013-035. CMS PAS SUS-12-022, JHEP 1211, 147 (2012) [arXiv:1209.6620 [hep-ex]],ATLAS-CONF-2013-035.

[26] ATLAS, Search for supersymmetry in events containing a same-flavour opposite-sign dilepton pair, jets, and large missing transverse momentum in $\sqrt{s} = 8$ TeV pp collisions with the ATLAS detector, arXiv:1503.03290v1 [hep-ex] 11 Mar 2015

[27] A. Heister *et al.* [ALEPH Collaboration], Phys. Lett. B **526**, 206 (2002) [hep-ex/0112011]; A. Heister *et al.* [ALEPH Collaboration], Phys. Lett. B **583**, 247 (2004); P. Achard *et al.* [L3 Collaboration], Phys. Lett. B **580**, 37 (2004) [hep-ex/0310007]; J. Abdallah *et al.* [DELPHI Collaboration], Eur. Phys. J. C **31**, 421 (2003) [hep-ex/0311019]; G. Abbiendi *et al.* [OPAL Collaboration], Eur. Phys. J. C **32**, 453 (2004) [hep-ex/0309014];

[28] CMS,arXiv:1206.2892.

[29] ATLAS-CONF-2013-028, ATLAS-CONF-2013-036, ATLAS-CONF-2013-035.

[30] "Search for electroweak production of charginos, neutralinos, and sleptons using leptonic final states in pp collisions at $\sqrt{s} = 8\,\text{TeV}$ - CMS PAS SUS-12-022;

[31] J. R. Espinosa and M. Quiros, Phys. Lett. B **279**, 92 (1992). U. Ellwanger, C. Hugonie and A. M. Teixeira, Phys. Rept. **496**, 1 (2010) [arXiv:0910.1785 [hep-ph]].

[32] L. J. Hall, D. Pinner and J. T. Ruderman, JHEP **1204**, 131 (2012) [arXiv:1112.2703 [hep-ph]].

[33] P. Batra, A. Delgado, D. E. Kaplan and T. M. P. Tait, JHEP **0402**, 043 (2004) [hep-ph/0309149].

[34] CMS SUS-13-004, CMS SUS-13-011, ATLAS-CONF-2013-024, ATLAS-CONF-2013-037.

[35] The ATLAS collaboration, ATLAS-CONF-2013-054; The ATLAS collaboration, ATLAS-CONF-2013-061; [ATLAS Collaboration], ATLAS-CONF-2012-151; [ATLAS Collaboration], ATLAS-CONF-2013-007; [ATLAS Collaboration], ATLAS-CONF-2013-037; The ATLAS collaboration, ATLAS-CONF-2013-053; G. Aad *et al.* [ATLAS Collaboration], Phys. Lett. B **720**, 13 (2013) [arXiv:1209.2102 [hep-ex]]; G. Aad *et al.* [ATLAS Collaboration], Phys. Rev. Lett. **109**, 211802 (2012) [arXiv:1208.1447 [hep-ex]]; G. Aad *et al.* [ATLAS Collaboration], Phys. Rev. Lett. **109**, 211803 (2012) [arXiv:1208.2590 [hep-ex]]; G. Aad *et al.* [ATLAS Collaboration], JHEP **1211**, 094 (2012) [arXiv:1209.4186 [hep-ex]].

[36] G. Aad *et al.* [ATLAS Collaboration], "Measurement of $W^+W^-$ production in $pp$ collisions at $\sqrt{s} = 7$ TeV with the ATLAS detector and limits on anomalous $WWZ$ and $W\gamma$ couplings," arXiv:1210.2979 [hep-ex].

[37] "Measurement of WW production rate" - CMS-PASSMP-12-005

[38] "Measurement of WW production rate" - CMS-PASSMP-12-013

[39] "Measurement of the $W^+W^-$ cross section in pp collisions at $\sqrt{s} = 8$ TeV and limits on anomalous gauge couplings" - CMS PAS SMP-14-016

[40] S. Chatrchyan *et al.* [CMS Collaboration], arXiv:1402.4770 [hep-ex]; S. Chatrchyan *et al.* [CMS Collaboration], arXiv:1311.4937 [hep-ex]; CMS Collaboration [CMS Collaboration], CMS-PAS-SUS-13-016; CMS Collaboration [CMS Collaboration], CMS-PAS-SUS-13-013; CMS Collaboration [CMS Collaboration], CMS-PAS-SUS-13-008.

[41] ATLAS-CONF-2013-012 (http://cds.cern.ch/record/1523698).

[42] CMS-PAS-HIG-12-015.

[43] CMS-PAS-HIG-13-005.

[44] M. Carena, S. Gori, N. R. Shah, C. E. M. Wagner and L. -T. Wang, JHEP **1207**, 175 (2012) [arXiv:1205.5842 [hep-ph]]; T. Kitahara and T. Yoshinaga, arXiv:1303.0461 [hep-ph]. M. Carena, S. Gori, N. R. Shah, C. E. M. Wagner and L. -T. Wang, arXiv:1303.4414 [hep-ph].

[45] CMS Collaboration [CMS Collaboration], CMS-PAS-SUS-13-009; The ATLAS collaboration, ATLAS-CONF-2013-068.

[46] G. Aad *et al.* [ATLAS Collaboration], arXiv:1403.4853 [hep-ex].

[47] [ATLAS Collaboration],[arXiv:1208.4305 [hep-ex]]

[48] [ATLAS Collaboration], ATLAS-CONF-2013-018; G. Aad *et al.* [ATLAS Collaboration], Phys. Lett. B **718**, 1284 (2013) [arXiv:1210.5468 [hep-ex]]; S. Chatrchyan *et al.* [CMS Collaboration], Phys. Lett. B **716**, 103 (2012) [arXiv:1203.5410 [hep-ex]].

[49] P. Meade and M. Reece, Phys. Rev. D **74**, 015010 (2006) [hep-ph/0601124].

[50] A. De Simone, O. Matsedonskyi, R. Rattazzi and A. Wulzer, JHEP **1304**, 004 (2013) [arXiv:1211.5663 [hep-ph]].

[51] Y. Kats and D. Shih, JHEP **1108**, 049 (2011) [arXiv:1106.0030 [hep-ph]]; C. Brust, A. Katz and R. Sundrum, JHEP **1208**, 059 (2012) [arXiv:1206.2353 [hep-ph]]; Z. Han, A. Katz, D. Krohn and M. Reece, JHEP **1208**, 083 (2012) [arXiv:1205.5808 [hep-ph]]; C. Brust, A. Katz, S. Lawrence and R. Sundrum, JHEP **1203**, 103 (2012) [arXiv:1110.6670 [hep-ph]]; J. A. Evans and Y. Kats, JHEP **1304**, 028 (2013) [arXiv:1209.0764 [hep-ph]].

[52] D. Curtin, P. Jaiswal and P. Meade, Phys. Rev. D **87**, 031701(R) (2013) [arXiv:1206.6888 [hep-ph]].

[53] D. Curtin, P. Jaiswal, P. Meade and P. -J. Tien, JHEP **1308**, 068 (2013) [arXiv:1304.7011 [hep-ph]].

[54] Curtin, David and Meade, Patrick and Tien, Pin-Ju, Natural SUSY in Plain Sight, Phys. Rev. D **90**, 115012 (2014)

[55] H. K. Dreiner, S. Heinemeyer, O. Kittel, U. Langenfeld, A. M. Weber and G. Weiglein, Eur. Phys. J. C **62**, 547 (2009) [[arXiv:0901.3485 [hep-ph]]

[56] G. Aad *et al.* [ATLAS Collaboration], Phys. Rev. D **87**, no. 11, 112001 (2013) [Erratum-ibid. D **88**, no. 7, 079906 (2013)] [arXiv:1210.2979 [hep-ex]].

[57] CMS Collaboration [CMS Collaboration], CMS-PAS-SMP-12-005.

[58] CMS Collaboration [CMS Collaboration], CMS-PAS-SMP-12-013.

[59] [ATLAS Collaboration], ATLAS-CONF-2013-030.

[60] M. Czakon, A. Mitov, M. Papucci, J. T. Ruderman and A. Weiler, Phys. Rev. Lett. **113**, no. 20, 201803 (2014) [arXiv:1407.1043 [hep-ph]].

[61] K. Rolbiecki and K. Sakurai, JHEP **1309**, 004 (2013) [arXiv:1303.5696 [hep-ph]].

[62] Kim, Jong Soo and Rolbiecki, Krzysztof and Sakurai,Kazuki and Tattersall, Jamie JHEP **1412**, 010 (2014) [arXiv:1406.0858 [hep-ph]].

[63] R. Contino, arXiv:1005.4269 [hep-ph]; B. Bellazzini, C. Csaki and J. Serra, arXiv:1401.2457 [hep-ph].

[64] J. Girrbach, S. Mertens, U. Nierste and S. Wiesenfeldt, JHEP **1005**, 026 (2010) [arXiv:0910.2663 [hep-ph]].

[65] G. F. Giudice, P. Paradisi, A. Strumia and A. Strumia, JHEP **1210**, 186 (2012) [arXiv:1207.6393 [hep-ph]].

[66] P. H. Chankowski, A. Dabelstein, W. Hollik, W. M. Mosle, S. Pokorski and J. Rosiek, Nucl. Phys. B **417**, 101 (1994);

[67] B. Aubert *et al.* [BaBar Collaboration], Phys. Rev. Lett. **105**, 051602 (2010) [arXiv:0912.0242 [hep-ex]];

[ALEPH and CDF and D0 and DELPHI and L3 and OPAL and SLD and LEP Electroweak Working Group and Tevatron Electroweak Working Group and SLD Electroweak and Heavy Flavour Groups Collaborations], arXiv:1012.2367 [hep-ex];

D. Abbaneo *et al.* [ALEPH and DELPHI and L3 and OPAL and LEP Electroweak Working Group and SLD Heavy Flavor and Electroweak Groups Collaborations], hep-ex/0112021.

[68] D. Curtin, P. Jaiswal and P. Meade, JHEP **1208**, 005 (2012) [arXiv:1203.2932 [hep-ph]]; T. Cohen, D. E. Morrissey and A. Pierce, Phys. Rev. D **86**, 013009 (2012) [arXiv:1203.2924 [hep-ph]]; T. Cohen and A. Pierce, Phys. Rev. D **85**, 033006 (2012) [arXiv:1110.0482 [hep-ph]].

[69] J. Fan and M. Reece, arXiv:1401.7671 [hep-ph].

[70] M. Carena, S. Gori, N. R. Shah, C. E. M. Wagner and L. -T. Wang, JHEP **1308**, 087 (2013) [arXiv:1303.4414, arXiv:1303.4414 [hep-ph]].

[71] N. Arkani-Hamed, S. Dimopoulos and S. Kachru, hep-th/0501082. R. Mahbubani and L. Senatore, Phys. Rev. D **73**, 043510 (2006) [hep-ph/0510064].

[72] B. Giebels [H. E. S. S. Collaboration], arXiv:1303.2850 [astro-ph.HE].

[73] G. -C. Cho, K. Hagiwara, Y. Matsumoto and D. Nomura, JHEP **1111**, 068 (2011) [arXiv:1104.1769 [hep-ph]].

[74] Private email communication with Matt Reece, March 6 2014.

[75] G. Aad *et al.* [ATLAS Collaboration], JHEP **1404**, 169 (2014) [arXiv:1402.7029 [hep-ex]]; G. Aad *et al.* [ATLAS Collaboration], arXiv:1403.5294 [hep-ex].

[76] V. Khachatryan *et al.* [ CMS Collaboration], arXiv:1405.7570 [hep-ex].

[77] CMS Collaboration [CMS Collaboration], CMS-PAS-SUS-13-017.

[78] The ATLAS collaboration, ATLAS-CONF-2013-093.

[79] G. D. Kribs, A. Martin and T. S. Roy, JHEP **0901**, 023 (2009) [arXiv:0807.4936 [hep-ph]].

[80] The ATLAS collaboration, ATLAS-CONF-2013-049.

[81] ATLAS-CONF-2012-165

[82] ATLAS-CONF-2012-167

[83] LEPSUSYWG: ALEPH, DELPHI, L3, and OPAL Collaborations.

[84] [CMS Collaboration] EXO-11-059, "Search for Dark Matter and Large Extra Dimensions in Mono-jet Events in pp Collisions at sqrt(s)=7TeV"

[85] [D0 Collaboration], Phys. Lett. B **693**, 95 (2010); [arXiv:1005.2222 [hep-ex]]

[86] Ezequiel Alvarez and Yang Bai, [arXiv:1204.5182 [hep-ph]].

[87] K. Blum, R. T. D'Agnolo and J. Fan, JHEP **1301**, 057 (2013) [arXiv:1206.5303 [hep-ph]].

[88] N. Arkani-Hamed, A. Delgado and G. F. Giudice, Nucl. Phys. B **741**, 108 (2006) [hep-ph/0601041].

[89] P. A. R. Ade *et al.* [Planck Collaboration], arXiv:1303.5076 [astro-ph.CO].

[90] G. Belanger, F. Boudjema, A. Pukhov and A. Semenov, Comput. Phys. Commun. **176**, 367 (2007) [hep-ph/0607059].

[91] First results from the LUX dark matter experiment at the Sanford Underground Research Facility; [arXiv:1310.8214v2[astro-ph.CO]]

[92] pdg, http://pdg.lbl.gov/2012/reviews/rpp2012-rev-g-2-muon-anom-mag-moment.pdf

[93] A. Djouadi, Phys. Rept. **459**, 1 (2008) [hep-ph/0503173].

[94] [CMS Collaboration], CMS-PAS-HIG-13-001.

[95] [ATLAS Collaboration], ATLAS-CONF-2013-012.

[96] S. Dawson, I. M. Lewis and M. Zeng, Phys. Rev. D **88**, no. 5, 054028 (2013) [arXiv:1307.3249].

[97] T. Gehrmann, M. Grazzini, S. Kallweit, P. Maierhfer, A. von Manteuffel, S. Pozzorini, D. Rathlev, L. Tancredi, Phys. Rev. Lett. 113 (2014) 212001, arXiv:1408.5243 [hep-ph].

[98] F. Cascioli, T. Gehrmann, M. Grazzini, S. Kallweit, P. Maierhfer, A. von Manteuffel, S. Pozzorini and D. Rathlev *et al.*, arXiv:1405.2219 [hep-ph].

[99] [ATLAS Collaboration], ATLAS-CONF-2013-020; CMS Collaboration [CMS Collaboration], gauge couplings in lll'l' decays at sqrt(s) = 8 TeV at the LHC," CMS-PAS-SMP-13-005.

[100] Patrick Meade, Harikrishnan Ramani, Mao Zeng, Phys. Rev. D **90** (2014) 114006, arXiv:1407.4481.

[101] Prerit Jaiswal, Takemichi Okui, Phys. Rev. D **90** (2014) 073009 arXiv:1407.4537.

[102] E. Aprile *et al.* [XENON100 Collaboration], Phys. Rev. Lett. **109**, 181301 (2012) [arXiv:1207.5988 [astro-ph.CO]].

[103] J. S. Lee, A. Pilaftsis, M. S. Carena, S. Y. Choi, M. Drees, J. R. Ellis and C. E. M. Wagner, Comput. Phys. Commun. **156**, 283 (2004) [hep-ph/0307377]; J. S. Lee, M. Carena, J. Ellis, A. Pilaftsis and C. E. M. Wagner, Comput. Phys. Commun. **180**, 312 (2009) [arXiv:0712.2360 [hep-ph]]; J. S. Lee, M. Carena, J. Ellis, A. Pilaftsis and C. E. M. Wagner, Comput. Phys. Commun. **184**, 1220 (2013) [arXiv:1208.2212 [hep-ph]].

[104] Abdelhak Djouadi, Margarete Mhlleitner and Michael Spira, Decays of Supersymmetric Particles: the program SUSY-HIT (SUspect-SdecaY-Hdecay-InTerface), hep-ph/0609292

[105] T. Sjostrand, S. Mrenna and P. Z. Skands, Comput. Phys. Commun. **178**, 852 (2008) [arXiv:0710.3820 [hep-ph]]. T. Sjostrand, S. Mrenna and P. Z. Skands, JHEP **0605**, 026 (2006) [hep-ph/0603175].

[106] M. Cacciari and G. P. Salam, Phys. Lett. B **641**, 57 (2006) [hep-ph/0512210]; M. Cacciari, G. P. Salam and G. Soyez, Eur. Phys. J. C **72**, 1896 (2012) [arXiv:1111.6097 [hep-ph]].

[107] J. Alwall, M. Herquet, F. Maltoni, O. Mattelaer and T. Stelzer, JHEP **1106**, 128 (2011) [arXiv:1106.0522 [hep-ph]].

[108] W. Beenakker, R. Hopker and M. Spira, hep-ph/9611232. W. Beenakker, M. Klasen, M. Kramer, T. Plehn, M. Spira and P. M. Zerwas, Phys. Rev. Lett. **83**, 3780 (1999) [Erratum-ibid. **100**, 029901 (2008)] [hep-ph/9906298].

[109] Piotr H. Chankowski, Andreas Dabeistein, Wolfgang Hollik, WolfM. Mosle, Stefan Pokorski, Janusz Rosiek, $\Delta$r in the MSSM, Nucl. Phy. B. **417**,101,1994

[110] Janusz Rosiek, Complete set of Feynman rules for the MSSM – ERRATUM, hep-ph/9511250v3

[111] A. Arvanitaki, N. Craig, S. Dimopoulos and G. Villadoro, JHEP **1302**, 126 (2013), [arXiv:1210.0555 [hep-ph]].

[112] C. Kilic, T. Okui and R. Sundrum, JHEP **1002**, 018 (2010), [arXiv:0906.0577 [hep-ph]].

[113] N. Arkani-Hamed, A. Gupta, D. E. Kaplan, N. Weiner and T. Zorawski, arXiv:1212.6971 [hep-ph].